Structural Response of Bow Structures with Sonar Domes

Thijs Velner

Faculty of Mechanical, Maritime and Materials Engineering
Delft University of Technology

TU Delft Delft University of Technology

TNO innovation for life

Structural Response of Bow Structures with Sonar Domes

by

Thijs Velner

to obtain the degree of Master of Science
at the Delft University of Technology,
to be defended publicly on Tuesday July 19, 2016 at 15:00 AM.

Student number:	4085809	
Project duration:	November 1, 2015 – July 19, 2016	
Thesis committee:	Assoc. prof. dr. ing. A. Romeijn,	TU Delft, supervisor
	Dr. ir. J.T. Tuitman,	TNO, daily supervisor
	Dr. ir. J.H. den Besten,	TU Delft
	Dr. ir. M. Godjevac,	TU Delft

This thesis is confidential and cannot be made public until July 19, 2016.

If the highest aim of a captain were to preserve his ship,
he would keep it in port forever

-Thomas Aquinas

Abstract

Naval vessels are designed to remain operational in severe conditions, sea-state 6 or higher, and have to maintain a minimum forward speed in these conditions. These seakeeping conditions may result in severe impact loads on the bow of the vessel, called slamming. Sonar domes are often used at naval vessels to detect objects under water and are located at the forefoot of the vessel. The sonar dome used by the Royal Netherlands Navy is a composite structure connected under the steel bow structure of the vessel and is filled with water. Slamming and other seakeeping loads at the composite sonar dome have to be transferred to the steel bow structure through the composite and water inside the dome. Slamming loads have an impact type of character, which is described as a sudden quick increase of the load and with a short duration. Previous research has shown that neglecting the loads at the dome structure results in a serious underprediction of local structural response of the bow of the vessel. Besides that, little is known about the load transfer from the dome towards the bow structure.

First, the dynamic response of a fluid filled composite sonar dome is studied. Different load types are applied at the sonar dome model to study the influence of the internal fluid on the response. Second, the effect of the loading transferred from the sonar dome on the stress levels in steel bow structure is studied.

Slamming loads at the dome structure do not result in a highly dynamic response for the considered design. The rise-times of the loads have a relative long duration compared to the lowest natural response period of the sonar dome. The rise-times observed in the studied seakeeping conditions is in general much longer compared to the natural response periods of the dome.

Including the internal fluid in the dome results in a reduction of the deformation and stresses of the composite shell. During seakeeping loading the pressure in the internal fluid rises, resulting in a pressure load on the bow structure above the dome. The reduction of internal pressure due to the outflow of water from the dome to an expansion container seems to be rather limited

The presence of a sonar dome results in additional loads at the bow structure. These loads are a force at the dome flange and a pressure load on the bow structure above the dome. This leads to an increased stress level of the structural elements directly above the dome.

It is concluded that the contribution of the internal pressure within the dome to the stress levels of the bow structure is most relevant. Vessels without a sonar dome do not have a deck in the forefoot of the vessel that is loaded by a fluid pressure. It is concluded that the loads from the sonar dome should not be neglected in a structural analysis of the bow structure.

Acknowledgements

The project has been assigned for by the department of Structural Dynamics at TNO to investigate the effects of the presence of a sonar dome in the bow structure. The project has been carried out to obtain the MSc. degree in Maritime Technology with the specialization 'Ship and Offshore Structures'. This thesis project is my final independent assignment in obtaining this degree. Although the project has a individual character, it could not be successfully carried out without the help of a number of people.

My sincere thanks go out to Johan Tuitman as my daily supervisor at TNO. Thanks to his critical feedback I was able to learn and improve a lot during my master thesis. Many thanks go out to my other colleagues of the department Structural Dynamics at TNO for the interesting discussions during the brakes.

Thanks go out to the people of DMO and the 'Marine werf Den Helder' for guiding me through the Zr. Ms. Mercuur, answering all my questions and giving me insight in the previous studies performed on the sonar domes.

I want to thank Arie Romeijn for his guidance throughout the process and Henk den Besten for his critical attitude and being always prepared to answer my questions.

I want to thank my parents, brother, family and friends. For their support, interest and love during al stages of my study at the TU Delft. They always encouraged me to explore and improve myself.

Finally I want to thank my housemates Elmer, Menno and Stan. Especially for the good atmosphere at home, the (mostly bad) jokes and deep discussions on our balcony.

Thijs Velner
Delft, july 2016

x

Contents

Appendices

List of Figures

List of Tables

Nomenclature

General mathematical notation

a	Scalar
$\bar{a}$	Vector
a	Matrix
$\dot{a}$	First derivative to time of a
$\ddot{a}$	Second derivative to time of a

Abbreviations

BEM	Boundary Element Method
BVP	Boundary Value Problem
DOF	Degrees Of Freedom
EOS	Equation Of State
GWM	Generalized Wagner Method
PS	Port side
RAO	Response Amplitude Operator
SB	Starboard
SWBM	Still Water Bending Moment

Symbols seakeeping part

$\bar{\delta}$	Nodal displacements
μ	Heading
ω	Wave frequency
ω_e	Encounter frequency
$\bar{\zeta}$	Modal displacement vector
a	Accelerations in body system at node
A	Hydrodynamic added mass
B	Hydrodynamic damping
B	Vessel width
$B_{lin}^{U\neq0}$	Linear roll damping (with forward speed)
$B_{quad}^{U\neq0}$	Quadratic roll damping (with forward speed)
$B_{lin}^{U=0}$	Linear roll damping (zero speed)
$B_{quad}^{U=0}$	Quadratic roll damping (zero speed)
C	Stiffness matrix
$\mathbf{c_s}$	Structural stiffness matrix (HETIME)
$\bar{f}_t$	Total nodal force vector
$\bar{f}_{A(\infty)}(\bar{\zeta}, t)$	Frequency independent radiation force vector
$\bar{f}_{rd}(\bar{\zeta}, t)$	Viscous roll damping force
$\bar{f}_d(\bar{\zeta}, t)$	Diffraction force vector
$\bar{f}_g(\bar{\zeta})$	Force due to gravity acceleration
$\bar{f}_h(\bar{\zeta})$	Hydrodynamic wave excitation and restoring force vector
$\bar{f}_r(\bar{\zeta}, t)$	Frequency dependent radiation force vector
$\bar{f}_s(\bar{\zeta}, t)$	Slamming force vector
$\bar{f}_a^n(\bar{\zeta}, t)$	Nodal acceleration force vector
$\bar{F}_t$	Total force vector

$\bar{F}$	External force vector
F_{slam}	Sectional slamming force
M	Structural mass matrix
$\mathbf{M}_A$	(Fluid) Added mass matrix
N	Matrix with element shape functions
g	Gravity acceleration
GM	Metacentric height
$H_{1/3}$	Significant wave height
K	Retardation function
K_{xx}	Roll radius of gyration
K_{yy}	Pitch radius of gyration
K_{zz}	Yaw radius of gyration
L	Vessel length
LCG	Longitudinal centre of gravity
$\bar{n}$	Normal vector
$S(\omega)$	Wave spectrum
T_{aft}	Draft aft
T_{fore}	Draft fore
V	Ship speed
VCG	Vertical centre of gravity

Symbols structural part

α_L	Linear thermal expansion coefficient
μ	Dynamic viscosity
ν	Flow speed
A	Cross-sectional area
$\bar{\delta}$	Nodal displacements
ϵ	Strain tensor
σ	Stress
C	Structural damping matrix
d	Pipe diameter
D	Matrix with differential operators to transform displacements to strains
f	Friction factor
g	Gravity acceleration
K	Structural stiffness matrix FEA
$\mathbf{K}_G$	Geometrical stiffness matrix
L	Pipe length
m	Nodal mass
M	Structural mass matrix
N	Matrix with element shape functions
$\bar{n}$	Normal vector
p	Pressure
P	Pressure
$P_friction$	Frictional pressure loss
Q	Flow rate
V	Volume

Frame of reference

Hydrodynamic models
The bow of a vessel is defined as the front end of the vessel, looking forward. The stern is the aft part of the vessel. Looking forward, starboard is on the right hand side, on the negative y-axis and port side is on the left hand side, on the positive y-axis. The six ship motions with respect to the axis system defined at the vessel's centre of gravity are illustrated in Figure 1, and defined as follows:

surge	longitudinal x-direction, positive forwards
sway	lateral y-direction, positive to portside
heave	vertical z-direction, positive upwards
roll	about the x-axis, positive right turning
pitch	about the y-axis, positive right turning
yaw	about the z-axis, positive right turning

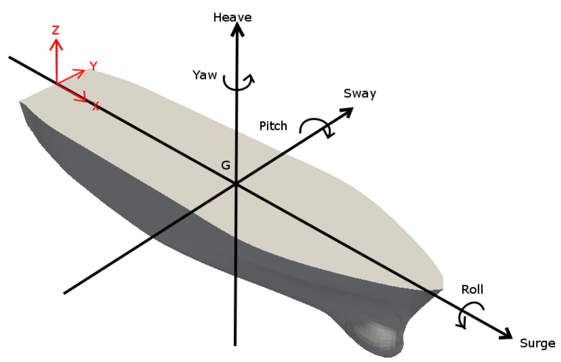

Figure 1: Frame of reference

Frame of reference 3D structural models
The frame of reference used for the 3D structural models is defined as indicated in red in Figure 1.

Frame of reference 2D structural models
In the 2D models the coordinate system is as shown in Figure 2, with the x-axis pointing to the right hand side, and the y-axis pointing upwards.

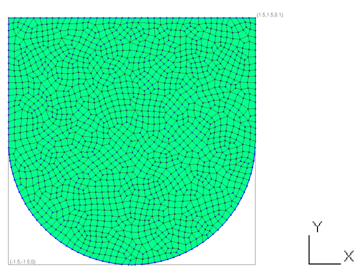

Figure 2: Frame of reference 2D dome model

1 Introduction

Naval vessels are designed to remain operational in severe conditions, sea-state 6 or higher, and maintain a minimum forward speed in these conditions. Figure 1.1 shows the emergence of the bow in waves of a M-Fregat. These seakeeping conditions may result in severe impact loads on the bow of the vessel, called slamming. Sonar domes are often used at naval vessels to detect objects under water and are located at the forefoot of the vessel. The sonar dome used by the Royal Netherlands Navy is a composite structure connected under the steel bow structure of the vessel and is filled with water (see Figure 1.2 and 1.3). The sonar dome structure is made of a composite material and is filled with water to provide the environment in which acoustic waves can propagate easily. This structure at the bow will experience wave and impact loads, known as slamming, as result of the seakeeping response of the vessel. These loads at the sonar dome are transferred through the composite dome structure and internal water into the steel hull structure of the vessel. The main research question of this master thesis is: How does a sonar dome respond to different types of loads and what is the influence of the loads at the dome on the structural response of the steel bow structure in heavy seakeeping conditions?.

Figure 1.1: Zr.Ms. Van Nes emerges from the waves. [18]

Relevance of the current research

The Royal Netherlands Navy is currently modifying the Zr.Ms. Mercuur to extend the lifetime. At the same time the Royal Netherlands Navy is developing the succeeder of the current M-Frigate class. In order to sail safely into the future, the structural strength has to be assessed. The assessment of the local structural response has previously been done by Tuitman in [21] and [23] for the 'Luchtverdedigings- en CommandoFregat' (LCF) of the Royal Netherlands Navy, where local response of a trim tank was calculated. The effect of the presence of a sonar dome on the local structural response of the bow is investigated in this thesis. Tuitman has shown that neglecting the load at the dome structure results in a serious under prediction of local structural

Figure 1.2: Bow of the Zr.Ms. Mercuur (A900) [19]

Figure 1.3: Interior sonar dome structure [2]

response. He also performed a brief study in which he incorporates the dome loads by assuming that the volume inside the dome doesn't change during loading, allowing to calculate loads due to internal pressures. Beside the aforementioned reports, little is known on the occurring loads in and around the heavy loaded flexible and fluid filled sonar dome. In order to predict the loads accurately, insight in the effects of a sonar dome on the structural response of the bow as whole is crucial. This study focuses on the local impact loads in rather extreme seakeeping conditions.

Research question

The main research question for this master thesis is stated:
'How does a sonar dome respond to different types of loads and what is the influence of the loads at the dome on the structural response of the steel bow structure in heavy seakeeping conditions?'

This question is investigated within the context of an existing vessel of the Royal Netherlands Navy, the Zr.Ms. Mercuur.

For the determination of the hydrodynamic loading, the *'Hydrodynamic Toolbox'*, developed by Tuitman [22] is used to determine the hydrodynamic loads. This set of programs is used to obtain the seakeeping loads including non-linear Froude-Kryloff and slamming loading. The structural response is determined by the results from the seakeeping analysis which are used as input in an FE-analysis of the bow structure. Using different structural models, describing the combination of the sonar dome and steel bow structure, the following questions will be answered:
'How does the sonar dome respond to seakeeping loads, and is this response dynamic?'

'Does the outflow of fluid from the dome result in a different response?'

By setting up different models describing the combination of the bow structure and the sonar dome the following question is investigated:
'How is the load on the sonar dome transferred to the structure and what is the effect of the internal fluid of the sonar dome on the load transfer?'

Finally, the effect of different measures to reduce the structural response are investigated:
'Which measures could reduce the stress levels?'

Approach

A schematic overview of the content of the report is given In Appendix A. The following paragraphs will briefly explain the content of the different used methods.

Seakeeping response and hydrodynamic loading
The bow of the vessel, which contains the sonar dome is subjected to hydrodynamic loads which also includes the impact of slamming. The seakeeping loads are calculated using a method that includes the slamming, non-linear Froude-Kryloff and hydrostatic loads. Because of the high non-linearity of the hydrodynamic forces, it is not possible to use any linear seakeeping response method. A suitable method is solving the seakeeping problem in time domain, which allows to include non-linear loads and evaluation of non-linear responses at each time step. Therefore the linear seakeeping calculation is coupled with a BEM slamming module which calculates the pressures due to the water entry of the bow sections of the vessel. Once the seakeeping loads are derived, these are transferred to a finite element model of the bow structure of the vessel. In general the hydro mechanical and structural models differ in characteristics and a proper method has to be set up to transfer the seakeeping loads, including pressures and accelerations, onto the structural model. This part is captured within the blue box in Appendix A. The seakeeping calculation method and results can be found in Chapter 2.

Structural analysis methods
Two types of analysis will be used for the structural analysis of the bow structure and the sonar dome. The response of the whole bow structure is calculated quasi static using an implicit FE code, VAST. The response of the fluid filled sonar dome is calculated using dynamic simulation in order to study possible dynamic effects in the response and to incorporate time dependent effects such as the outflow of water from the dome. Using an explicit FE program, LS-DYNA the response of the sonar dome due to the hydrodynamic loading is calculated in time domain. Both methods and programs are discussed in more detail in Chapter 3

Dynamic sonar dome analysis
The sonar dome is a composite shell structure filled with water located at the forefoot of the vessel, where it will experience slamming impact loads. An overview of this part is given within the red box in Appendix A. Chapter 4 will focus on two aspects: is there is a loading component that results in a dynamic response of the sonar dome and what is the effect of the outflow of fluid from the dome.
The dome is assumed to have a lower structural stiffness compared to the surrounding steel structure, and has a relative high mass due its containing fluid, which will result in lower natural periods of the structural response of the dome. These dynamic response periods are studied including the internal fluid for all the different expected load components. Especially the slamming loads seem to be of interest due to its impulsive character.
The second time dependent aspect is the in- and outflow of water through the expansion pipe during loading. A mathematical description of the expansion pipe will be derived based on pipe flow theory and incorporated in the dynamic simulations to study this effect. The models and results are presented in Chapter 4.

Structural response

The third part of this research consists of the response due to loads transmitted to the hull by the sonar dome. This part is indicated by the yellow box in Appendix A.
The dome is connected to the hull structure through flanges which are connected by a series of bolts. In Chapter 4 the dynamic load on the flange and deck above the dome are calculated. These loads are used as input at the dome flange and the deck above the dome in the quasi static bow model in order to calculate the stress in the steel structural members above the sonar dome. Special attention is drawn on the knees and stiffeners directly above the K-deck since this area has shown to be prone to high loads.
Since the structural analysis of the steel bow structure is linear elastic, a superposition of all load components can be made. The pressure load at each hull panel of the bow structure is calculated using the seakeeping results from Chapter 2. Combining all load components gives insight which structural members have the highest stress levels and which load components are the main contributors to this response. The models and results are described in more detail in Chapter 5.

Structural response reduction

In order to improve the structural integrity, areas with high stress levels are investigated. Based on the results from Chapter 3 areas which are likely to be highly stressed are identified. This part focuses on these areas and take a look at the possibilities to reduce the response in these highly stressed areas. This is done by looking at a few possible design modifications ,as shown within the green box in Appendix A. The modifications and results are discussed in Chapter 6.

2 Seakeeping method

Seakeeping

Seakeeping describes the 6-DOF motions that a ship experiences when sailing. When a linear potential panel method is used the actual position of the vessel and wave surface is not taken into account. Therefore this method only is not able to calculate (local) impact loads due to slamming. Which can only be resolved using free-surface capturing methods. To resolve the impact problem a method has to be used which incorporates the slamming loads. This chapter is about some detail of the problem and the method used to solve.

Slamming

Slamming is described as the hydrodynamic impact load of a body entering the water surface. In literature the following types of slamming are found [9]:

- Bottom slamming
  Occurs when an emerged part of the bottom re-enters the water surface.
- Bow-flare slamming
  Occurs when a high relative velocity between the bow-flare and water surface is attained.
- Breaking wave impact
  Occurs when a wave brakes at the ship structure
- Wet-deck slamming
  Occurs when waves hits the wetdeck of multihull or offshore structure.

The highly dynamic slamming loads may result in serious damage on the hull structure, which can also be related to serious accidents as an example, the ferry Estonia in 1994 which suffered from bow flare slamming at the bow doors [24].

The effects of impulse pressure on structures can results in large contributions in the structural response. For impulse loading this is the case when the high pressures have a short duration relative to structural natural periods of modes that give dominant contributions to the structural stresses [7]. The first research conducted on slamming loads can be identified with the publication of 'The impact on seaplane floats during landing' by von Karman in 1929. Since then many researchers have studied the impact problem. And many questions raised are still not answered since slamming is a complicate process in which the effects of forward speed and 3D flows are not fully captured. [9].

When investigating the global response of a vessel, from the structural dynamics point of view the time-scales of interest lies in the order of seconds for large seagoing vessels. The time-scales of effects such as air bubbles are typically much smaller. Under these assumptions it may be possible to simplify the problem by excluding these kind of interactions. This has lead to the development of analytical and numerical methods to described the problem using potential flows. Tuitman [20] applied the Generalize Wagner Method (GWM) within a hydro-elastic seakeeping method in order to be able to calculate the global whipping responses.

A more detailed problem arises when one investigates the local impact problem. Studies have shown that there is a large variation in maximum pressure observed in experiments. An example are the experiments conducted by Faltinsen [8], who performed vertical drop-test with aluminium and steel plates on waves and calm water. During the experiments performed by Faltinsen maximum pressures were observed ranging from 10 to 80 bar for the same impact velocity. One explanation is that the maximum pressure is highly localized in space and time, so a pressure gauge should be sufficient small with a sufficient high sampling rate to catch the peak pressures. Other aspect which may be important may be the presence of air cavities and acoustic waves.

2.1 Method

For this research, the vessel response is calculated using the Hydro-Elastic method developed by J.T. Tuitman [20]. This method is able to calculate the seakeeping response of the vessel which consists of the rigid body motions and the dynamic response of the vessel. One way to compute this response is to constantly calculate the dynamic structural response and update the seakeeping problem. However, this results in a very computationally extensive method. In [20] the calculation of the flexible response of the vessel is calculated using generalized modes. These generalized modes consist of the rigid body modes and a number of pre-calculated elastic responses which describe the flexible behaviour of the vessel. Combining the degrees of freedom from the rigid body and flexible modes results in the coupled system used for the hydro-elastic calculation of the seakeeping problem. However in this research the vessel is assumed to be rigid, since the vessel is relatively short, and therefore relative stiff in longitudinal direction. Only the 6-DOF rigid body motions will be solved within the seakeeping problem.

2.2 Hydrodynamic toolbox

The hydrodynamic toolbox is a set of programs created to calculate the seakeeping behaviour according to the hydro-elastic theory described in [20]. The following subsections will describe the different components of the programs.

Meshing
For the calculations of the hydrodynamic response, a BEM mesh of the wetted hull has to be generated. This mesh is generated from a geometric model of the vessel which can be a structural model or lines plans of the vessel. The program AMG [22] generates the hydrodynamic mesh of the vessel. The wetted part of the vessels mesh and the inner free surface is used within the boundary value problem. The inner surface panels of the mesh are used to prevent resonance within the vessel resulting in so called irregular frequencies in the output.
For the slamming calculation, 2D sections of the forward part of the vessel have to be generated. This is done using the program AMGCUT [22] which cuts through the mesh on predefined locations and ensures that the sections are smooth. This is to ensure stability of the GWM calculation method. The modified slamming sections are shown in Figure 2.1.

Linear seakeeping
Using the mass distribution, the model is first balanced. This means that the modal displacements of the model are calculated in still water. This is done till there is an equilibrium between internal and external forces in the still water condition. The modal displacements will be used to re-mesh the hydrodynamic model. This approach prevents initial responses at the start of the simulations due to a difference in internal and external forces.
The Boundary Value Problem (BVP) can be solved for a range of headings and encounter wave frequencies. The problem is solved using the potential flow assumptions with an infinite water depth. This problem is formulated using the program

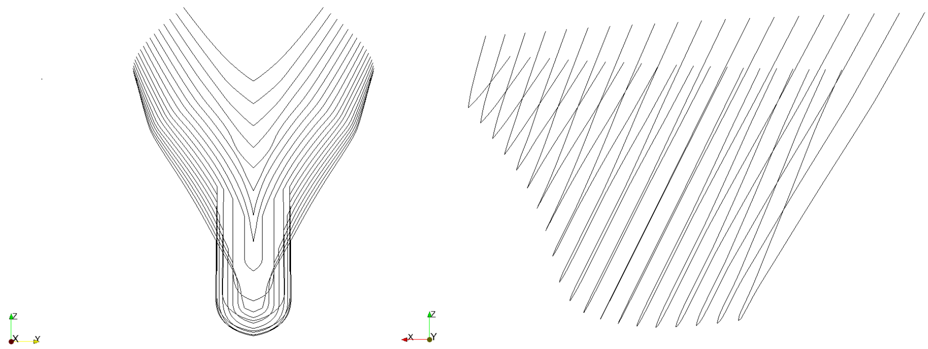

Figure 2.1: Slamming sections

HEPRE [22] and solved using the program HYDROSTAR [25]. The results of the programs are the hydrodynamic pressures due to diffraction, radiation and the incoming wave. The radiation pressures are integrated over the wetted surface to obtain the added mass and damping coefficients for the defined frequency range. The forward speed of the vessel is taken into account using the encounter frequency approach and the results for a base flow. The encounter frequency is calculated using Equation (2.1). Using a uniform base flow the pressure contributions on the hull due to forward speed are calculated and incorporated in the results.

$$\omega_e = \omega - \frac{\omega^2}{g} V \cos\mu \tag{2.1}$$

Where:

V	Ship speed
μ	Heading
ω	Wave frequency
ω_e	Encounter frequency

Frequency domain calculation

Using the results from HYDROSTAR the response to different wave components can easily be obtained, giving an estimate for the linear response of the vessel in waves. The natural frequencies of all rigid body modes are calculated by solving the equation of motion (2.2).

$$(\mathbf{M} + \mathbf{A}(\omega)) \cdot \ddot{\bar{\zeta}} + \mathbf{B}(\omega) \cdot \dot{\bar{\zeta}} + \mathbf{C} \cdot \bar{\zeta} = 0 \tag{2.2}$$

Where:

$\bar{\zeta}$	Displacement vector
M	Mass matrix
A	Added mass matrix
B	Damping matrix
C	Stiffness matrix

Slamming loads

The slamming load is calculated using the Generalized Wagner Model (GWM). This theory describes the drop of 2D objects in still water. The GWM uses the Boundary Element Method (BEM) to solve the water impact problem and to calculate the pressures. Since the GWM is not able to model flow separation, the sections used

should be smooth. The applied method only allows for shapes that are monotonically increasing. This is not the case for the 2D sections near the bow of the vessel. These sections are modified such that this condition is fulfilled by evaluating all points at the slamming section starting at the keel. For each point the y-coordinate is evaluated and points for which the previous y-coordinate is larger are removed.
For each section a slamming calculation is started when the relative velocity between the water surface and the section reach a certain threshold, and the section has to be in contact with the water surface. With small increments in time, which are usually an order smaller than the time domain seakeeping simulation time step, the development of the pressure is calculated. The pressures are integrated over the section to find the total slamming force. The calculated force is equal to Equation (2.3) where the surface integral over the section is reduced to a line integral over a section with a constant width.

$$F_{slam} = \sum_{n=1}^{N} l \cdot \int_{C_s} p_{slam} \cdot \bar{n} \mathrm{d}C_s \tag{2.3}$$

Where:

N	Number of slamming sections
C_s	Contour length of section
l	Width slamming section
p_{slam}	Slamming pressure

Time domain simulations
The program HETIME [22] computes the seakeeping response in time domain. It includes the non-linear slamming and Froude-Kryloff forces, which means that the momentary position of the vessel and wave elevation are taken into account to determine the pressures on the hull. This results in a non-linear pressure depending on the local wave height of the incoming waves with a discontinuity at the mean water level as illustrated in Figure 2.2.

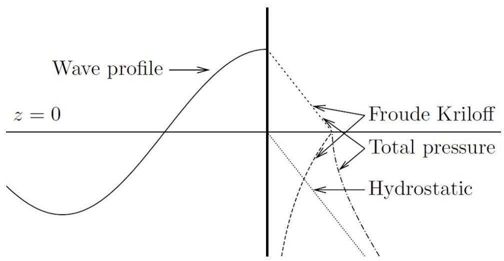

Figure 2.2: Non-linear Froude-Kryloff force [14]

Also the slamming force calculated using the routine as described in the previous section is taken into account. Other force components, added mass, damping and diffraction forces are taken from the frequency domain calculations. The main equation solved in this program is the Cummings equation of motion [5] shown in Equation (2.4). The infinite frequency values for the added mass and damping are calculated in the frequency domain in HYDROSTAR. The retardation functions are calculated using extrapolated damping curves and the total force is composed of the following elements: Hydrodynamic wave excitation and restoring force, diffraction force, radiation force, gravity acceleration force and the slamming force. The equation of motion is solved using a fourth order Runge-Kutta integration scheme.

$$
\begin{aligned}
&(\mathbf{A}(\infty) + \mathbf{m}) \cdot \ddot{\bar{\zeta}} + \mathbf{B}(\infty) \cdot \dot{\bar{\zeta}} + \int_{-\infty}^{t} \mathbf{K}(t-\tau) \cdot \dot{\bar{\zeta}}(\tau) d\tau = \bar{f}_t \\
&\bar{f}_t = \bar{f}_h(\bar{\zeta}, t) + \bar{f}_d(\bar{\zeta}, t) + \bar{f}_{rd}(\bar{\zeta}, t) + \bar{f}_g(\bar{\zeta}) + \bar{f}_s(\bar{\zeta}, t)
\end{aligned} \tag{2.4}
$$

Where:

$\bar{\zeta}$	Modal amplitude
A	Added mass
m	Modal mass matrix
B	Damping
K	Retardation function
$\bar{f}_t$	Total force
$\bar{f}_h(\bar{\zeta}, t)$	Hydrodynamic wave excitation and restoring force
$\bar{f}_d(\bar{\zeta}, t)$	Diffraction force
$\bar{f}_{rd}(\bar{\zeta}, t)$	Viscous roll damping force
$\bar{f}_g(\bar{\zeta})$	Force due to gravity acceleration
$\bar{f}_s(\bar{\zeta}, t)$	Slamming force

Generating structural load cases

Structural load cases are generated by post-processing the seakeeping results. The loads can be derived for all time steps in the seakeeping simulation, but the interest lies in the intervals with the most extreme loading occurs. By selecting the intervals of most extreme loading the computational effort to calculate the load cases is reduced. The program MARGENL is used to calculate the load cases to be used in the FEA program VAST. The loads are derived using the seakeeping calculations. The total nodal force is constructed using the force components shown in Equations (2.5) and (2.6).

$$
\bar{f}_t^n = \bar{f}_d^n(\bar{\zeta}, t) + \bar{f}_r^n(\dot{\bar{\zeta}}, t) + \bar{f}_{A(\infty)}^n(\ddot{\bar{\zeta}}, t) + \bar{f}_h^n(\bar{\zeta}, t) + \bar{f}_s^n(\bar{\zeta}, t) + \bar{f}_a^n(\bar{\zeta}, t) \tag{2.5}
$$

$$
\bar{f}_a^n(\bar{\zeta}, t) = m^n(\bar{a}_l + \bar{g}) \tag{2.6}
$$

Where:

n	Indicates the node
m	Nodal mass
a	Accelerations in body system at node
g	Gravity acceleration vector in body system
$\bar{f}_t$	Total nodal force vector
$\bar{f}_d(\bar{\zeta}, t)$	Diffraction force vector
$\bar{f}_r(\bar{\zeta}, t)$	Frequency dependent radiation force vector
$\bar{f}_{A(\infty)}(\bar{\zeta}, t)$	Frequency independent radiation force vector
$\bar{f}_h(\bar{\zeta})$	Hydrodynamic wave excitation and restoring force vector
$\bar{f}_s(\bar{\zeta}, t)$	Slamming force vector
$\bar{f}_a^n(\bar{\zeta}, t)$	Nodal acceleration force vector

A further derivation of the individual force components can be found in [20] and [23]. The total nodal hydrodynamical and acceleration forces are combined to form the load cases to be used in a (quasi) static FEM analysis for each individual time step.

2.3 Input

This section describes the input values and models used for the seakeeping simulations.

Hydrodynamic properties
DMO provided TNO with a model of the hull lines of the Hr.Ms Mercuur in PIAS format. Together with the model, DMO provided the hydrodynamic properties of the Mercuur as listed in Table 2.1.

Table 2.1: Hydrodynamic properties of the Zr.Ms. Mercuur

L	64.8	$[m]$
B	12.0	$[m]$
T_{aft}	4.67	$[m]$
T_{fore}	4.06	$[m]$
∇	1496	$[t]$
LCG	26.25	$[m]$
VCG	5.23	$[m]$
GM	1.19	$[m]$
K_{xx}	4.8	$[m]$
K_{yy}	15.0	$[m]$
K_{zz}	15.0	$[m]$
$B_{lin}^{U=0}$	6.24E+5	$[Nms/rad]$
$B_{quad}^{U=0}$	7.6E+5	$[Nms^2/rad^2]$
$B_{lin}^{U\neq0}$	6.38E+5	$[Nms/rad]$
$B_{quad}^{U\neq0}$	-5.91E+4	$[Nms^2/rad^2]$

Meshes
The first mesh used is the hydrodynamical mesh, shown including the slamming sections at the bow in Figure 2.3. Note that for the BVP only the wetted part of the hull in still water is used. This BEM mesh is used to solve the BVP and construct the response in frequency domain and to obtain the linear hydrodynamic coefficients used in the time domain analyses. The mesh including the non-wetted panels and the slamming sections is used also in the time domain seakeeping calculations.

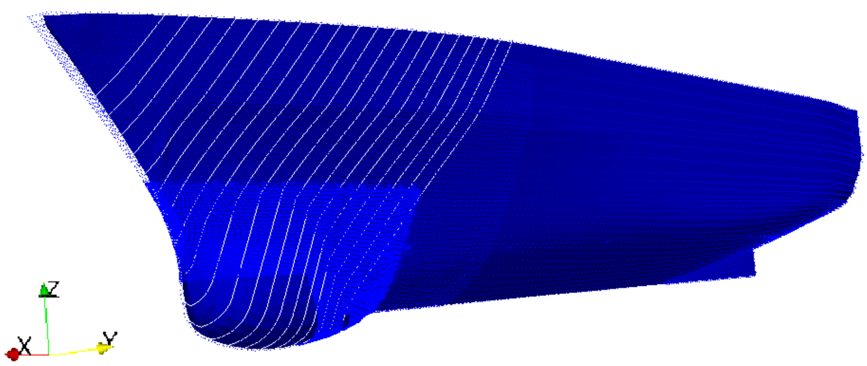

Figure 2.3: Hydrodynamic mesh of Zr.Ms. Mercuur

The second mesh used within the hydrodynamic analysis, is the wetted part of the structural mesh. This mesh contains a sub-model of the real structure, since only the forward part of the vessel is modelled within the structural model. This mesh contains of the elements of the structural model at the outer hull and weather deck, and all nodes of the structural mesh including all nodal masses. The hydrodynamical and structural mesh describe the same geometry, but the meshes are very different due to the differences in mesh requirements between the intended seakeeping and FEM calculations.

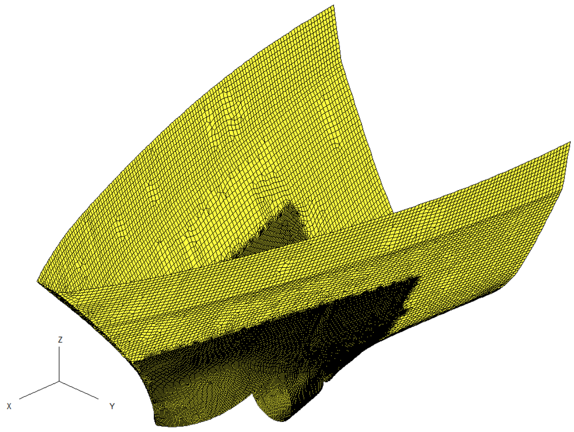

Figure 2.4: Structural sub-mesh to calculate seakeeping loads

The last mesh to be defined is the integration mesh. This mesh is used to be able to transform the pressure loads from the BVP to modal or sectional loads within the program. In this analysis a copy of the hydrodynamic mesh is cut at a number of sections in order to obtain sectional forces at these locations, and this mesh is used as integration mesh. The integration consist of evaluating the pressure at each panel using the "Gaus quadrature" to obtain the contributions of the panel load on the nodal forces at the panel.

Structural properties
Within the seakeeping analysis the structural model is assumed to be rigid. Therefore the results consist only the 6 modes described by the 6 degrees of freedom of the vessel to describe the displacements.

Seakeeping condition parameters
A number of parameters are defined simulate a seakeeping condition. These parameters are:

- Speed, V
- Heading, ϕ
- Wave height, $H_{1/3}$
- Wave period, T_p
- Wave peakiness factor, γ

2.4 Results

Using different input parameters the vessels response is simulated for a number of cases. Use is made of the relations between total slamming force, wave height and wave period derived in [21]. From the seakeeping simulations the following output is stored:

- Wave realization info
- Ship motions (Frequency RAOs and time domain results)
- Slam and sectional forces
- Nodal forces on FE models

From the seakeeping results one simulations of $300s$ is selected to be used as load case throughout this study. The parameters used are listed in Table 2.2. The first $30s$ of the simulation will not be used in the analysis due to initialization effects.

Table 2.2: Concerned seakeeping conditions

V	5	$[knts]$
ϕ	180	$[deg]$
$H_{1/3}$	10	$[m]$
T_p	10.3	$[t]$
γ	3.3	$[-]$

Using the frequency response from the linear seakeeping results, the global response can be reflected upon. In head waves largest expected motions are in heave and pitch direction. In Appendix C in Figure C.1 the RAO is plotted for the heave and pitch motions. The heave motion RAO is close to one up to a wave frequency of $1rad/s$. However the pitch RAO show a clear maximum around a wave period of $0.9rad/s$. Using the wave spectrum peak period and the vessel speed, the encounter frequency is calculated according Equations (2.1). This results in a peak encounter frequency of $1.05rad/s$. Using this method and Equation (2.7) the mean wave frequency is calculated to be $0.72rad/s$ for a wave spectrum with a peakiness factor of, $\gamma = 3.3$. This range corresponds with the peak of the pitch RAO. This verifies that a condition is chosen where large pitch motions occur.

$$T_z = \frac{4 * T_p^4}{5\pi}^{\frac{1}{4}} \tag{2.7}$$

In Figure C.2 the total slam force at the bow section is shown. Based on this result one slamming event is selected. To include the wave and acceleration loading during the slamming event the time range of the event is chosen from $114s$ to $120s$ resulting in a load case of 6 seconds.
In Appendix C, Figure C.5, the acceleration level at the centre of the are plotted. From the whole time trace one could observe that slamming loads and vertical accelerations are related using a rigid body. However, a high peak in the accelerations does not always corresponds to a high peak in the slamming loads.
The selected slamming event is based on the highest loading which is found in 5 realisations of 300 seconds simulation each. The slamming force at a part of the bow section is calculated to compare the maximum values for each slamming event. Through the data points of the maximum slam force for each slamming event a Weibull fit is made. The results are shown in figure 2.5. The top figure shows the distribution of the slamming force on Weibull paper, the bottom figure shows the probability of exceedance of a certain slam force. Of interest are the highest peaks in the distribution, normally the Weibull fit is extrapolated to the desired level of exceedance. Based on the peaks, two fits are made, one with the total dataset, the purple line and one with only the highest 10% of the slams. From the figures is observed that extrapolating the Weibull fit for the whole dataset clearly underestimates the probability of exceedance for higher slamming amplitudes.

It is concluded that the probability of exceedance does not drop quickly for large values of the slam force. So one could expect higher slam forces when performing more seakeeping simulations.

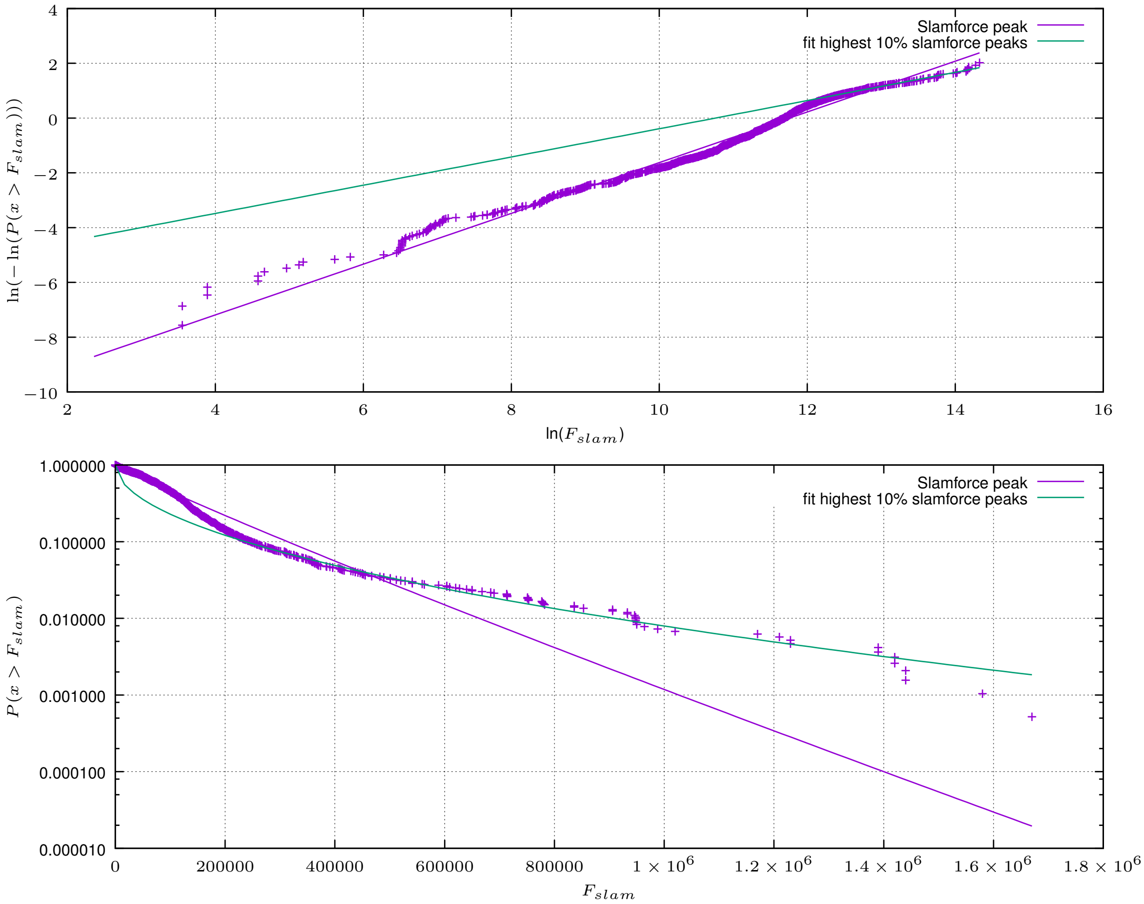

Figure 2.5: Weibull fit of maximum slam forces

3 Structural analysis methods

The structural response can be described by deformations, velocities, accelerations, strains and stresses depending on the type of analysis.
Within the structural analysis two domains can be described. The (quasi) static domain (independent of time) and the dynamic domain (time dependent). A load in the (quasi) static domain can be described as a load that varies very slowly compared to the structures natural periods. A load in the dynamic domain varies quickly in time, where quickly is defined relative to the structures ability to react to this load.
In [13] the behaviour of panels under impact pressure is grouped into three domains based on the ratio between the duration of the load τ and the relevant natural frequency of the considered structure T.

- Quasi-static domain when $3 \leq \tau/T$
- Dynamic domain when $0.3 \leq \tau/T < 3$
- Impulsive domain when $\tau/T < 0.3$

(Quasi) Static Analysis
The (quasi) static analysis is preformed using a FE program. When constant global inertial forces are incorporated in the loading one can speak of an quasi-static analysis. Within this analysis, at each time step a static calculation is performed. The governing equation solved in this analysis is Equation (3.1). For different loading conditions in time, load cases will be generated. These load cases will be solved independently.

$$\mathbf{K}\bar{\delta} = \bar{f} \tag{3.1}$$

Where:

$\mathbf{K}$	Structural Stiffness matrix
$\bar{\delta}$	Nodal displacements
$\bar{f}$	Nodal forces

Displacements
The displacements are the first order nodal quantity to be calculated in the analysis. The nodal displacements are solved by inverting the stiffness matrix and to multiply it with the nodal force matrix. This is illustrated by Equation (3.2).

$$\bar{\delta} = \mathbf{K}^{-1}\bar{f} \tag{3.2}$$

Stress and strains
A second order quantity of the solution are the element strains and stresses. For this step the already obtained nodal displacements are evaluated using the element shape functions to obtain the displacements at every location within the elements. This results is multiplied with a matrix consisting of differential operators on the displacements to obtain the strain tensor. The differential operators are based on the strain-displacement relationships. The stresses are calculated from the strains using 'Hooke's Law'. The governing equation is given in Equation 3.3.

$$\begin{aligned} \sigma &= S\epsilon \\ \epsilon &= \mathbf{DN}\bar{\delta} \end{aligned} \tag{3.3}$$

Where:

σ	Stress tensor
ϵ	Strain tensor
S	Stress strain relationship matrix based on Hooke's law
D	Matrix with differential operators to transform displacements to strains
N	Matrix with element shape functions to describe displacement within elements

Dynamic Analysis
The method used to calculate the dynamic response is a time domain analysis. The governing equations is given in Equation (3.4)

$$(\mathbf{M})\ddot{\bar{\delta}} + \mathbf{C}\dot{\bar{\delta}} + (\mathbf{K})\bar{\delta} = \bar{f}(t) \tag{3.4}$$

Where:

K	Structural Stiffness matrix
$\bar{\delta}$	Nodal displacements
$f\bar{(t)}$	forces
C	Structural damping matrix
M	Structural mass matrix

The problem can be solved using a modal superposition method or by direct integration. The modal superposition requires the natural frequencies and mode shapes obtained by an eigenvalue analysis of the system shown in Equation (3.4) for $\bar{f}_t = 0$. However, this method requires to calculate the full mass and stiffness matrices an its inverse. Thereby has the fluid material model in FEM no shear strength which makes it difficult to derive the natural frequencies.
Proposed is to use the direct integration method, which makes use of the direct calculation of all contributions by integrating the accelerations and velocities. The governing equation used is the momentum equation. The procedure is further described in Section 3.3. The mass and stiffness have only to be determined on element level, avoiding the expensive matrix inversion procedure. However, the time step is limited by the element size, and is related by the time it takes for sound waves in the material to travel within one element and the number of integration points within the elements used to assure stability.

Failure modes for stiffened panels
Once the results with respect to displacements, stresses and strains are derived these have to be analysed to determine whether this state can results in failure of the structure. A stress above the yield strength of the material will result in plasticity, redistributing the load over the structure. The yield strength could be used as criteria to determine when the structure fails. However failure could be very locally in a point that is not critical for the overall structure.
In ship-structures one could focus on the collapse of a stiffened panel. In [13] the following types of structural failure of stiffened panels are identified:

- Collapse mode I: Overall collapse of the plating and stiffeners as a unit, global buckling
- Collapse mode II: Biaxial compressive collapse without failure of the stiffeners, local plate failure
- Collapse mode III: Beam-column type collapse
- Collapse mode IV: Local buckling of the stiffener web (after the inception of the buckling collapse of the plating between the stiffeners)
- Collapse mode V: Flexural-torsional buckling or tripping of the stiffeners

- Collapse mode VI: Gross yielding

However, assessing the collapse of stiffened panels includes the post yielding behaviour of the structure resulting in a non-linear elastic-plastic structural analysis and possibly a non-linear buckling analysis as well. On the other hand, a yield criteria can be directly compared with the stresses from the linear structural analysis.

3.1 Programs

TRIDENT/VAST is an advanced finite element analysis software package for naval architecture and marine engineering applications, which consists of a graphical user interface (GUI) program and a finite element solver [16]. The program TRIDENT/VAST is based on an implicit solver. Making the program suitable to preform large (quasi) static simulations.

The dynamic response of the sonar dome is investigated using the program LS-DYNA. LS-DYNA is an advanced general-purpose multi-physics simulation software package. The code's origins lie in highly non-linear, transient dynamic finite element analysis using explicit time integration [15].

3.2 TRIDENT/VAST

3.2.1 Input

The input for the FE solver VAST consist of the structural mesh, loading file, boundary condition file, nodal mass file and an execution file controlling the calculations progress.

Mesh

Figure 3.1 shows the FE-model of the bow structure of the Zr.Ms. Mercuur. The model consists of in total 196,279 nodes and 164,857 elements. Figure 3.1 shows a darker area around the sonar dome indicating the area where a reduced element size is used for the mesh in order to calculate the local stress peaks more accurately. All hull panels, web frames, decks and stiffeners are modelled using shell elements. A number of brackets connecting stiffeners with the decks are modelled using stiffened shell elements, which allow to give panels an offset. On the free edge of these brackets, beam elements are modelled with a close to zero stiffness in order to obtain the axial strain along this edge more accurately, this are so called numerical strain gauges.

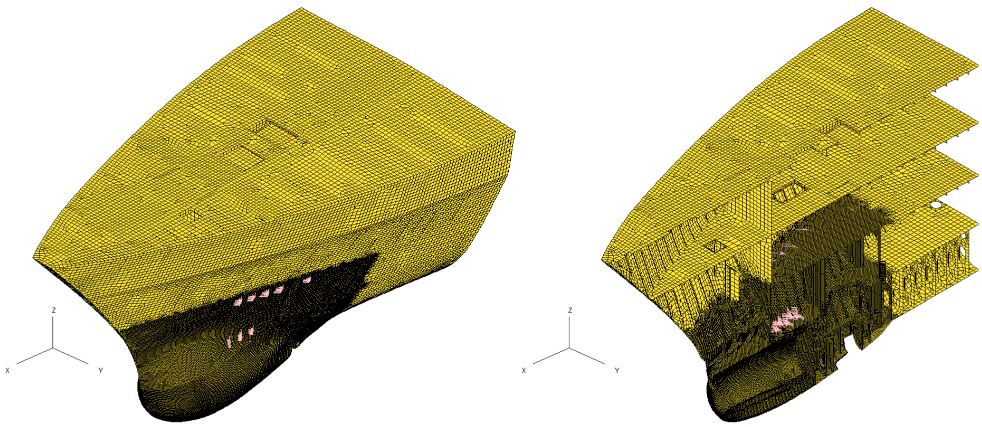

Figure 3.1: FE-model of the bow structure of Zr.Ms. Mercuur

Loads
The loads for the structural model are determined by post processing the seakeeping results as described in Section 2.2. The loads are already written in an input file by the program MARGENL which can be directly read into the finite element solver, VAST.

Boundary conditions
Figure 3.2 shows the mesh of the Zr.Ms. Mercuur with the applied boundary conditions. All nodes at the end of the bow section are fixed in all translational and rotational degrees of freedom. This support is in reality too stiff, since the remaining part of the vessel will deform in reality. This may result in element loads that will be overestimated close to the boundary conditions. However the interest lies in the local deformations and stresses at the bow and these results seem to be not influenced by the applied boundary conditions. This is validated by comparing the model with a varying stiffness of the boundary conditions. The stiffness of the boundary conditions is reduced by a factor 10 in the input files. This resulted in a difference in total displacement of less than 0.01% for the node located at the foremost part of the bow. In the stress at the knees and stiffeners above the sonar dome, no significant differences are observed.

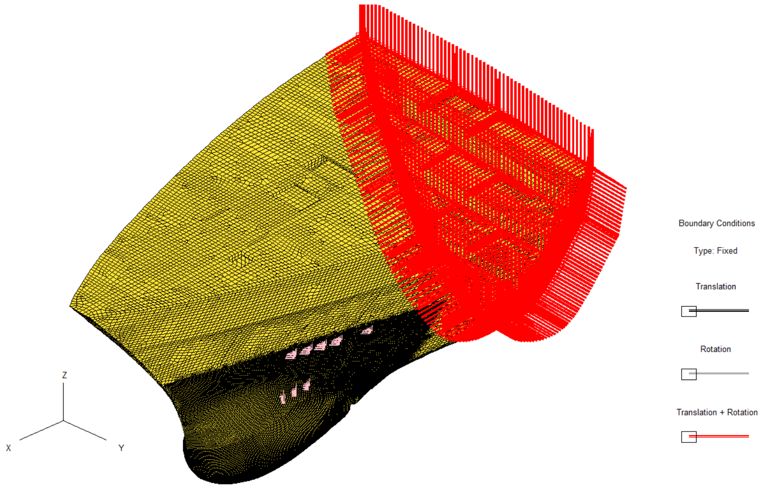

Figure 3.2: Boundary conditions at the FE-model of the bow structure of Zr.Ms. Mercuur

3.2.2 *Output*

The following results are obtained for each load case by performing the FE analysis:

- Nodal displacements
- Element stress and strain components

These results will be used to relate the characteristics of the slamming event obtained from the seakeeping analysis to the occurring structural response.

3.3 LS-DYNA

The explicit formulation refers to the numerical method used to represent and solve the time derivatives in the momentum equations. For a given state, the displacement at all nodes at time level t are known. A system of explicit algebraic equations are written for all the nodes in the mesh at time level $t + \Delta t$. Each equation is solved in-turn for the unknown nodal displacements. This method is computational fast but only conditionally stable. The time step, t, must be less than the length of time it

takes a signal travelling at the speed of sound in the material to traverse the distance between the nodes. Which implies that large differences in mesh size in the model would affect the calculation time step significantly
The governing equation for a certain state, indicated by the superscript n is given in Equation (3.5). This is the Lagrangian formulation of the momentum equation containing the equation within the body and the equation of momentum on the body contour [3].

$$\begin{cases} \rho \ddot{x}^n = \nabla \sigma^n + f^n_{ext} & \text{on body } \Omega \\ \sigma^n \cdot n = p & \text{on body countour } \delta\Omega \end{cases} \tag{3.5}$$

Where:

ρ	Material density
$\ddot{x}$	Acceleration vector
$\nabla\sigma$	Stress divergence or traction vector
f_{ext}	External force vector
n	Surface normal vector
p	Surface pressure

Equation (3.5) can be multiplied with and displacement vector, and integrated over the body and body contour. This yields in an equation which states the principle of virtual work.

$$\begin{aligned} &\int\limits_{\Omega} \rho \ddot{x}^n N_i dx = -\int\limits_{\Omega} \sigma^n \nabla N_i dx + \int\limits_{\Omega} f^n_{ext} N_i dx + \int\limits_{\delta\Omega} p^n N_i dx \\ &M\ddot{x}^n = -F^n_{int} + F_{ext} \\ &\text{With:} \\ &M\ddot{x}^n = \int\limits_{\Omega} \rho \ddot{x}^n N_i dx \\ &F^n_{int} = \int\limits_{\Omega} \sigma^n \nabla N_i dx \\ &F_{ext} = \int\limits_{\Omega} f^n_{ext} N_i dx + \int\limits_{\delta\Omega} p^n N_i dx \end{aligned} \tag{3.6}$$

The accelerations are place and time dependent. By introducing the discretized vector for the displacement the accelerations can be written as in Equation (3.7). With this formulation of the accelerations, the mass matrix can be derived.

$$\begin{aligned} \ddot{x}^n(x,t) &= \sum_j \ddot{x}^n(t) \cdot N_i(x) \\ M &= \int\limits_{\Omega} \rho N_j \cdot N_j dx \end{aligned} \tag{3.7}$$

Using this result the accelerations can be solved using Equation 3.8

$$\ddot{x}^n = (F^n_{ext} - F^n_{int}) M^{-1} \tag{3.8}$$

One could notice that here the dynamic problem is solved with a weak formulation. In this formulation the total stiffness matrix will not be calculated. The structural stiffness will only be evaluated on element level to calculate the internal forces. This results in that the time step used will be related to the natural frequency of a single element which is determined by the sound of speed trough the element. Also the integration method used will affect this time step.

Input
The input used for the dynamic simulations in LS-DYNA consist of a structural mesh of the dome. Material definitions, boundary conditions and time dependent load curves. The exact details of the input is dependent on the simulations and will be described in Chapter 4.

Output
As result from the simulations, time dependent output is generated. Used is the nodal displacements, the element pressures evaluation, the boundary reaction forces, total energy evaluation and stresses in the shell elements.

4 Dynamic analysis sonar dome

The goal of modelling the sonar dome is to gain insight in the forces, bending moments and pressures introduced into the hull structure by the response of the sonar dome. Expected are time dependent values for different load components at the boundary between the dome and the steel hull. A model of the dome is generated to study the effects of the internal fluid. The hydrodynamic model, describing outer geometry is available, which is used as basis to model the outer composite shell of the dome. To be able to compare and validate the results a comparison of the global response will be made with previous studies performed on the sonar domes of the M-frigates. A visit to the current builder of the sonar domes, Marinebedrijf Den Helder, confirmed that the dome originates from the same mould. The only difference in the dome structure is that the dome of the Mercuur is somewhat shortened by placing the most aft ward bulkhead more forward.

2D dome model
From the sonar dome, a cross-section is taken to set up a 2D model. This simplified 2D model is created to study the behaviour of a fluid filled shell structure. Using this model the material properties and different calculation settings for LS-DYNA are studied.

3D dome model
Based on the geometry of the hydrodynamic model of the vessel a 3D model of the dome is made. Using this geometry a mesh is created with shell elements at the outside, and solid element at the interior to simulate the fluid.
The sonar dome is connected to the ship structure at the top-side by a large flange using a bolt connection. This connection is, in the current models, made by merging the nodes at the steel hull flange and composite dome flange. In the dynamic simulations the details of this connections are avoided and not modelled. For the current research of interest are the total load components at the whole interface and the spatial distribution of these loads, not the individual stress concentrations at the flange details.
The 3D model will be compared with previous calculations performed without internal fluid to check whether the global stiffness and response of the composite shell is comparable. Differences in the response are expected since the dome considered in this research is shorter compared to the dome in the previous analysis.
Using the model with and without fluid, the response to different load components will be investigated. Loads considered are: slamming loads, wave loads and acceleration loads. The resulting displacements, internal pressures and total loads at the boundary conditions is studied for each load.

Water management system
A property which has to be included in the model is the water management system of the sonar dome. This system consist of an expansion container and an expansion pipe controlling the pressure inside the sonar dome. A survey at the Zr.Ms. Mercuur provided more insight in the system and its dimensions. It was observed that a scale is fitted on the expansion container indicating the fluid level. The experience of the crew is that no large differences on the scale could be observed during heavy seakeeping conditions. Since the vessel and fluid in the container is already moving due to the vessel motions. However at least it is confirmed that the total container of 50 litres will not drain fully, or that fluid flows out at the top.

Seakeeping loads
Using a load case based on the seakeeping simulations, the response of the dome is calculated. The results are post processed to derive the pressure at deck K and the total force at the flange connections.

Comparison with (quasi) static methods
In previous studies on the response of the sonar dome a (quasi) static method has been used. The results form the dynamic simulations will be compared.

4.1 2D dome model

The first geometry studied is a simplified 2D representation of a sonar dome cross-section. The geometry and mesh used is shown in Figure 4.1.

Geometry
The geometry created is a rectangular box of $3m$ by $1.5m$ with on de lower side a half circle with a radius of $1.5m$. The created surface is extruded over $0.1m$ to generate a volume, as LS-DYNA is mainly a 3D code.

Mesh
The volume is meshed using tetrahedron elements. In the interior solid elements are created. The outer contour consist of shell elements.

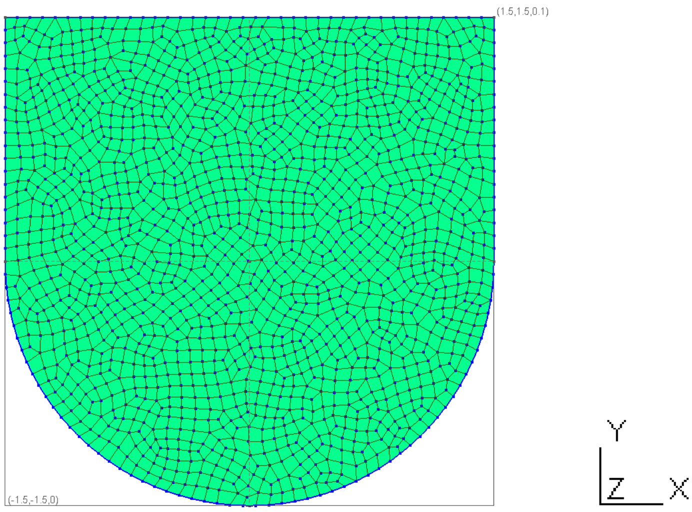

Figure 4.1: 2D model of a sonar dome cross-section and internal fluid

Load and boundary conditions
The model is fully clamped at the top, representing the steel hull structure. All other nodes are restricted in z-direction to invoke a response in only x and y direction. The rotations are restricted about the x- and y-axis. A sub-selection of the contour shell elements is selected to be loaded with a pressure pulse. The load vectors are graphically shown in Figure 4.2.

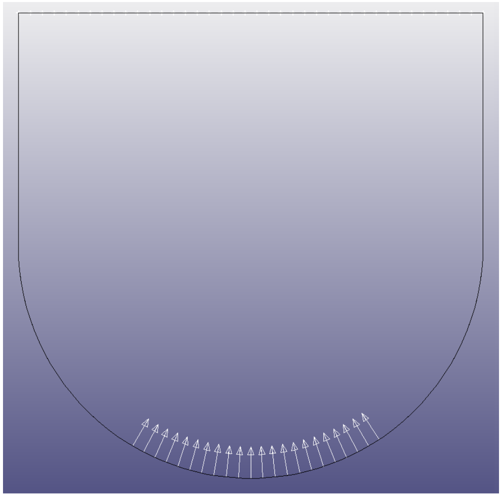

Figure 4.2: Load at the 2D dome model

Elements
The model is build up of a combination of solid and shell elements. In the interior solid elements are created using solid element formulation 1 of LS-DYNA, which is a 8-node constant stress solid element. The outer contour consist of 4-node shell elements using shell element formulation 16 of LS-DYNA [4]. The shell element is a fully integrated shell formulation based on the Reissner-Mindlin kinematic assumption. Which can be related to the Kirchhoff-Love assumptions including shear. The reason for this formulation is that it is able to control the warping stiffness to prevent hourglassing effects which may occur when using the default under integrated elements within LS-DYNA.

Shell
The shell elements represent the composite material on the outer contour. The material parameters used are listed in Table 4.1

Table 4.1: Material parameters composite shell elements

Thickness t	0.032	$[m]$
Density ρ	2600	$[kg/m^{-3}]$
Modulus of elasticity E	17	$[GPa]$
Poisson ratio p	0.3	$[\nu]$

Solid
The solid elements represent the fluid elements in the interior of the dome. In the model different material models for the fluid are compared. The following two cases are compared:

- Material using Grüneisen Equation Of State (EOS)
- Material using only the fluid bulk modulus

The material using the Grüneisen EOS is modelled using the `Mat_Null` material formulation from LS-DYNA together with the definition of the EOS parameters. The formulation of the EOS is given in derived from [17]. The EOS describes the relation between the deviatoric stresses an pressures for the fluid material. The parameters used for the EOS are derived from numerical models to model underwater shock waves [1]. The values used for the `Mat_null` and EOS models are listed in Table

4.2 and 4.3. The model using only the material bulk modulus is created by using the `Mat_Elastic_Fluid` formulation from LS-DYNA. One should note that the cavitation pressure is reduced to -1.5 time the atmospheric pressure to account for the constant pressure head resulting from the overflow piped which is fitted to approximately $5m$ above the sonar dome.

Table 4.2: Parameters LS-DYNA Mat_null material formulation

Mass density ρ	1005.0	$[kgm^{-3}]$
Cavitation pressure cut-off PC	-150 000	$[Pa]$

Table 4.3: Parameters LS-DYNA EOS model

C_0	1005.0
S_1	2.5599999
S_2	-1.980
S_3	0.22679
γ_0	0.5

The last model uses only the bulk modulus of the material. For this the `Mat_Elastic_Fluid` material model is used. The parameters used are listed in Table 4.4.

Table 4.4: Parameters LS-DYNA Mat_Elastic_Fluid material formulation

Density ρ	1005.0	$[kg/m^3]$
Bulk modulus k	2.1830E+9	$[Pa]$
Cut-off pressure cp	-150 000	$[Pa]$

Results
The response of the dome is investigated by defining 3 cases. The first case is the model without the fluid elements. The second model is the model including the internal fluid with the Grüneisen EOS which is assumed to be the most detailed description of the fluid. The third model uses the elastic fluid formulation. On these three models a pressure pulse is applied at $t = 1.0s$ with a duration of $\Delta T = 0.1s$ and an amplitude of $P = 0.1bar$.

Deformations
The first quantity investigated is the deformation of the model. Figure 4.3 shows the deformed shape of the model including the fluid with EOS during the pressure pulse loading. The images shown are respectively the undeformed configuration, and the two maximum deformations where the model oscillates in between. In order to compare the models, one node is selected. This node is located at the bottom of the model on the centreline, and is referred to as node 122 in the next sections. It is expected that the node will show a vertical oscillating motion in the y-direction after the pressure load is applied. The displacement in time is shown for all three cases in Figure 4.4. From this plot can be seen that the presence of the fluid significantly reduces the response amplitude and frequency. The two models for the fluid elements, the Grüneisen EOS and the linear EOS containing only the bulk modulus result in these cases in almost the same results, the two lines in Figure 4.4 overlap.

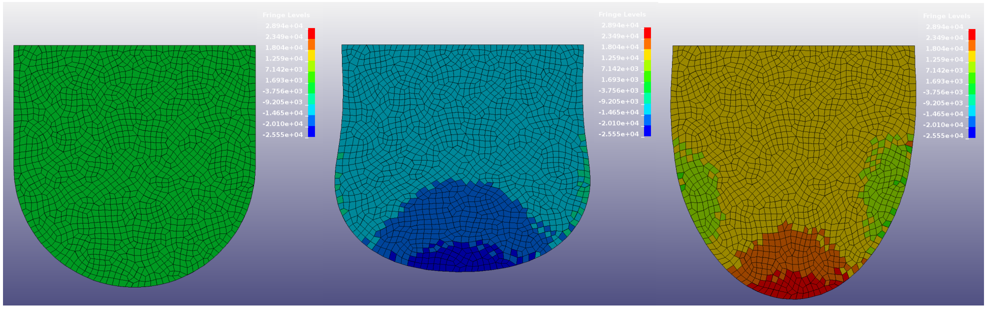

Figure 4.3: Left: Undeformed model, middle: maximum deformation, right: minimum deformation

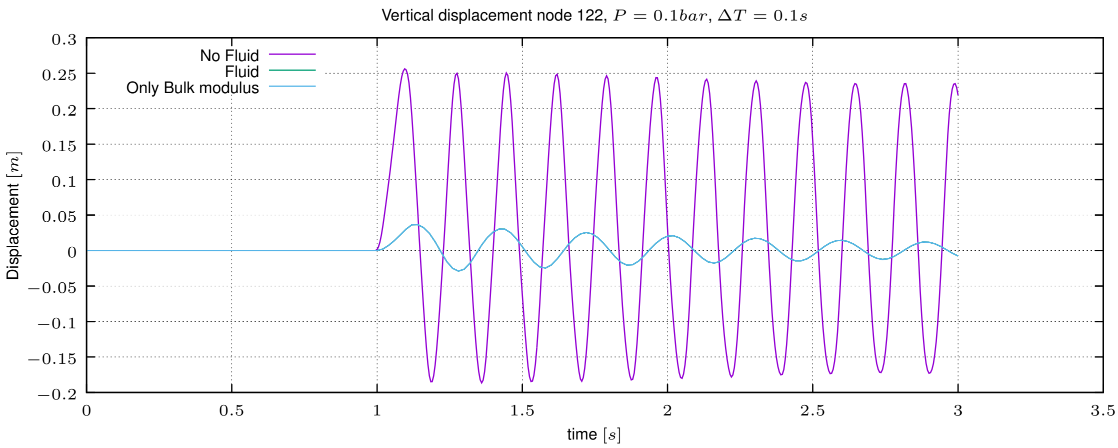

Figure 4.4: Vertical displacement node 122, effect internal fluid on 2D dome model

Effect fluid model

As mentioned in the previous section, the use of two different fluid models seem to have the same result. This effect is investigated in some more detail. The pressure load is increased to $1.0bar$ to see whether this introduces larger differences between the two models. A plot of the displacement results for a load case with a 1.0 bar pressure pulse with a duration of $\Delta T = 0.s$ shown in Figure 4.5. It shows a small growing difference between the methods in time, however for especially the first cycles the difference is not significant. From these calculations is concluded that the Grüneisen EOS, which includes which is optimized to capture shock waves is not necessary to model the sonar dome response accurately. The model using only the fluid bulk modulus will be used for all calculations.

Effect load amplitude

This section investigates the effect of the load amplitude on the simplified model to study whether the response is highly non linear. Figure 4.6 shows the load to three different pressure pulse amplitudes. The durations of the pressure pulse is $\Delta T = 0.1s$ for all three cases. From Figure 4.6 can be observed that the response is not fully linear, and that the relative response decreases with increasing amplitudes.

Unstable model behaviour

During the first simulations unstable behaviour in the response is observed when applying higher loads. This effect could clearly been observed in the pressure response. Figure 4.7 shows the internal pressure in time. One should note that the external pressure load is applied from $t = 1.0$ till $t = 1.1$, and that the pressure shows

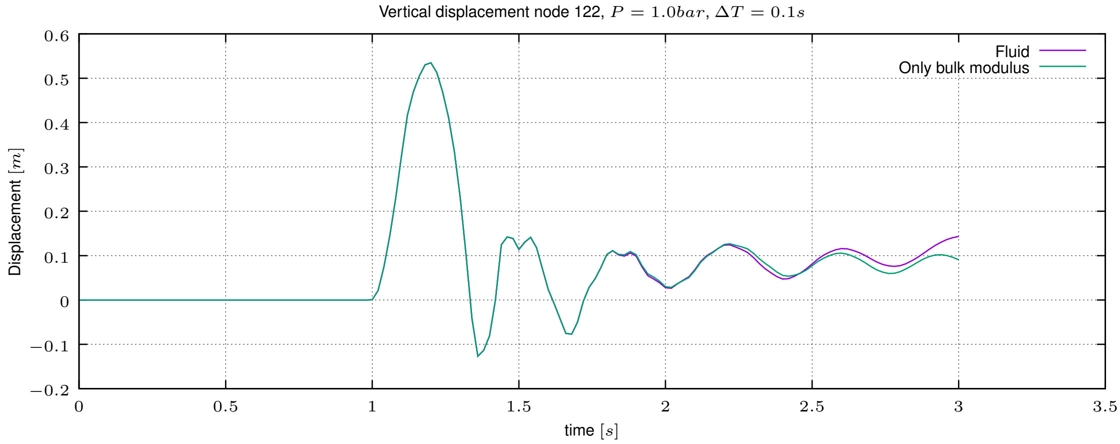

Figure 4.5: Vertical displacement node 122, comparison EOS fluid model with linear bulk modulus

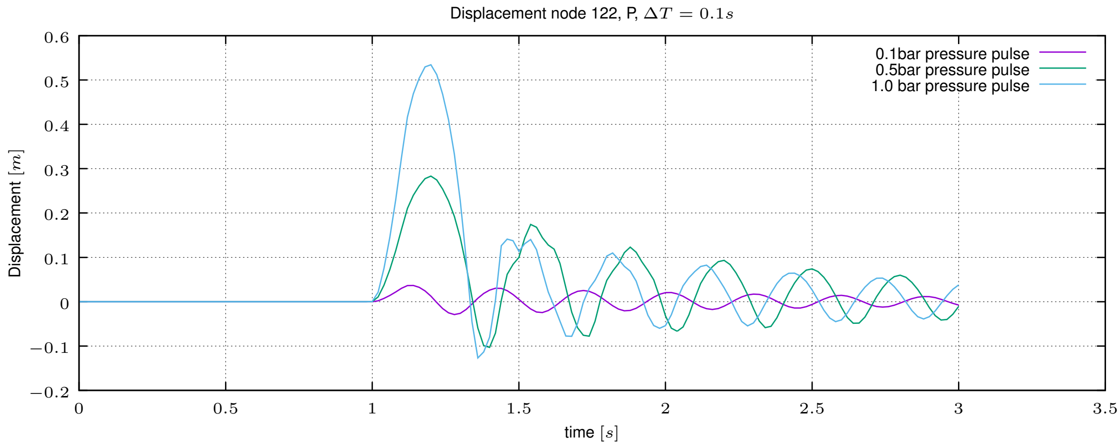

Figure 4.6: Displacement response of 2D dome model to $0.1bar$, $0.5bar$ and $1.0bar$ pressure pulse load

a significant increase around $t = 1.4$ which is a order higher with respect to the applied external pressure load. Figure 4.6 shows the displacements of the bottom node for three different loads. The instability is not that obvious compared to the pressure response. However distortions in the response are observed.
Since the problem is expected to be stable for all loads, the models an parameters used are studied in great detail. One of the aspects investigated is the geometry of the 2D model. The so far introduced model has vertical sides of $1.5m$. These sides show buckling behaviour due to the loading, which can be observed in Figure 4.3, the dome in the middle of the figure shows inward buckling of the side shell, and the right hand figure shows the outward buckling of the shell. In order to investigate this effect a new mesh is generated where the height of the vertical shell part is reduced to $0.5m$, the resulting mesh in shown in Figure 4.8. Using the new mesh a new model is created using an ALE formulation for the fluid to check whether this problem is mesh dependent. This method updates the fluid mesh using transport terms to ensure a smooth mesh for every calculation and avoids large deformations in individual elements. The results for the new mesh, loaded with a load pulse of $1.0bar$ with a duration of $\Delta T = 0.1s$ are shown in Appendix D. In Figure D.1 is observed that the new mesh reduces the response significantly for the original Lagrangian fluid formulation as well as for the ALE formulation. This can be expected as the reduction in height result in a less slender structure for the dome shell. The main difference

observed between the ALE and Lagrangian formulation is that the ALE formulation results in a lot more numerical damping. However looking at the pressure response in Figure D.2 for both models, the unstable and non-physical pressures are not avoided using this method.
A solution for the instability problem is not found. However, the following practical working solution is used. The instability may result from the large deformations found in the response of the 2D structure. The 2D model is less stiff compared with the 'real' 3D geometry. Introducing additional stiffness in the shell elements avoids the instability problem.

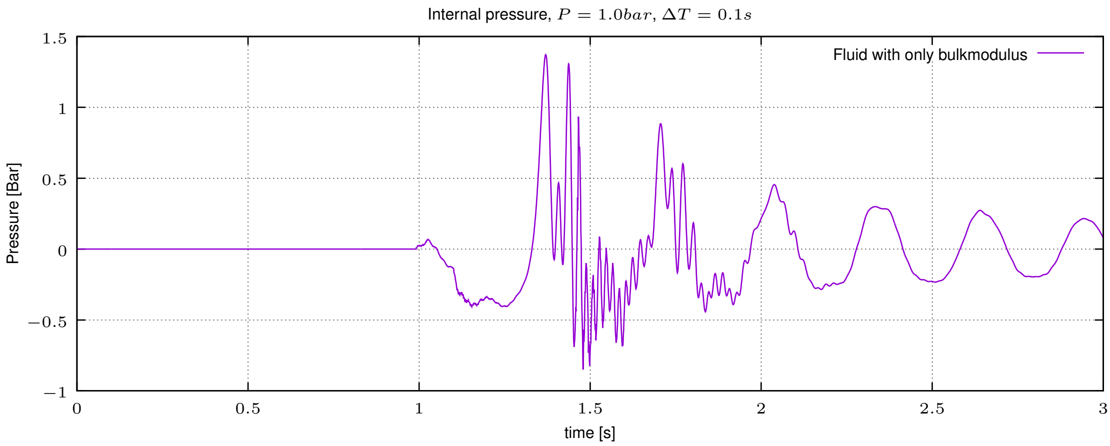

Figure 4.7: Internal pressure response showing unstable 2D dome model behaviour

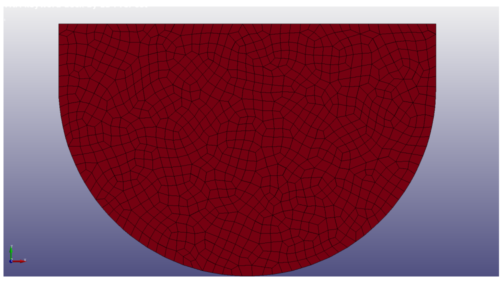

Figure 4.8: 2D Dome model with reduced height of vertical sides

4.1.1 *Dome with increased stiffness*

In the first analysis of the fluid filled dome there was a large difference in relative mass and stiffness of the 2D model. In the cases presented in the section the stiffness is modified to produce more realistic response amplitudes. The vertical displacement of the bottom node of the 2D model is taken as reference. For this location the vertical displacement for a static load case is calculated in [12] and is about $19mm$ with a loading amplitude of $5bar$ at the bottom of the dome. The stiffness of the shell of the 2D dome is modified such that the vertical displacement of the bottom node is close to $19mm$. After this the fluid properties are included and the results for both cases are compared.
Figure 4.9 shows the vertical displacement of the bottom node for the model with increased shell stiffness. It can be observed that the presence of the fluid increases the dynamic and static response amplitude. However due to the relative stiff shell static results show almost no difference indicating that most of the loading is in the

composite shell and not in the fluid.

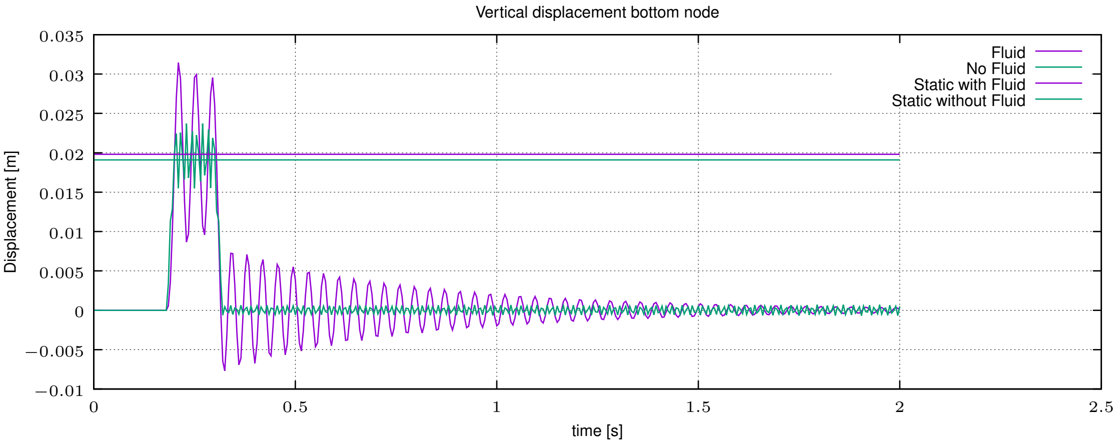

Figure 4.9: Vertical displacement bottom node with and without fluid for 2D dome with increased stiffness

The pressure inside the dome is shown for an element in the centre of the model and for one close to the shell where the load is applied in Figure 4.10. A pressure cut-off is used in the material model to simulate the vapour pressure at -1.5 bar ($1bar$ atmosphere + $5m$ head). This cut-off pressure is reached more close to the shells. This will result in additional damping in the model.

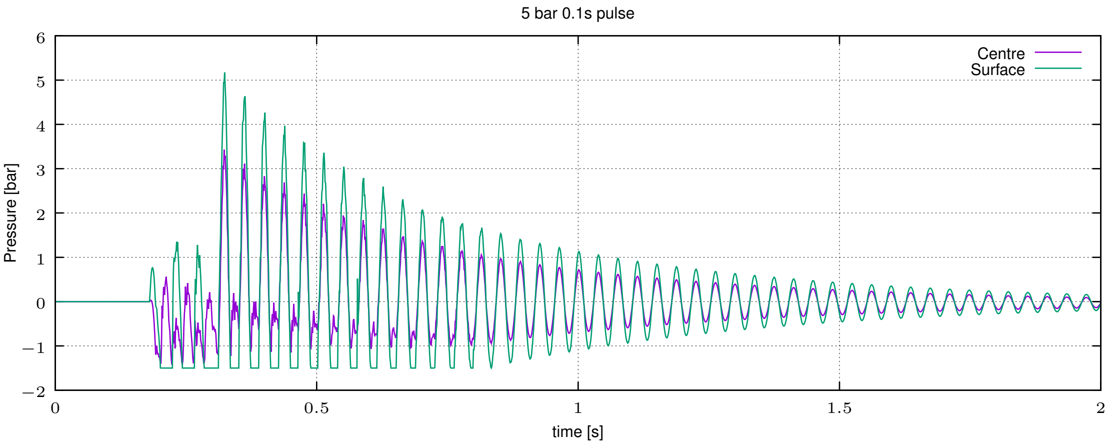

Figure 4.10: Internal fluid pressure response for 2D dome with increased stiffness

From the the results of the model with increased stiffness and previous models can be concluded that the stiffness and mass of the system has a large influence on the response. For the last case it is observed that the internal fluid may significantly increase the response amplitude.

4.1.2 *Hourglass control*

The model including the fluid shows clearly that the system is damped. However no 'real' damping such as viscosity is applied. The damping observed is assumed to be a result from the viscous hourglass energy control method. Figure 4.11 shows the total energy for two simulations. One with a viscous hourglass coefficient of 0.15 and one with a viscous hourglass coefficient close to zero, $1.0E{-}9$. It can easily been observed that the higher hourglass coefficient has as results that the total energy will decay in time. However this coefficient is needed to prevent zero energy modes in the shell and solid elements. These distortions are visualised by taking a screen shot of the simulation with the low hourglass coefficient, shown in Figure 4.12.

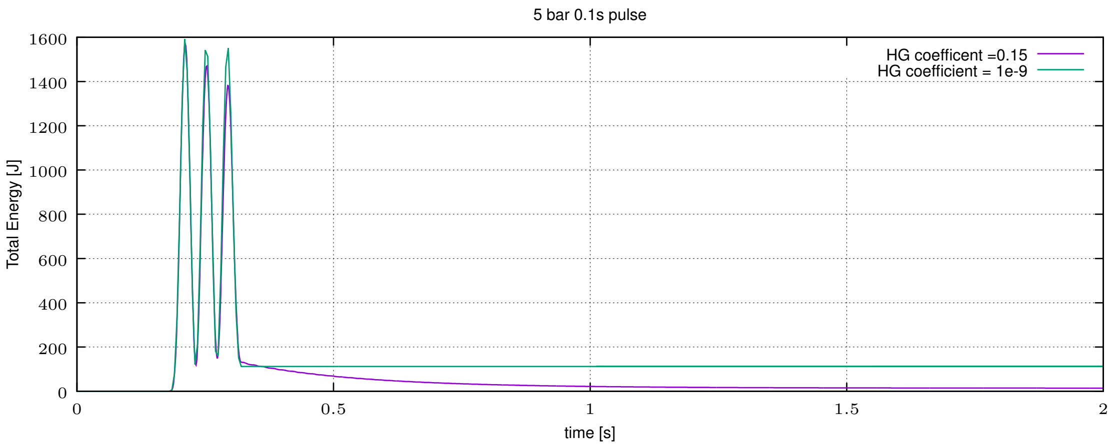

Figure 4.11: Hourglass control

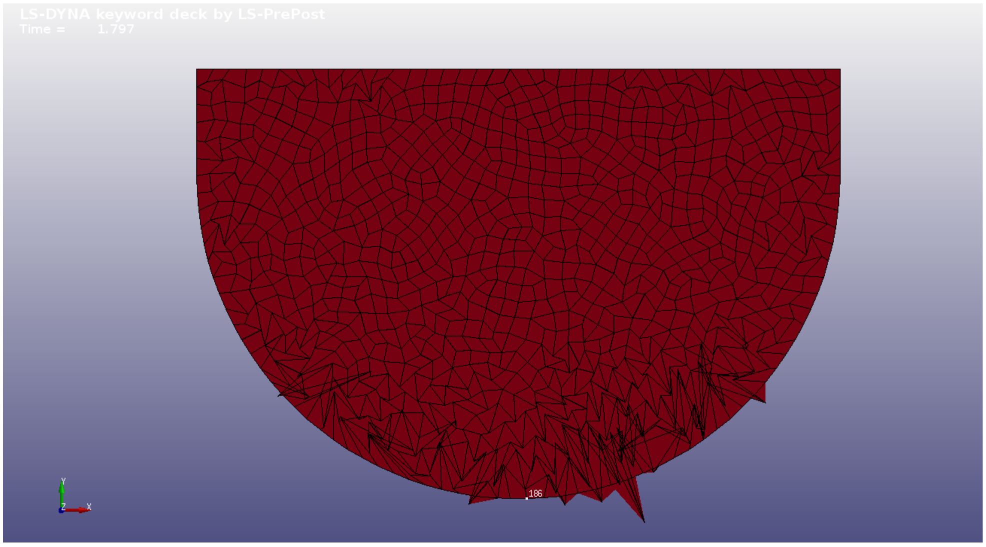

Figure 4.12: An example of one zero energy element distortion mode

Conclusion simplified dome analysis
From the simplified analysis is concluded that it is possible to couple the shell and fluid elements to represent the dynamic response of a fluid filled structure. In order to determine which dynamic effects are present in the sonar dome a more detailed 3D model has to be made to derive the total response. Based on the presented simplified analysis is chosen to model the internal fluid using only the bulk modulus of the water. However, un physical oscillations in the pressure may arise due to large deformations and should be reflected upon for the 3D case. The different load amplitudes shows that the response is non-linear however, this effect is small for the case considered.

4.2 3D dome model

So far a 2D cross-sectional representation of the dome is used to study the effect of the internal fluid. Using the investigation into the 2D dome model it was shown that the stiffness in the 2D model was too low compared to the mass. Using representative values for the composite sonar dome material and thickness this should be more in balance for the 3D model. The 3D sonar dome model is set up and calculated for different types of loading such as slamming, wave loading and acceleration loads.

4.2.1 Geometry and mesh

The 3D dome geometry is difficult to mesh automatically with solid quad elements internally and quadrilateral shell elements at the surface, which share common nodes. The mesh is generated by taking a simple geometry and relocating the boundary nodes and recalculate the positions of the internal nodes. The internal nodes are repositioned using a radial basis function. This method is derived from [6]. An illustrative 2D example is shown in Figure 4.13. The method of generating the whole mesh using radial basis function interpolation is described in more detail in Appendix E.

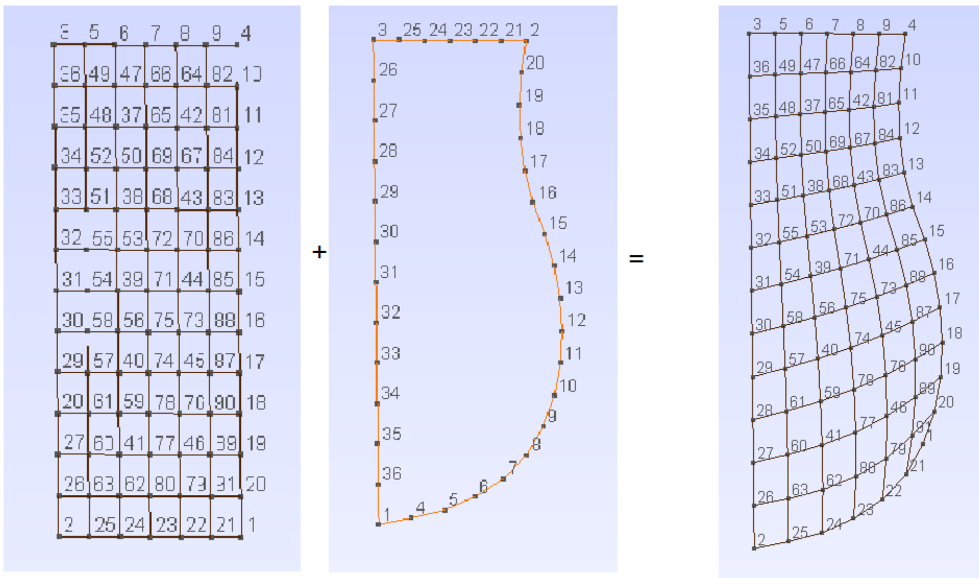

Figure 4.13: Mesh generation example in 2D

Figure 4.14 shows the resulting mesh as used for the simulations. The blue elements represent the composite shell, the red elements represent the solid fluid elements.

Simplifications

The model is simplified by neglecting the flange connection and stiffeners within the sonar dome. This simplifies the structure to a composite material shell with a uniform thickness. It is assumed that this model represents the sonar dome accurately enough to allow to investigate the effect of the presence of the internal fluid.
No additional damping is added to the fluid nor structure. The damping observed in the results originates from the hourglass control as show in Section 4.1.2 or may be partly the result of the cavitation of some of the fluid elements close to the shell.
The forward part of the dome is due to the curved geometry relatively stiff compared to other areas of the dome. The forward bulkhead with the longitudinal boundary conditions is assumed to be accurately enough within this study to represent this curved part.
The structure is assumed to be undeformed when at rest. This means that all pressures are given with respect to the hydrostatic pressure at rest which is approximately $0.5 bar$ since the free surface of the fluid in the expansion container is located about 5

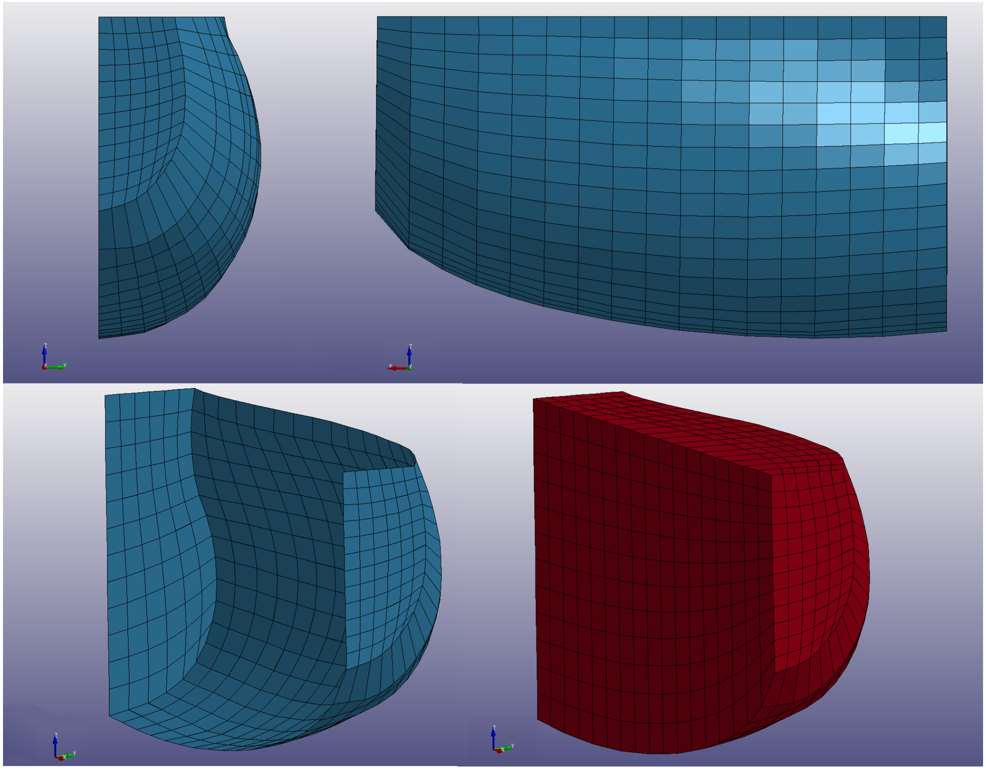

Figure 4.14: 3D dome mesh

meters above the dome.

4.2.2 *Boundary conditions*

The top side of the dome model is located at the K-deck on the bow of the vessel, this steel and stiffened deck is assumed to be relatively stiff compared to the dome shell structure. The upper boundary of FE model the dome is therefore fully clamped. The front and aft bulkheads are constrained in longitudinal direction. On the longitudinal cross-section at the centreline a symmetry plane boundary condition is applied.

4.2.3 *Material properties of the fluid*

The study of the 2D model showed that the elastic fluid material model is sufficiently accurate for the sonar dome response calculations. The parameters used for this material model are listed in Table 4.5.

Table 4.5: Fluid material model parameters 3D dome model

Mass density ρ	1005.0	$[kg/m^3]$
Bulk modulus k	2.183E+9	$[Pa]$
Cut-off pressure cp	-1.5E+5	$[Pa]$

Material properties of the shell

The shell elements represent the composite structure of the sonar dome. Material properties are derived from [12] and listed in Table 4.6.
The thickness of the shell elements is chosen to be uniform and is $32mm$.

Table 4.6: Shell material model parameters 3D dome model

Composite mass density ρ	2600	$[kg/m^3]$
Shell thickness t_p	0.032	$[m]$
Modulus of Elasticity k	11.0E+9	$[Pa]$
Poison ratio pr	0.3	$[\nu]$

Calculations
Using the model, three different settings are used for the simulations:

- Static without fluid
- Static with fluid
- Dynamic simulation

The static simulations are performed using the 'dynamic relaxation' method of LS-DYNA, which is an explicit calculation with an optimized amount of damping to converge quickly to a stable static solution.
For the simulations without the fluid, the solid fluid elements are removed from the model.

4.2.4 *Impulse Loading*

An impulse load is applied to the model to study the dynamic response. The distribution of the load investigated is chosen similar to the loading conditions used in an analysis of the dome without internal fluid [12]. This makes it possible to validate the global response of the model by performing a static calculation without internal fluid and compare the displacements of the bottom of the dome.
The load used is an external pressure load with a maximum of $5.0bar$ at the bottom of the dome. A cosine distribution of the pressure amplitude over the height is used resulting in an external pressure of $0bar$ at the top of the dome. For the dynamic calculations the impulse load is applied at $t = 0.2s$ with a rise time for the load of $0.02s$.

Displacements
A node on the centre line at the bottom of the dome is selected to study the vertical displacements. The node experiencing the largest displacements is node 218 located at the centreline halfway along the length of the dome. The displacement of this node is plotted in Figure 4.15. From this can been observed that in a static case, the fluid reduces the maximum displacement. However, in a dynamic situation the static values are exceeded. From Figure 4.15 can be concluded that the presence of the fluid increases the dynamic response for this load case.
Despite simplifications of the geometry, the displacements observed for the static load case corresponds well with the displacement reported in [12], which where at a maximum of $19mm$ at the bottom of the dome. In Appendix F Figures F.1, F.2 and F.3 shows the deformed model with the maximum resultant displacements for the three cases. It shows that the fluid reduces the localized displacements and result into a more distributed displacement. Which possibly may also influence the buckling behaviour of the dome, which is investigated in [10] where the internal fluid is neglected.

Pressure
Due to the external load, the internal pressure within the fluid will rise. This internal pressure is plotted for dynamic and static load cases in figure 4.16. It is observed that the relative differences between the dynamic and static results are much smaller with

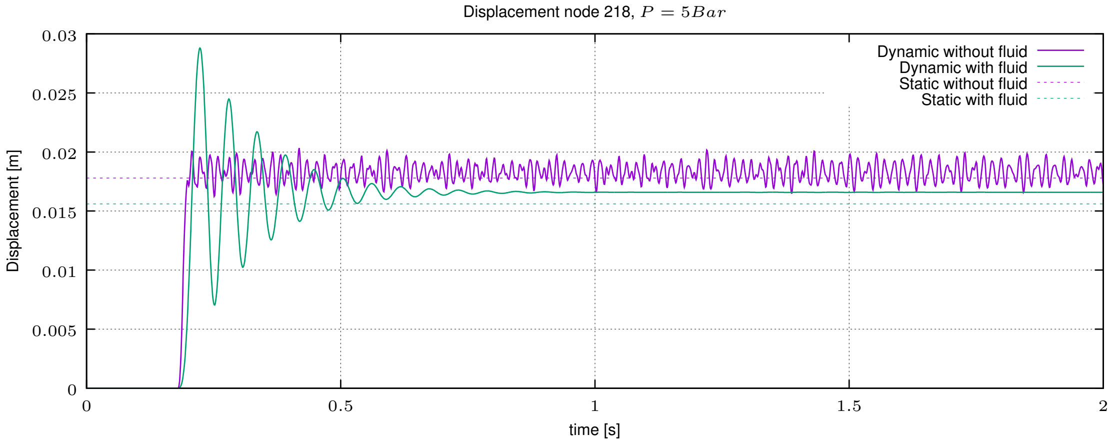

Figure 4.15: Vertical displacement of bottom node 218 to design pressure pulse load

respect to the displacement results.

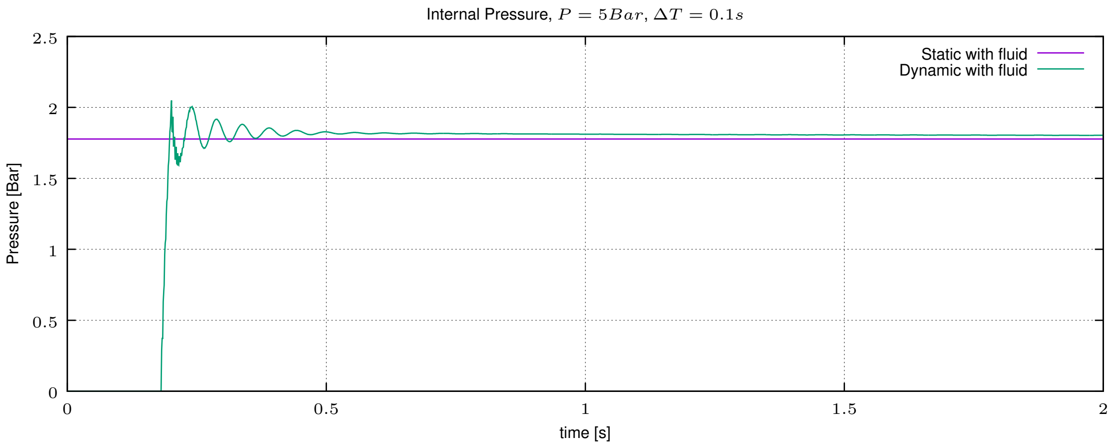

Figure 4.16: Internal fluid pressure response to design pressure pulse load

Effect Load pulse length and shape

The duration and shape of an impulse loading has an effect on the response. However for the sonar dome, the expected slamming pulse has a significant longer duration (1s to 2s) with respect to the natural periods observed in the response signals, typically about $0.05s$, resulting in a more or less quasi static response. However during impact, a fast ramp up of the pressure may result in a initial overshoot of the response with respect to the static response. Figure 4.17 shows the response to a constant pressure load with varying ramp-up times.

In order to determine whether the observed overshoot in the dynamic response is significant, seakeeping simulations are performed in more detail to derive accurate ramp-up times for the slamming loads. The response due to different ramp up times can be evaluated using Figure 4.18, which shows the relative difference between the static and dynamic displacement amplitude for a node at the bottom of the dome. It is observed that dynamic effect become fast more important when the rise-time is below $0.1s$. The response to seakeeping loads is studied in more detail in Section 4.4.

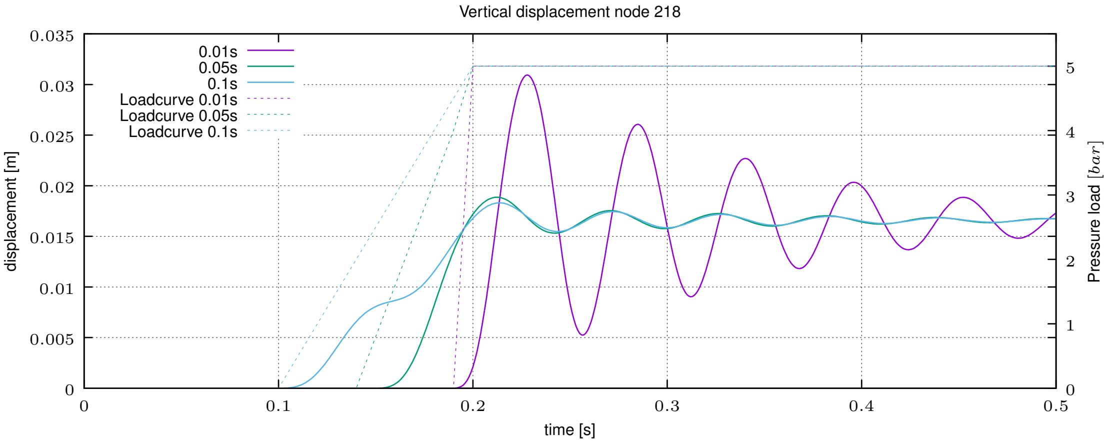

Figure 4.17: Effect of rise-time of the load on the displacement response of node 218 for three cases

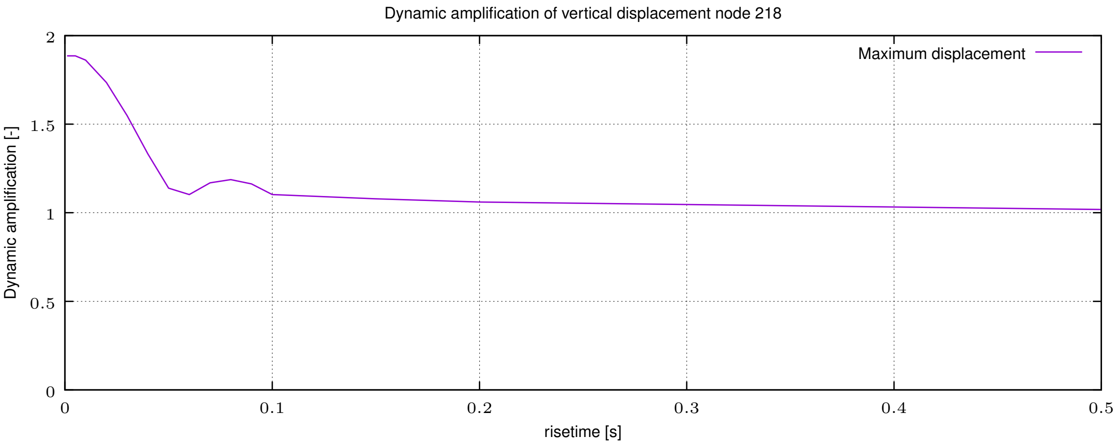

Figure 4.18: Dynamic amplification of vertical displacement node 218 due to different rise-times of the load

Forces at K-deck

For the structural response of the steel bow structure, one specific aspect of interest is the total force at the dome-hull connection. Therefore the reaction forces at the boundary condition at this deck are analysed. The total reaction force at the top of the dome is divided into two components, the reaction force through the shell and the reaction force due to the fluid pressure.

Figure 4.19 gives an overview of the total reaction forces in vertical direction observed in the dynamic and static analysis. The maximum load observed in the dynamic case exceeds the static calculation with about 20%. The total reaction force is subdivided in the contribution by the fluid pressure, and the contribution transferred through the composite structure. It is observed that the difference in total force between the dynamic and static calculation originates mainly from the difference in load transferred through the composite shell. Or in other words, the dynamic response occurs mainly in the composite shell.

Figure 4.20 and 4.21 compare the force in vertical direction in all shell elements for the case with and without fluid at the moment of maximum loading in time. Particular interest is the distribution of the vertical force around the upper boundary. For the case without fluid is can be observed that the highest force is at roughly half span of the dome. Which can be confirmed by a previous analysis concerning the flange loading along the length of the dome, shown in Figure 4.22. However including the

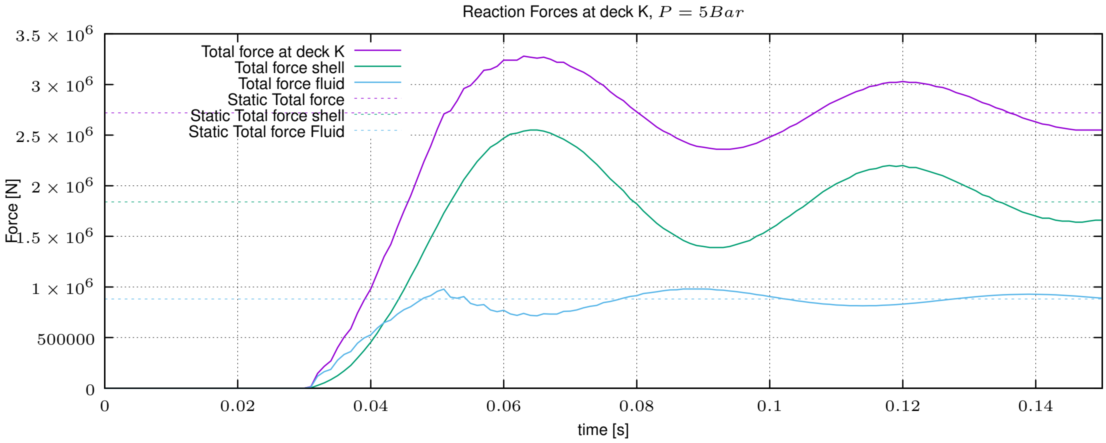

Figure 4.19: Vertical Reaction forces at deck K for the design pressure pulse load

internal fluid seem to alter the force distribution as observed in Figure 4.20. Here the maximum force amplitude occurs around the edges of the dome.

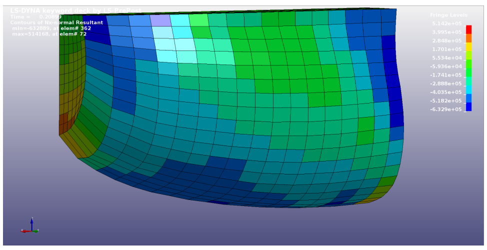

Figure 4.20: Vertical stress with internal fluid

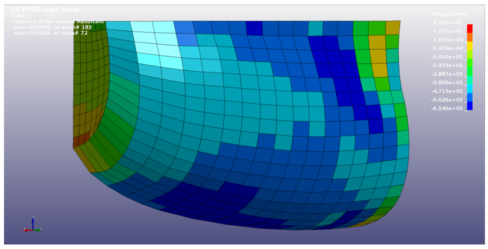

Figure 4.21: Vertical shell stress without internal fluid

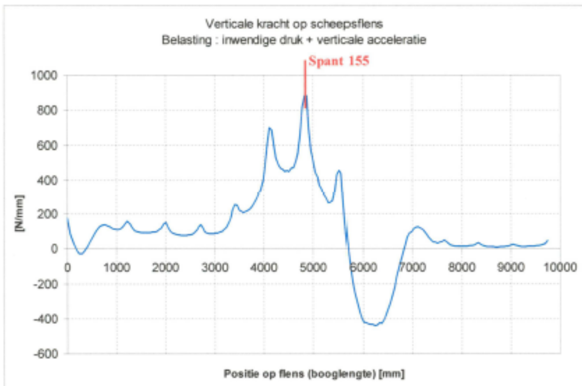

Figure 4.22: Vertical force along length dome as calculated in [11]

Another load component is the out of plane shear force in the shell due to the internal pressure which presses the shell outwards. Figure 4.23 shows the horizontal force at the boundary conditions at the K-deck. The maximum force observed is at least an order lower with respect to the vertical force component.
The last assumed main loading component is the bending load, the component around the x-axis. From Figure 4.24 and it is observed that the bending load is at its maximum at the boundary condition. And has a maximum in the opposite direction just below the boundary condition, where the dome flange is approximately fitted ($458mm$

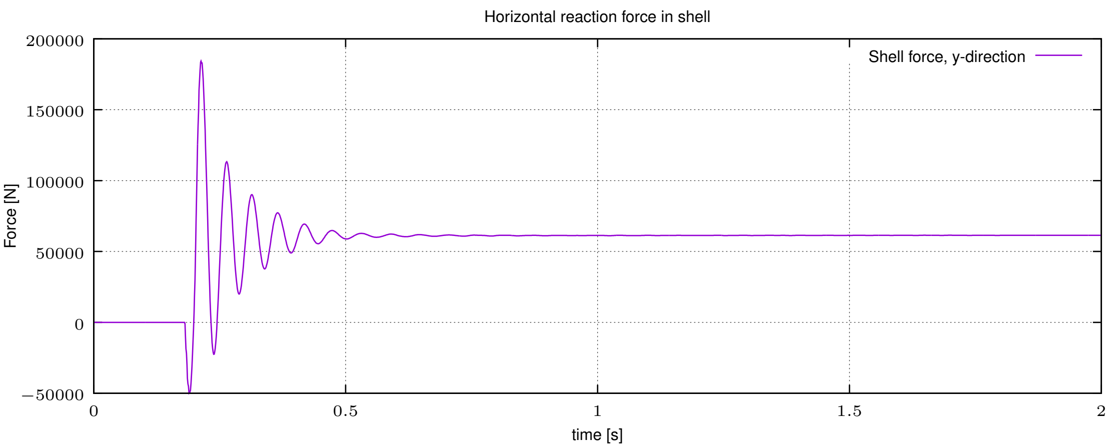

Figure 4.23: Horizontal reaction forces in shell due to design pressure pulse load

below the K-deck) which can be seen in Figure 4.26 where the red line indicate the flange position.

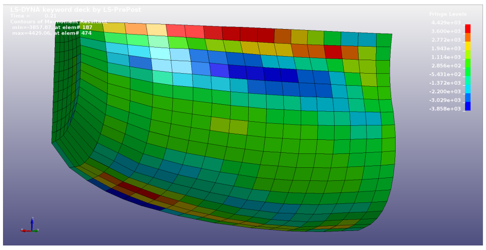

Figure 4.24: Shell bending moment around global x-axis with fluid

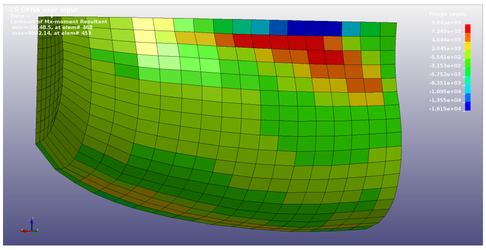

Figure 4.25: Shell bending moment around global x-axis without fluid

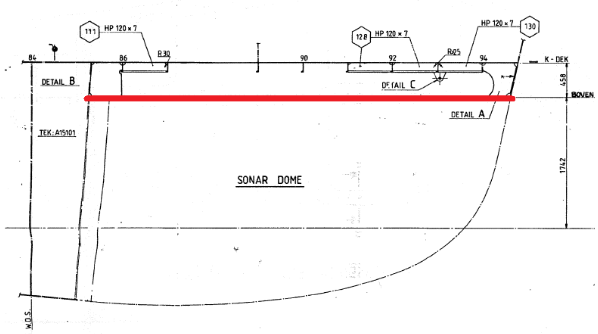

Figure 4.26: Structural drawing of sonar dome and flange location

4.2.5 *Accelerations loads*

The seakeeping of the vessel results in accelerations loads at the dome. An example of the resulting accelerations at the dome from a head sea seakeeping simulation is shown in figure C.5. Since this is a rather extreme seakeeping case for head seas, it is assumed that the maximum accelerations at the dome vary roughly between $+1g$ and $-1g$ with a period of about 10 seconds. This case is used to investigate the response to the acceleration loads. A sinusoidal input signal for the accelerations is used to load the dynamic model. This is done by invoking the acceleration loads on the mass

of all elements. The fluid of the overflow and expansion vessel is not modelled yet, the hydrostatic pressure calculated deviates from the actual values. This effect was discovered in the final stage of this study. The effects of this modelling error is studied in Section 4.7 but seem to be rather limited.
The periods observed in the acceleration signals are much longer compared to the dynamic response periods observed in the slamming load analysis. However in order to compare the magnitude of the response, these loads will be calculated using the dynamic model.
Figure 4.27 shows the displacement response of the bottom node to the acceleration load. The maximum displacement at this location is less than $1mm$ which is about a factor 20 smaller compared to the slamming load response.

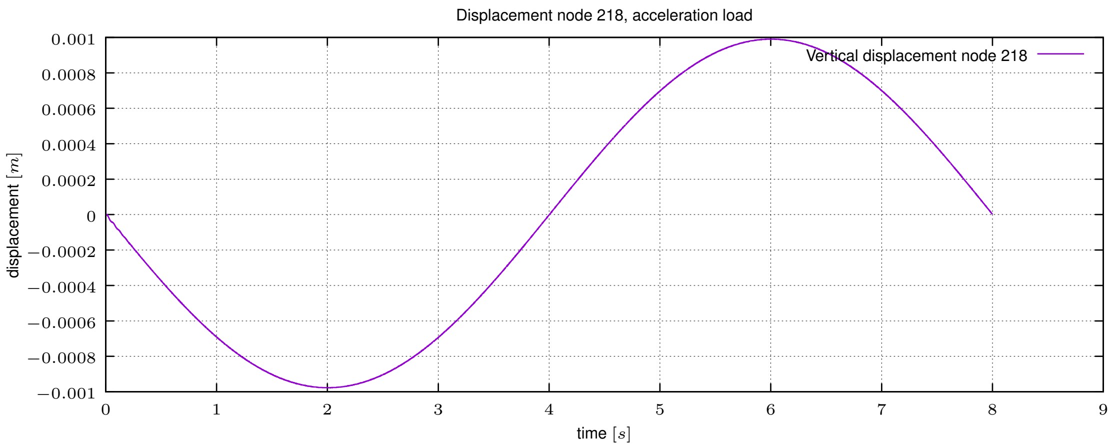

Figure 4.27: Vertical displacement node 218 due to acceleration load

Figure 4.28 shows the pressure at the K-deck which varies between + and - 0.065 bar. The pressure load is validated by comparing the pressure at the top and bottom elements. The difference is close to the hydrostatic pressure related to the height of the dome.

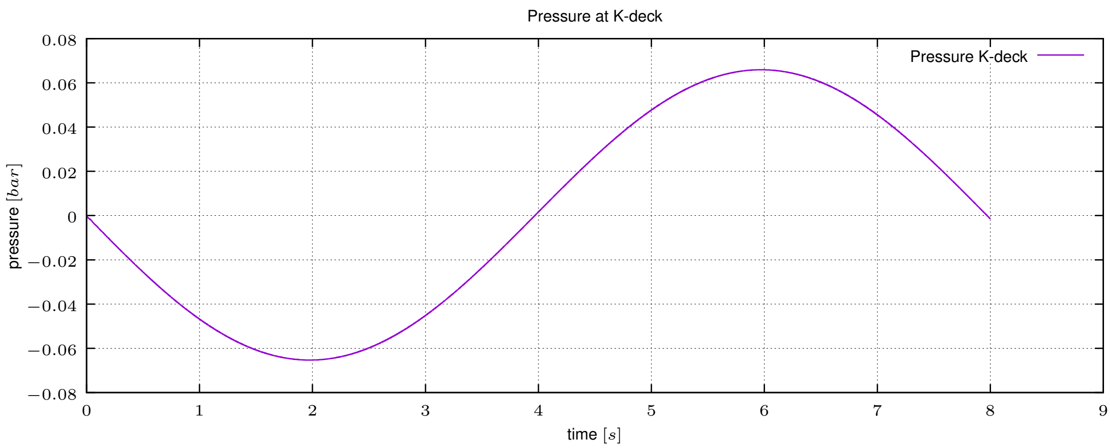

Figure 4.28: Pressure at K-deck due acceleration loads

The total force in the shell and fluid at the k-deck is derived using the reaction forces at the boundary. From this the contribution of each force component can be derived. The force components are shown in Figure 4.29.
Figures 4.27, 4.28 and 4.29 show the response of the sonar dome due to the accel-

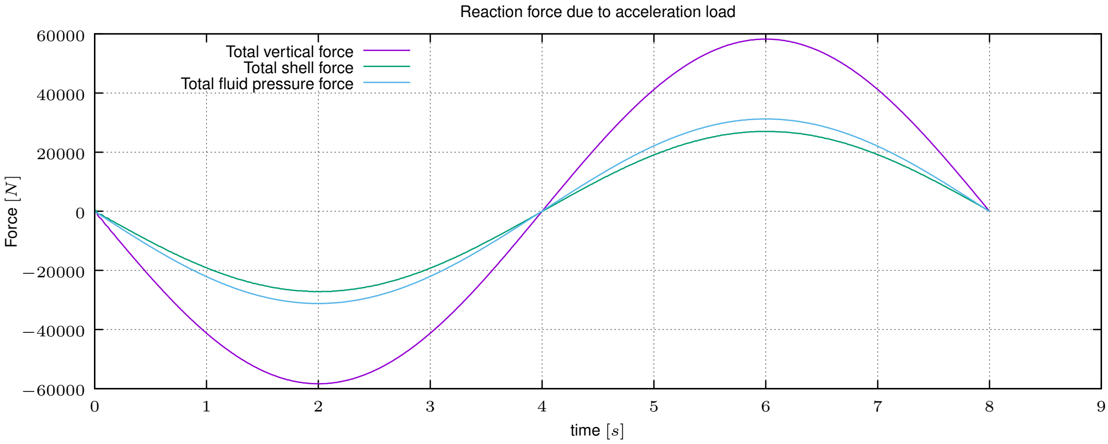

Figure 4.29: Reaction forces at K-deck due to acceleration loads

eration load. The response due to the acceleration load is significantly smaller when compared with the slamming response.

4.2.6 *Wave loading*

The wave loading due to the hydrostatic pressure is simulated under the following assumptions: the dome remain below the water surface, the pressure varies linearly over the height and the load can be described using a pure sine function.

Closely related to the method used for the acceleration load, a pressure load is defined using a pure sine signal. A total pressure amplitude of $1bar$ is used representing a wave with a height of 10 meter.

Figure 4.30 shows the displacement response of the bottom node to the wave load. The pressure applied on the dome is more uniform compared to the impulse load applied. This results in smaller deformations of the dome.

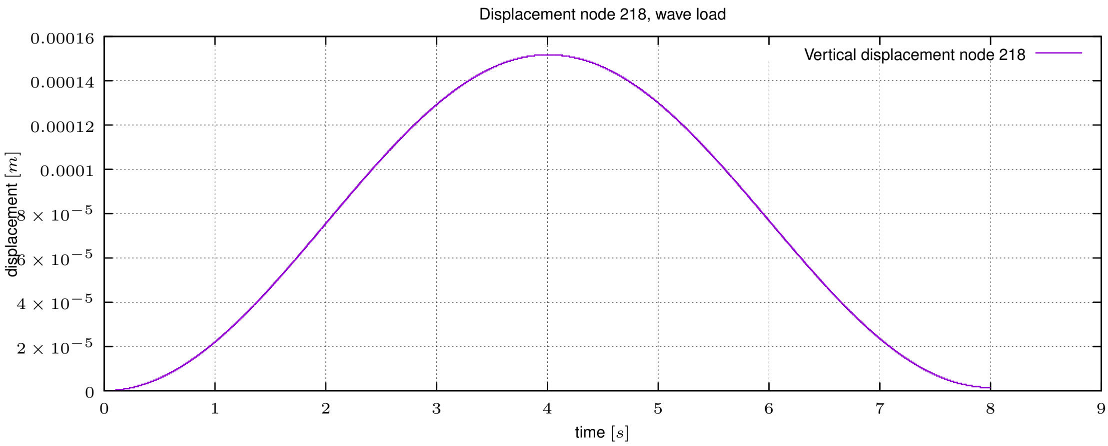

Figure 4.30: Vertical displacement node 218 due to wave loads

Figure 4.31 shows the pressure inside the dome, which is uniform. The pressure is expected to be the main contributor to the force at the boundary.

Figure 4.32 shows the vertical forces of the dome at the K-deck. The internal pressure is the main contributor to the total vertical force as shown in Figure 4.32. The total fluid force exceeds the total applied vertical force, resulting in tension loads in the shell near the flange.

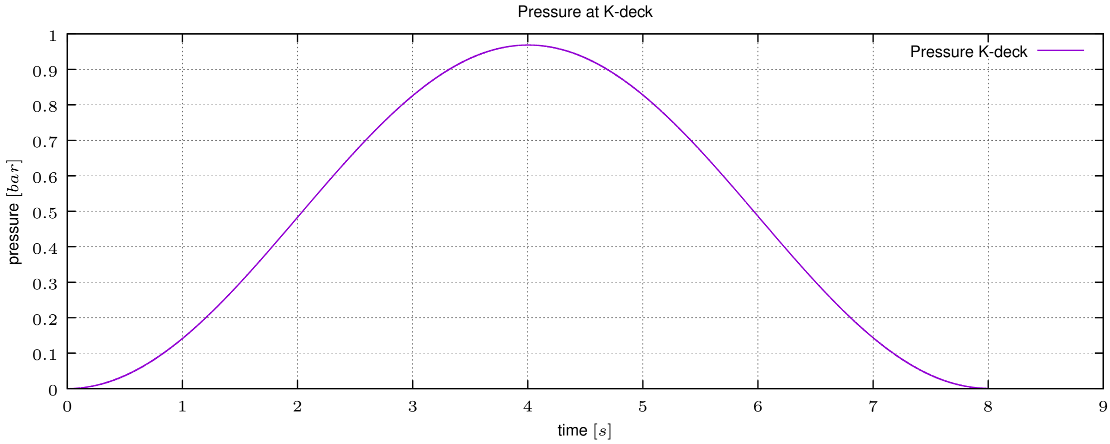

Figure 4.31: Pressure at K-deck due to wave loads

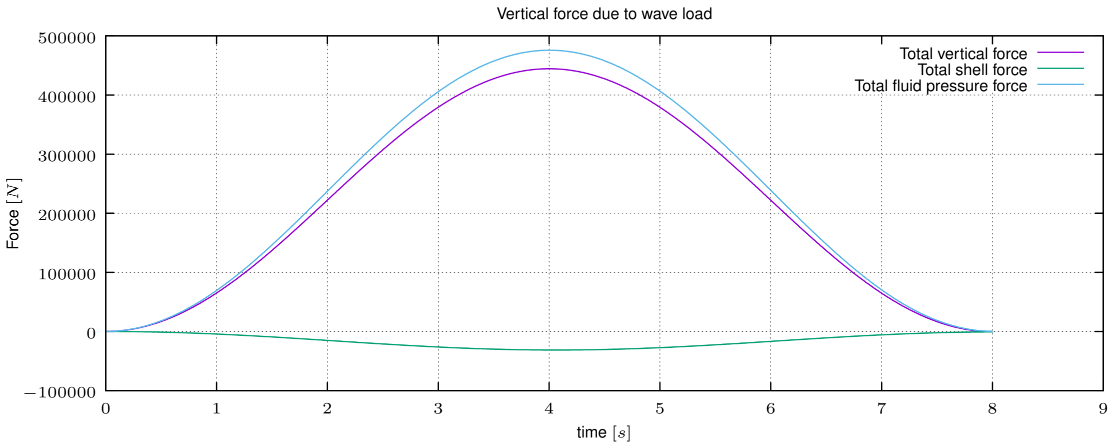

Figure 4.32: Forces at K-deck due to wave loads

4.3 Influence overflow pipe

The sonar dome is equipped wit an expansion container. The container is connected with the internal fluid of the sonar dome using a pipe of approximately $7m$ length. The container has a volume of approximately 50 litres and is placed roughly $5m$ above the dome, raising the free-surface of the internal fluid. The function of this expansion container is to be able to fill the sonar dome and to keep a constant head resulting in a pressure of roughly $0.5bar$ inside the dome. It is assumed that for slowly varying loads this container functions as expansion container to prevent a pressure build-up in the dome due to compression or expansion of the dome. However, this will possibly not be the case when te load is relatively short. When a high load with a short duration is applied, a large volume has to flow to the container in a fairly short time to prevent an increase in pressure. Tuitman [21] showed that with an empty sonar dome model the change in volume is roughly 50 litres. In order to prevent any pressure increase in the dome this volume should flow out through the pipe into the container. The relation between the pressure over the pipe and the flow speed is given by the Bernoulli equation, which is given in Equation (4.1) including a term for pressure losses due to wall friction in the pipe and the relation for the flow-rate.

$$
\begin{aligned}
P - P_{friction} &= \frac{1}{2}\rho v^2 \\
Q &= v \cdot A
\end{aligned}
\tag{4.1}
$$

Where:

P	Pressure difference over pipe $[Pa]$
$P_{friction}$	Pressure losses due to friction $[Pa]$
v	Flow speed $[m/s]$
Q	Flow rate $[m^3/s]$
A	Cross-sectional area pipe $[m^2]$

4.3.1 *Effect pipe frictional loss of pressure*

To calculate the flow speed based on the internal pressure, the pressure loss originating from the wall friction has to be determined. The pipe frictional loss is calculated using Equation (4.2).

$$
P_f = \left(f \cdot \frac{L}{d}\right)\frac{1}{2}\rho v^2 \tag{4.2}
$$

Where:

f	Friction factor
L	pipe length $[m]$
d	Pipe diameter $[m]$

Equation (4.2) makes use of the friction factor f which is estimated using the pipe flow Reynolds number, Equation (4.3). The relative roughness ϵ/d is estimated to be about 0.015. The friction coefficient is derived using the Moody charts for friction coefficients [26, Chapter 6, Figure 6.13]. For Reynolds numbers between $4.0E+3$ and $1.0E+9$ the fiction coefficient varies between 0.044 and 0.055. For this study a constant friction coefficient of 0.05 is taken.

$$
Re = \frac{\rho v d}{\mu} \tag{4.3}
$$

Where:

μ	Dynamic viscosity, $1.002 \cdot 10^{-3} Pa/s$

With the assumption that the friction factor will not vary in great extend Equations (4.1) and (4.2) are combined and rewritten in Equation (4.4).

$$
v^2 = \frac{2P}{\rho\left(1 + f \cdot \frac{L}{d}\right)} \tag{4.4}
$$

4.3.2 *Implementation overflow in dynamic model*

Previous paragraph describes the fluid dynamics of the overflow pipe attached to the dome. This section describes the implementation of this system in the dynamic sonar dome model.

Method

The outflow of fluid results in a reduction of the internal volume of the dome. This will be simulated by modifying the volume elements representing the fluid. The fluid elements will be given linear thermoelastic properties. The volume will be changed by cooling down thermoelastic elements, which results in an uniform volume reduction throughout the dome.

Another method was to reduce the size of a small number of elements close to the location of the overflow pipe. This resulted in a less stable calculation due to the large relative volume change of these few elements. The method used is to reduce the volume of all elements slightly, which result in a more stable pressure distribution. Since the time scale of the problem is much larger compared to the sound speed there should be no side effects due to this approach.
A calculation is done without altering the volume of the internal elements to check whether the introduction of the thermal properties at the elements influence the behaviour of the model in general and no differences where observed, the results can be viewed in Appendix G, Figure G.1.
Secondly the change of volume is calculated based on the pressure at each time step using Equation (4.5). Integrated over the time step this results in the total change of volume for the solid elements at each time step, which will be used as input for the next iteration of the calculations. In general are 3 iterations have shown to be sufficient to get a converged solution.

$$\frac{dV}{dt} = \sqrt{\frac{2P}{\rho\left(1 + f \cdot \frac{L}{d}\right)}}\frac{1}{4}\pi d^2 \tag{4.5}$$

Where:
V outflow volume
The thermodynamic elements have a thermal expansion coefficient of 1, the value defined by the thermal load curve represent the relative volume of the elements with respect to the initial volume of the thermal elements. The program used defines only the linear expansion coefficient. The total relative change in volume is equal to 3 times the linear expansion coefficient, Equation 4.6.

$$\frac{\Delta V}{V_0} = 3 \cdot \alpha_L \cdot \Delta T \tag{4.6}$$

Where:
α_L Linear thermal expansion coefficient

Results
Figure G.2, G.3 and G.4 in Appendix G show the effect of the reduction of internal pressure due to the outflow of fluid from the dome during slamming. Based on the results it is concluded that the overflow will not lead to a significant reduction in internal pressure during the initial impact peaks. For loads with a longer duration the internal pressure will decline gradually.
When observing the wave loading, typically cycles of about 10 to 15 seconds are seen. Due to the longer period more water may flow in and out of the dome based on the actual loading. Using a sine-shaped wave load the effect of the overflow is studied, and the results are shown in Figure G.5. It is observed that the overflow limits the increase of internal pressure with respect to the fully closed dome. During the wave loading, the volume of the dome has been reduced by at maximum $6.4 litres$. However in previous studies [21], a change of volume of about 50 litres has been found using a empty dome model. Which implies that to fully prevent any increase in uniform internal pressure, 50 litres has to flow out of the dome. This study has shown that a relative small outflow volume already result in a large reduction of pressure, namely a reduction from approximately $1bar$ to $0.25bar$ for the wave loading considered.

4.4 Seakeeping loads

In the previous sections of this chapter, individual load components which are assumed to be part of the total seakeeping loading are investigated. The total seakeeping load is calculated using the methods described in Chapter 2. To obtain the pressure loads at the shell elements of the dynamic dome model, a structural mesh of the outer shell elements is used as structural load projection mesh. An illustration of the hydrodynamic and structural mesh used is shown in Figure 4.33.

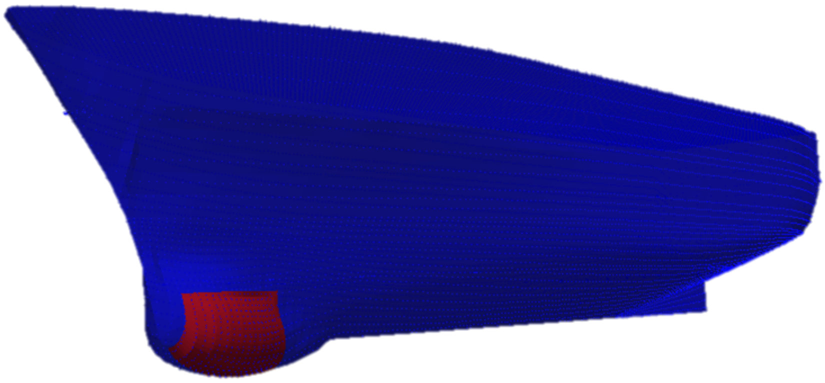

Figure 4.33: Structural dome mesh on hydrodynamic model

An overview of the programs and information flow used for the analysis is given by Figure 4.34. The first step is to calculate the seakeeping response of the vessel in frequency domain using HYDROSTAR the results are used to perform the seakeeping analysis in time domain, HETIME. The seakeeping pressures at the hull from HETIME are used in MARGENL to calculate node nodal forces at the structural mesh. The nodal forces, together with the accelerations at the centre of the dome are used in LS-DYNA to perform a dynamic simulation. This is done iteratively to account for the outflow using the outflow model from previous section. A more detailed description of the individual programs used are given in Chapter 2 and Section 3.3.
The recalculation of the seakeeping loading for the sonar dome mesh results in the pressure loads in time at the shell elements of the sonar dome. The accelerations are derived for the centre of the sonar dome, since it is assumed that these values differ not significantly throughout the dome.

Pressures
Figure 4.35 shows the development of the internal fluid pressure during the selected slamming event. In this plot the results for 4 calculations, representing the iterations for the overflow calculation are shown. It is observed that after the 3rd calculation the pressure does not differ significantly from the previous calculations and the results is assumed to be converged. Due to the hydrostatic pressure, the pressure at the to of the dome is expected to be $0.28bar$ lower compared to the bottom for an acceleration level of 1g, the pressure at the top of the dome is shown in Figure 4.36.

Displacements
The displacements of the bottom of the sonar dome show somewhat different behaviour as in the individual load cases investigated in the previous section. During the applied loading conditions, it is observed that initially the highest load is at the bottom, pushing the bottom of the dome upwards. A fraction of time later the pres-

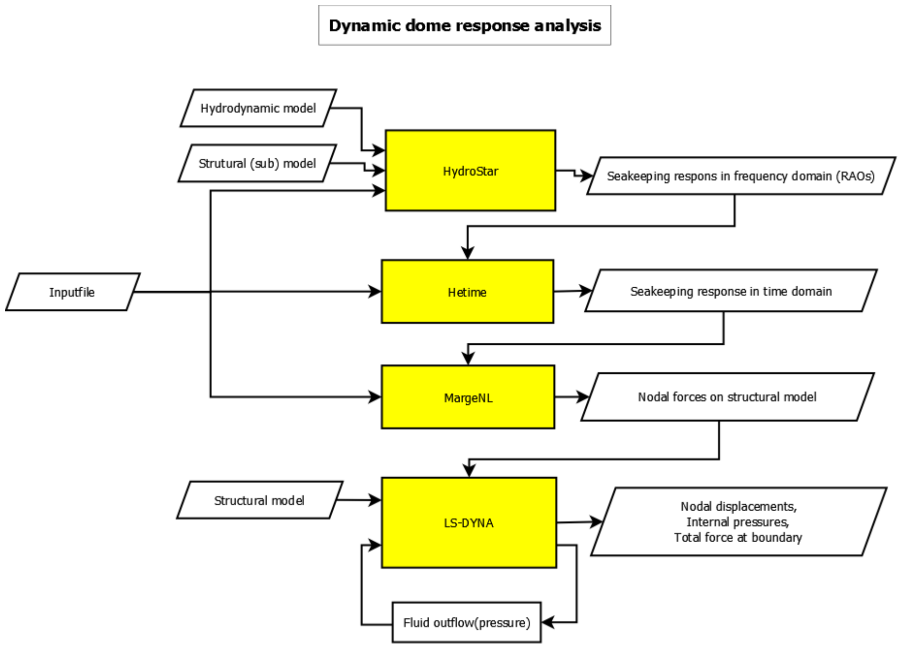

Figure 4.34: Overview calculation process for the dynamic dome response calculations

sure at the sides of the dome rise drastically, pushing the sides of the dome inward. Due to the increasing pressure in the dome, the bottom will displace downwards during this phase. When the pressure declines the bottom comes back up to the neutral position. The vertical motion of the bottom node of the dome is shown in Figure 4.37.

Internal volume
During loading, the volume of the dome is changed based on the calculated outflow of volume. The relative change in volume is shown in Figure 4.38. The initial volume of the modelled dome is $14.325m^3$, which is half of the dome. Using the total relative volume from Figure 4.38, the change in volume is calculated. From this it is concluded that the maximum change of volume for this slamming event is about 10 litres for the whole dome. From Figure 4.38 it is also observed that this change of volume is mainly due to the outflow of water through the overflow pipe rather than compression of the fluid.

Forces at K-deck
The forces at the K-deck exerted by the shell and fluid are shown in Figure 4.39. It is observed that there is a quite even distribution between the shell and fluid forces for this load case.
The horizontal force during the loading conditions shows a completely different behaviour and is quite small during the wave impact. However when the wave load on the sides of the dome increases this will result on a inward horizontal force at the flange. However this force component is approximately 20 times smaller compared to the vertical component.

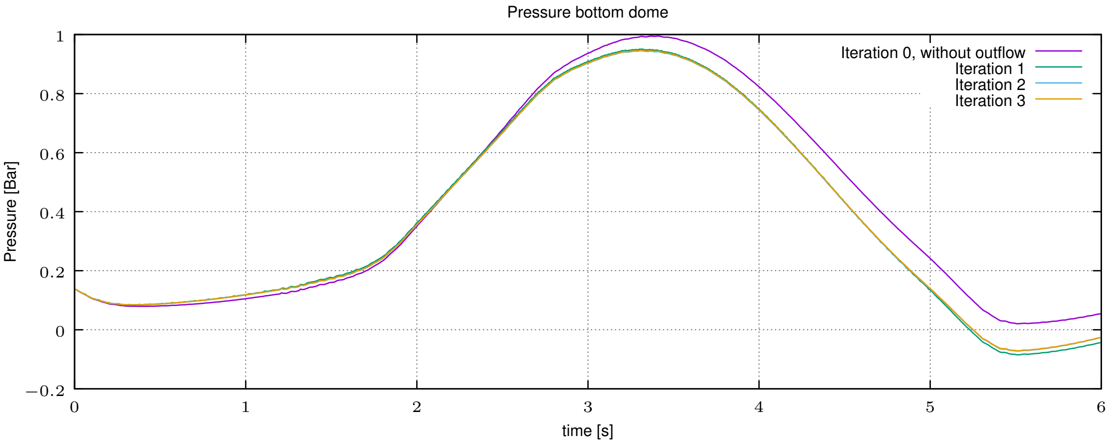

Figure 4.35: Internal pressure at bottom of the dome, showing the convergence of the iterations of the outflow of fluid

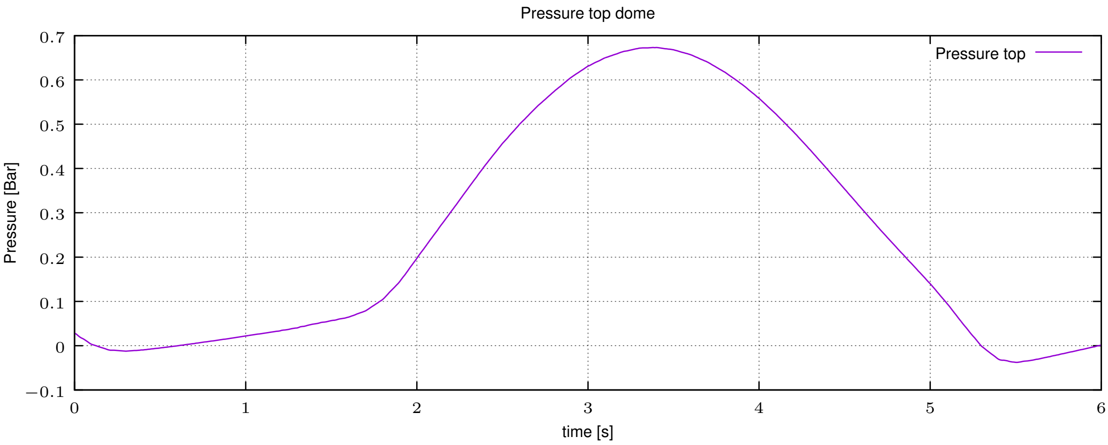

Figure 4.36: Internal pressure at top of the dome

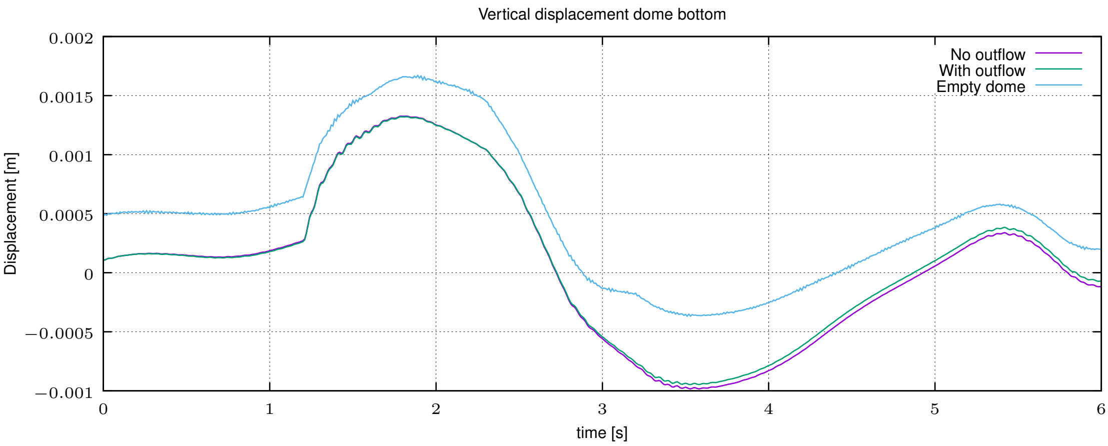

Figure 4.37: Vertical displacement dome bottom with and without outflow from the dome

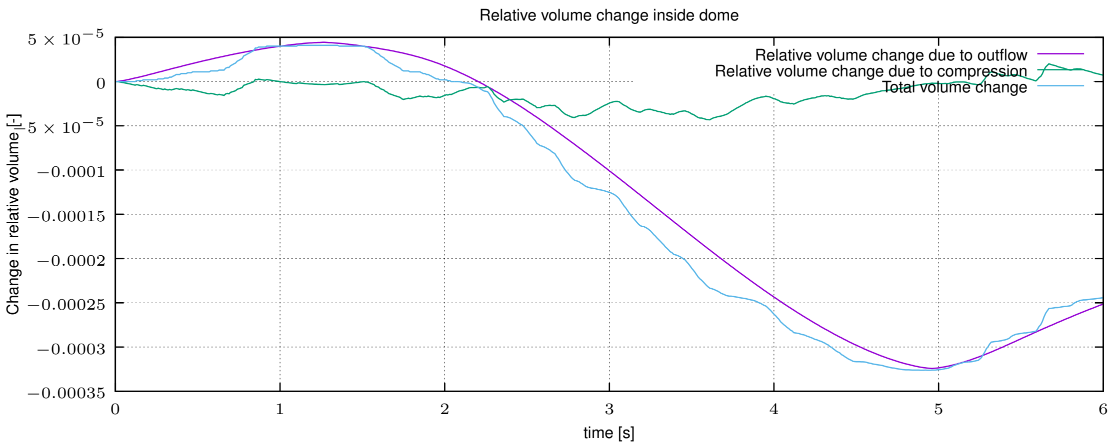

Figure 4.38: Change in relative internal volume of the dome

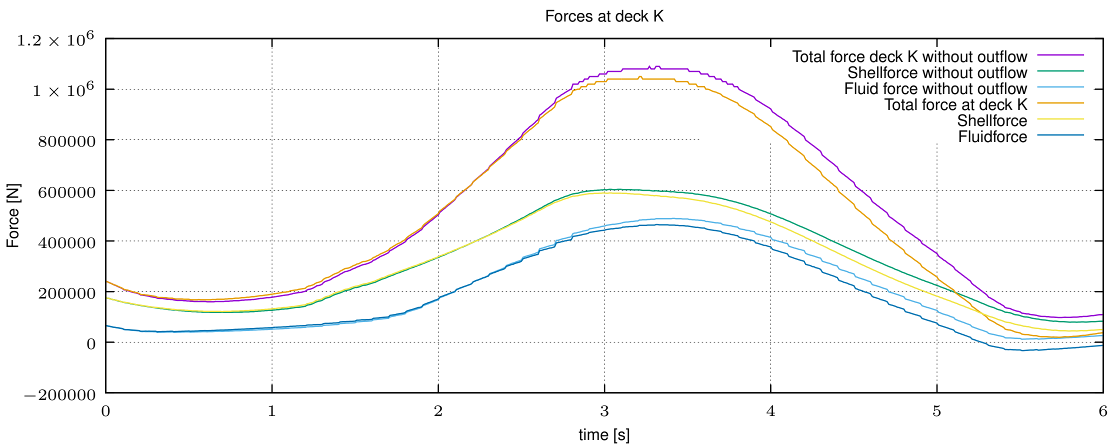

Figure 4.39: Forces at deck K with and without outflow

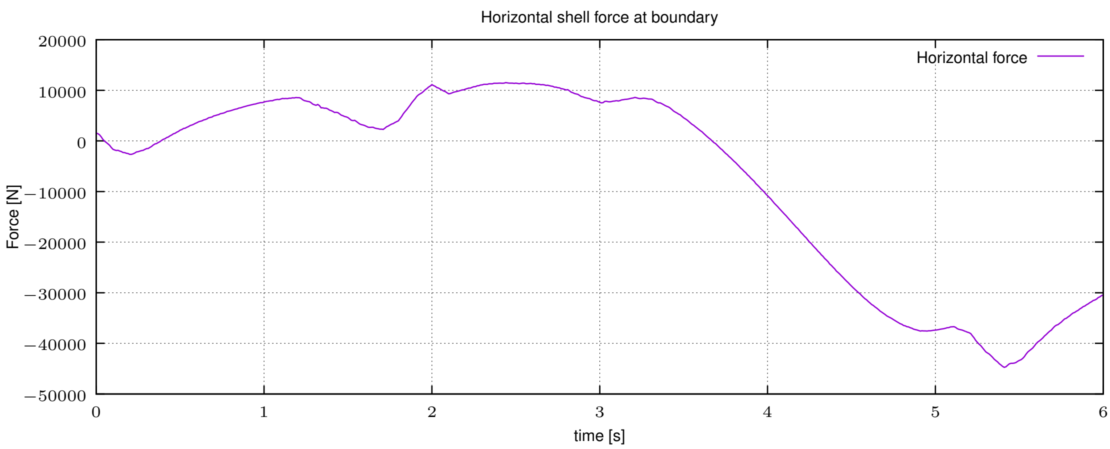

Figure 4.40: Horizontal forces at deck K

4.5 Stress dome structure

The sonar dome is modelled with the material parameters of the composite used. The dome does not represent exactly the real structure with respect to local thickness variations, geometry and internal stiffening. However a look at the stresses may give insight in the locations most prone to overloading and the order of magnitude of the occurring stresses. Another aspect that is studied is the effect of the internal fluid on the stress level.

In Appendix H, the maximum Von Mises stress in the shell elements is shown for a number of time steps. The right hand part of the figures show the actual vessel and wave position corresponding to the load case. In general is observed that the highest stresses are observed near the flange connection on the aft of the dome when the immersion of the dome is maximal.

Figure 4.41 shows the von mises stress level for 2 elements in the dome. The element locations for both cases are illustrated in Figure 4.42. These 2 elements are selected based on the highest stress level in the calculations. Element 409 has the highest stress level in the begin phase of the slamming event. Element 672 has the highest response in the last phase of the slamming event for the calculations with internal fluid. The dashed lines in Figure 4.41 represent the stress level when the fluid is removed from the dome.

Based on this figure it can be concluded that the internal fluid reduces the maximum stress level in the shell. The overall maximum stress level is reduced from $21MPa$ to $6.6MPa$, which is a reduction of 69% and is observed in Element 672. The presence of the internal fluid result in a different shape of the response as well. The peak of the maximum stress level has shifted in time.

Investigating the stresses in the dome shell structure when the fluid is included, 2 clearly distinct types of stress history can be observed. This is shown in Figure 4.41, here element number 409 is located at the forward bottom of the dome. Which shows clearly a peak at the initial slamming impact, which also corresponds with the maximum displacement in time as observed in Figure 4.37. However element number. 672 located more aftward at the top of the dome, close to the flange, experiences a larger load which is mainly the result of the seakeeping pressure on the outer sides of the dome which occurs in a later stadium of the loading.

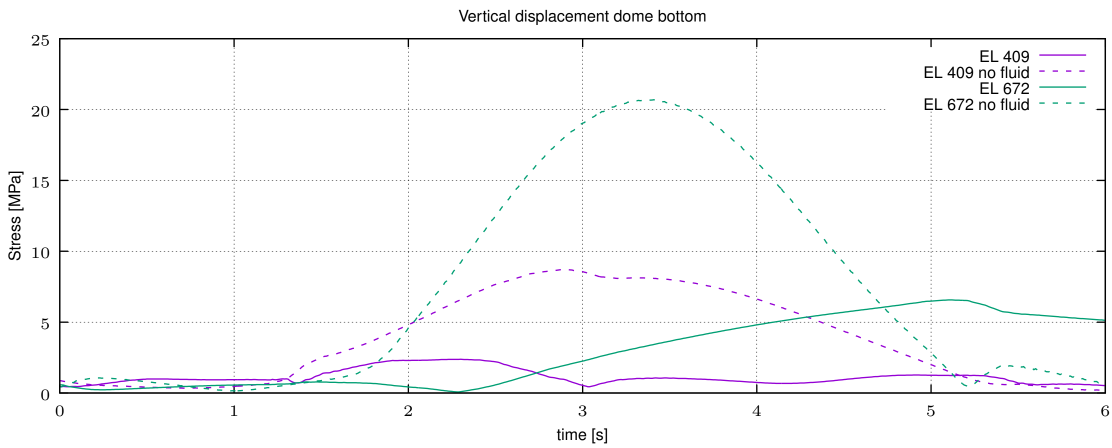

Figure 4.41: Stresses in composite shell

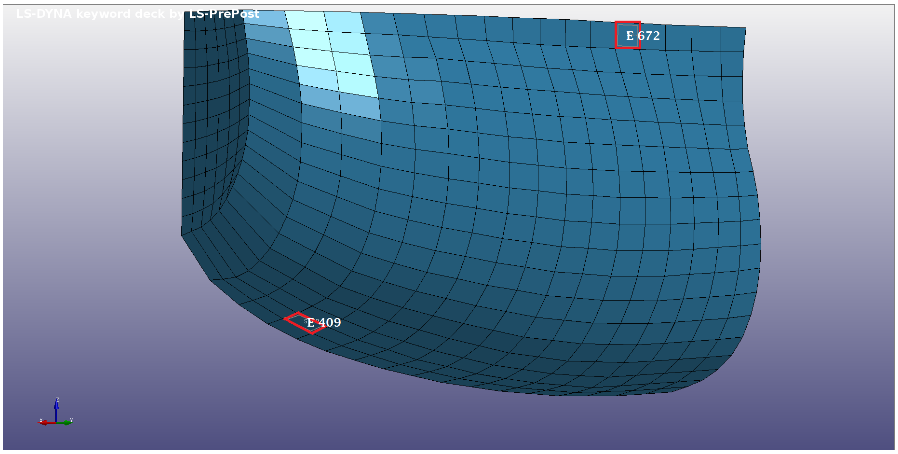

Figure 4.42: Element locations

4.6 Comparison with quasi static approach

In [21] a quasi static method is presented to account for the internal fluid of the sonar dome in a empty model, meaning that the actual fluid is not modelled. This method was applied using linear quasi static load cases within the program VAST. This linear approach allows for superposition of the individual load cases. The method is compared with the results from the fully dynamic method as presented in this chapter.
The explicit calculations performed in LS-DYNA are in general always non-linear. In order to be able to use the same model for this comparison the load on the model is scaled down, and the response is assumed to be approximately linear.

Method description
The method to calculate the response of the sonar dome without modelling the fluid is described in [21]. Within this method it is assumed that the total internal volume does not change in time. The method consist of two calculation steps. Figure 4.43 shows the 2 calculation steps performed. First the response of the empty dome due to the external pressure and acceleration loads is calculated. These loads result in a change in volume of the empty model. The second step is to increase the uniform internal pressure of the dome till the sum of the changes in volume of the 3 parts equals zero.

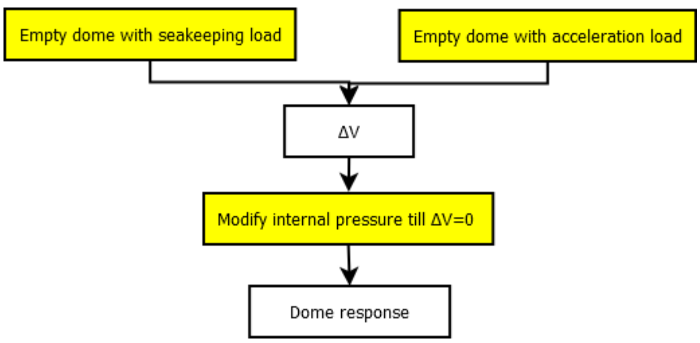

Figure 4.43: Quasi static linear pressure load calculation method

Validation load level
The load level is scaled down with a factor 100. In order to verify that the response for this load level is approximately linear, the response to a second load level is calculated where the load is scaled down a factor 50. Figure 4.44 shows the response to both load levels. The third line in the plot is twice the first line to check the linearity. Since the line of $0.02 * Load$ and 2 times $0.01 * Load$ are almost the same the results are assumed to be linear between both load ranges.

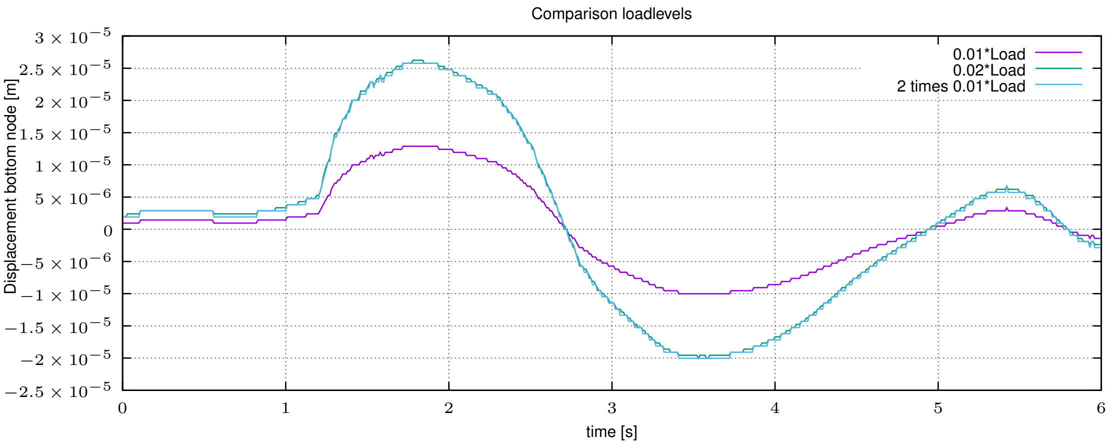

Figure 4.44: Comparison load levels to check linearity of the response

Removing fluid from model
The solid elements in the model are used to calculate the change in volume during the simulation. So it is preferred to keep the solid elements, but give them properties that will not introduce internal loads. In order to achieve this, the bulk modulus of the fluid and the density is reduced to close to zero. The results from two calculations, one with a relative reduction of $1.0E{-}9$ and one with $1.0E{-}12$ are compared to check whether result is still affected by a further reduction of density and stiffness. The ratio between the stiffness and density of the solid elements is kept constant in order to keep the speed of sound equal, since this is governing the time step of the dynamic simulations. Figure 4.45 shows the response calculated with both relative reduction of the mass and stiffness properties of the fluid.

Response due unit internal pressure
In previous cases with the full load applied, internal pressures around $1bar$ are observed. With the reduce load cases, the reference case for the internal pressure is set at $1kPa$. Assumed is that for this load range the volume change of the dome is linear with the internal pressure applied. The total change in volume is $5.0E{-}4m^3$ per $1kPa$ pressure.

Response due unit acceleration
As noted earlier, in the dynamic model the fluid surface is modelled at the K-deck, not at the top of the filling tank above deck. In order to keep both models the same, the fluid surface is in this case modelled at the K-deck as well. Using an unit acceleration of $0.01m/s^2$ the the hydrostatic pressure from the fluid on the interior of the dome is calculated and applied as load. The total change in volume due to unit acceleration is $1.6E{-}6m^3$. This change in volume is assumed to be linear with the accelerations.

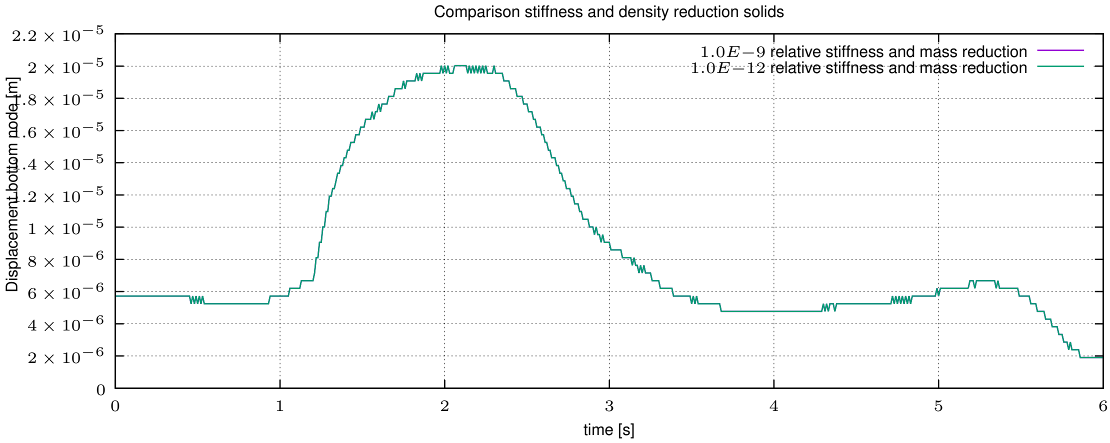

Figure 4.45: Comparison of two relative stiffness and mass reductions levels for the internal fluid, lines overlap no difference observed

Total response

The total change in internal volume is calculated according the external and acceleration loads. To counteract this change in volume, the internal pressure is increased till the total change in volume is zero. Use is made of the change in volume related to the introduced unit load which are listed in Table 4.7.

Table 4.7: Change in volume due to unit acceleration and pressure loads

Initial Volume	$14.32493m^3$
Volume change per $0.01m/s^2$ acceleration	$+1.60E{-}6m^3$
Volume change per $1kPa$ internal load	$+5.0E{-}4m^3$

The first load case observed is the first time step from the dynamic simulations. The change in volume resulting from this load case is listed in Table 4.8. The internal load results in a pressure of $-0.023kPa$. Assuming the system to be linear with all load components this result in a loading of $-0.023bar$ for the real load case.

Table 4.8: Quasi static internal pressure calculation at t=0

Load component	Change in volume
External pressure	$+0.15E{-}5m^3$
Accelerations	$+1.40E{-}5m^3$
Internal load	$-1.55E{-}5m^3$

The second load case is taken as the moment of maximum pressure at approximately $3.34s$. The change of volume from this load case is listed in Table 4.9. The resulting internal pressure is $0.586kPa$. Thus resulting in a pressure of $0.586bar$ in th real load case.

The results using the change in volume method are calculated statically using the load case from the dynamic simulations. The pressure is calculated statically for every $0.1s$. The resulting pressure is plotted against the pressures from the dynamic simulations without the outflow of water in Figure 4.46. From this plot is concluded that the pressure prediction for lower loads seem to be quite accurate. However it under predicts the pressure in the higher load regions.

Table 4.9: Quasi static internal pressure calculation at t=3.3

Load component	Change in volume
External pressure	$-3.20E{-}4m^3$
Accelerations	$+2.72E{-}5m^3$
Internal load	$+2.93E{-}4m^3$

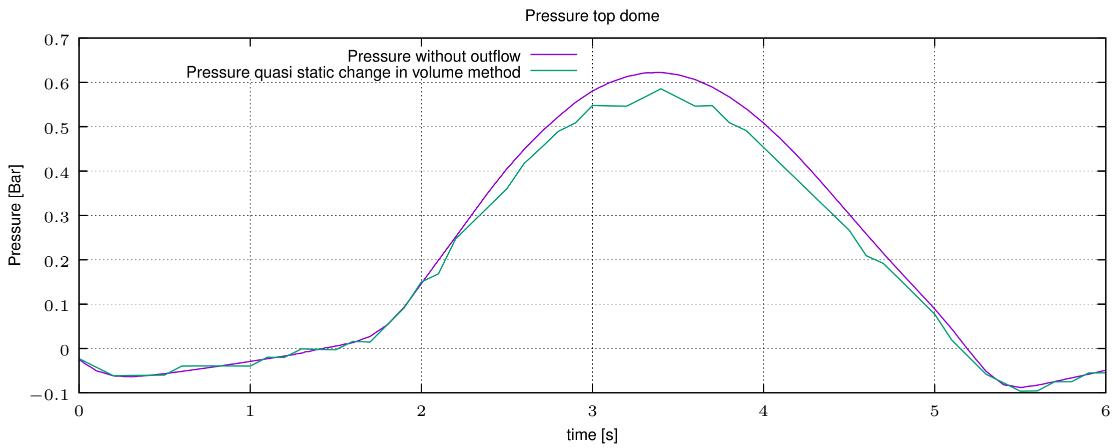

Figure 4.46: Comparison pressure calculation methods, dynamic calculation and quasi static linear method both without outflow

4.7 Effect free surface location

As mentioned earlier, the location of the free surface of the internal fluid is not modelled correctly in the dynamic model, since the mass and location of the fluid in the overflow and expansion vessel is not incorporated. The presence of this additional fluid height will result in a higher pressure inside the dome linearly related to the actual acceleration load. The set up of the dynamic model does not allow one to easily adjust the model to get results for the right internal free surface location. However the change of volume method models the acceleration load by calculating this contribution in pressure directly from the hydrostatic height and actual acceleration load. Therefore the effect of the free surface location is studied using this model.
Figure 4.47 shows the pressure response with respect to the hydrostatic pressure at rest. It can be observed that elevating the internal free surface of the fluid from the K-deck to $5m$ above this deck has an increasing effect on the pressure amplitude observed at the top of the dome. However, this effect is limited since the increase of pressure in the dome due to acceleration loads, reduces the increase of the uniform internal pressure force to get the total change of volume zero.
It can be concluded that the height of the internal free surface of the water can not be neglected. One could argue that water has to flow in the dome to increase its pressure. However, the increase in the acceleration load comes from the height of the expansion vessel, which results in a smaller or opposite pressure difference between the dome and the expansion vessel, reducing the outflow of water due to the external load on the dome.

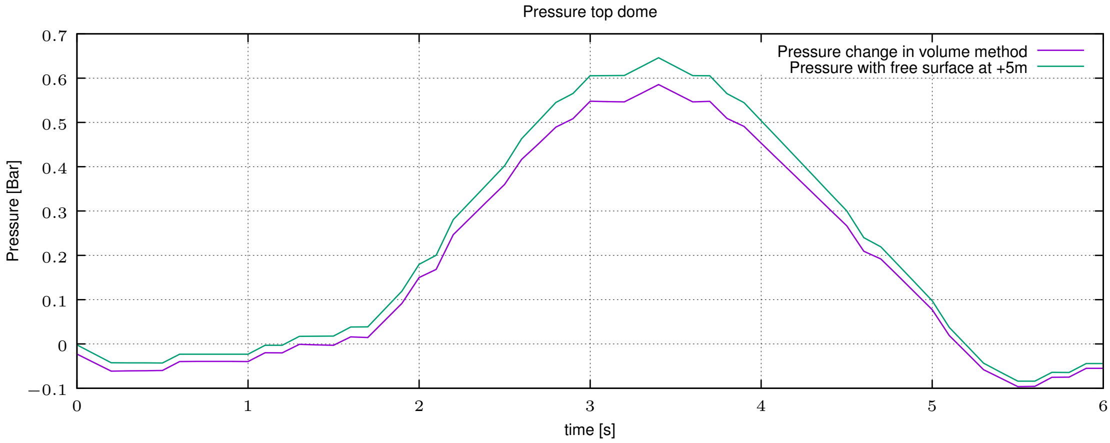

Figure 4.47: Effect fluid free surface location on internal pressure response

4.8 Conclusion

Using the simplified 3D dome model of the sonar dome, the global stiffness is validated by performing a calculations with a empty sonar dome with the same static load conditions as reported in [12]. For comparison the displacement of the bottom of the dome is taken. The maximum displacement reported in [12] is $19mm$. The response to the same load case using the simplified dome model is $17.6mm$.
From response due to the seakeeping pressure load case it is observed that the magnitude of the slamming load is clearly overestimated in the design calculations where a load of 5 bar at the bottom was assumed.
The presence of the internal fluid reduces the displacement response amplitudes due to a build up of internal pressure for the static load case. From the dynamic load cases is observed that the model including the fluid has a larger overshoot over the static response level. The observed dynamic response period of the model including fluid is much closer to the rise-time of the load compared to the model without internal fluid.
Within the fluid filled dome the total vertical force shows a distribution of the force over the shell and internal fluid. Due to the outflow of water, the contribution of the shell force tends to increase. However this is not significant during the initial loading phase where the load rises quickly. The force exerted on the ship structure by the composite shell and fluid are of the same order of magnitude.
The dynamic behaviour of the dome is governed by the rise time of the slamming impulse load. From the seakeeping results it is observed that the rise time of the load is in general above $0.2s$ which results in a very limited dynamic amplification of a factor 1.05 which damps out quickly.
The effect of the dynamic behaviour of the dome is mainly observed in the force transferred through the shell. The fluid pressure load shows less dynamic effects.
The horizontal shell forces are at least an order of magnitude smaller with respect to the vertical forces, however one should note that this may vary when not only looking at symmetric head sea conditions.
The different types of loading results in an increase of the internal pressure. The sonar dome is equipped with an overflow. Due to the small pipe used for this overflow, the reduction of internal pressure within the time frame of the different load components is relatively small. For slamming loads the pressure reduction could be neglected. For wave loading, the internal pressure shows a reduction during of about 20%
The presence of the internal fluid lowers the stress levels in the composite shell. A

reduction of 69% of the maximum stress level is calculated between the dome with and without internal fluid.
The presence of the fluid results in less localized deformations of the dome, which may result in a structure that is less prone to local responses such as buckling.
The location of the internal free surface relative to the dome has an increasing effect on the internal pressure. However this effect seems rather limited since an higher hydrostatic pressure component will be partly compensated by a smaller increase of the uniform internal pressure due to compression of the dome.

5 Response of the hull structure

In Chapter 4 the dynamic response of the dome is studied. The results and conclusions drawn on the dynamic dome analysis will be used to investigate the structural response of the steel hull structure of the bow of the Zr.Ms. Mercuur. The question investigated in this chapter is: *'how is the structural response of the bow structure affected by the additional loads resulting from the dome response'.*
Use will be made of the FE-model of the bow structure as introduced in Chapter 3. At the location of the dome, the loads originating from the dome response will be defined. On the steel part of the bow structure the seakeeping pressure loads will be applied. Since the FE-analysis is linear, a superposition of the separate load cases can be made to study the total response of the bow.
The first part of this chapter focus on the simplifications and loads applied to the bow model. In the second part the response to all described loads is calculated using the structural bow model. This is done to get insight in the locations where the highest stress levels occur and the sign of these stresses, tension or compression. The total response with and without dome load is studied to be able to conclude whether the additional load components from the dome locations results in an increase or decrease of the stress levels. The total load consist of a superposition of the seakeeping loads on steel hull structure and the dome loads, which where derived in Chapter 4. Finally the local response at a structural detail, the brackets at the K-deck, are studied. The contribution of each individual component to the total stress level in these brackets is studied.

5.1 Simplifications

The load will be applied at the dome flange. The applied load is equally distributed over all nodes of the flange. Each of these nodes is loaded with the same nodal force. The unit forces at the dome flange are scaled to result in a total load of 1kN at the boundary conditions.
On the aft end of the dome the composite bulkhead of the dome faces the steel bulkhead of the steel hull, indicated by the yellow line in Figure 5.1. The space between these two parallel bulkheads is filled using wood. Beside the wood there is no physical connection between the two bulkheads. The normal forces transferred via the bulkhead, can thus only be compressive in nature. The seakeeping loads at the dome results in a force component in longitudinal direction. It is assumed that a large part of this longitudinal force component will result in loads at the steel bulkhead. Using the dynamic model from Chapter 4 the total force in longitudinal direction has an amplitude of $202kN$. Applying this load as a uniform compressive load at the steel bulkhead results in a maximum stress level of $31MPa$ in some of the stiffeners directly behind this bulkhead. The observed stress levels are local and do not result in a noticeable contribution in the stress levels around the decks above the dome, which is the area of interest for this research. It is assumed that at least a large part of the loads in longitudinal direction are transferred through the steel bulkhead. Loads in longitudinal direction at the flange are assumed to be relatively small compared to the other load components and are neglected within this study. Only friction allows load transfer in sideward and upward direction at the dome bulkheads. In the current study this friction component is neglected.

5.2 Loads

loads will be transferred at the connections between the sonar dome and the steel hull structure. In Appendix B the general arrangement of the vessel is supplied to provide more insight in the location of the referred decks and frames. The load components considered in this chapter are:

- Vertical flange loads from the sonar dome
- Pressure load from internal pressure of the sonar dome
- Loads in sideward direction from the sonar dome
- Seakeeping loads at wetted hull

The loads are applied on three different locations:

- Dome flange
- K-deck
- Wetted steel hull

The locations are highlighted in Figure 5.1.

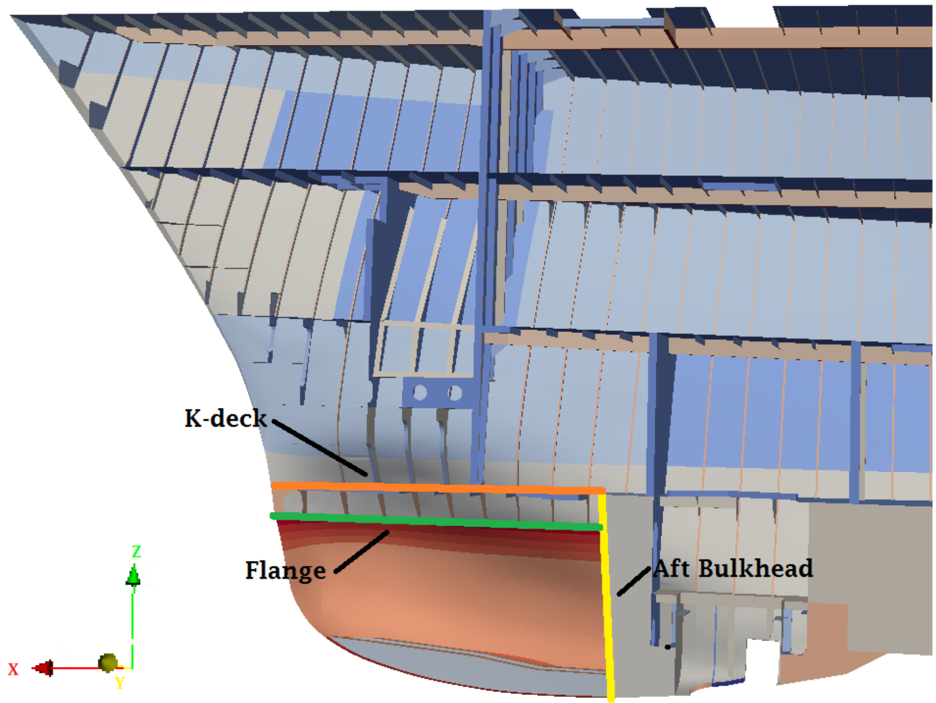

Figure 5.1: Location dome flange, K-deck and aft bulkhead

Dome flange

The dome is connected to the bow structure at the dome flange, the location of this connection indicated by the green line in Figure 5.1. At this location the following force components are applied to the steel flange:

- Vertical flange force, Nz
- Symmetric horizontal flange force, Ny
- Asymmetric horizontal flange force due to sideward dome load, Ny_sideforce
- Asymmetric vertical flange force due to global bending of the dome, GMx

In this analysis this total vertical flange force, Nz is distributed over the nodes of the flange. A unit force of $1kN$ is applied to the structure. This load is shown in Figure 5.2.

The external pressure on the sides of the dome when submerged results in an inward deflection of the dome sides, which results in out of plane shear forces in the dome shell near the flange. Appendix I, Figure I.4 shows this load component. On both sides, PS and SB a unit force of $0.5kN$ is distributed over all flange nodes.
Horizontal forces are introduced in the flange when the loading condition of the sonar dome is asymmetric, as found in oblique waves. This load is shown in Appendix I, Figure I.6.
The global bending load is simplified by introducing a force in z-direction at the flange, on one side in positive direction, and on the other side in negative direction. The flanges on SB and PS are loaded with a total vertical force of $-0.5kN$ and $+0.5kN$, shown in Appendix I, Figure I.10.
The direction of the loads is chosen such as can be expected during a slamming event. Figure 5.2 shows applied load vectors on the structural model for the vertical force. Figures for the other applied loads can be found in Appendix I.

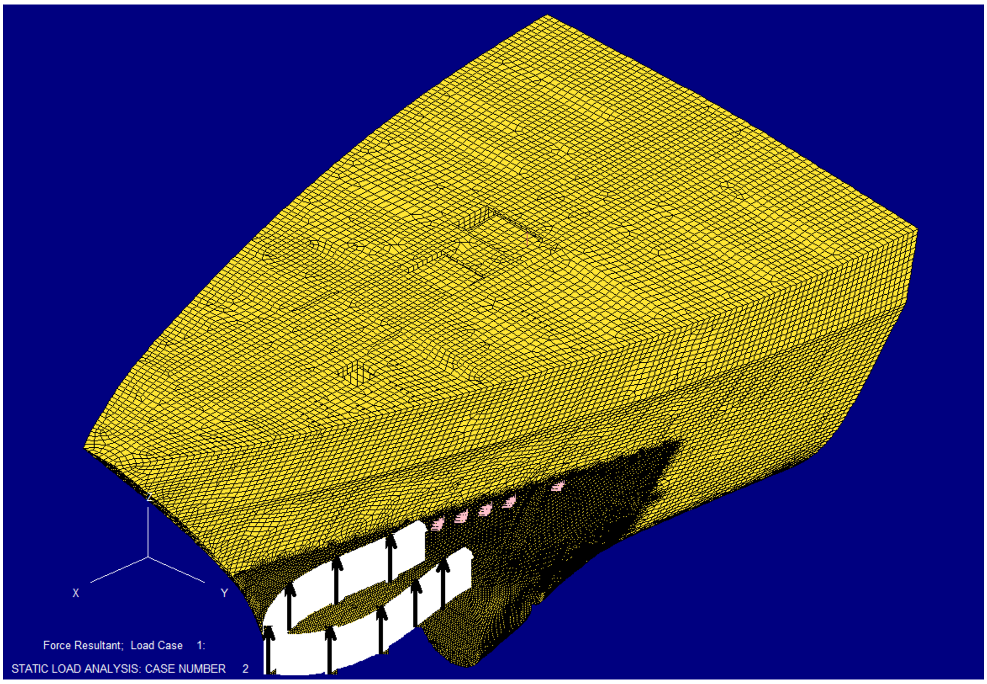

Figure 5.2: Vertical flange load, Nz

K-deck
The lower side of the K-deck, indicated by the orange line in Figure 5.1, is loaded by the internal fluid pressure of the dome. The applied pressure load, 'Press', is illustrated in Appendix I, Figure I.13 and has an unit amplitude of $1.0bar$.

Wetted steel hull
The wetted hull of the model experiences seakeeping loads applied as nodal forces onto the model. The seakeeping and slamming loading at $t = 3.4s$ of the considered slamming event is applied. Note that this load is not scaled to form an unit load.

5.3 Response to the individual load components

In this section the effects of different unit load components on the structural response is investigated. The responses to the individual load components are plotted using the maximum element stresses to get insight the amplitude and sign of the stress levels. Ideally the absolute maximum stresses are used, however this was not available within the program used.

Vertical flange loading, Nz
The response to vertical flange load, shown in Figure 5.2 is presented in Figure 5.3. Based on the load, compressive stresses in the structure directly above the dome are expected, however, positive maximum stresses are observed due to the bending load in the shell elements.
Figure I.3 shows a more detailed plot of the maximum stresses at the K-deck aft of frame 89. In this plot can be seen that the brackets are loaded in compression for this loading condition due to the curvature of the hull.

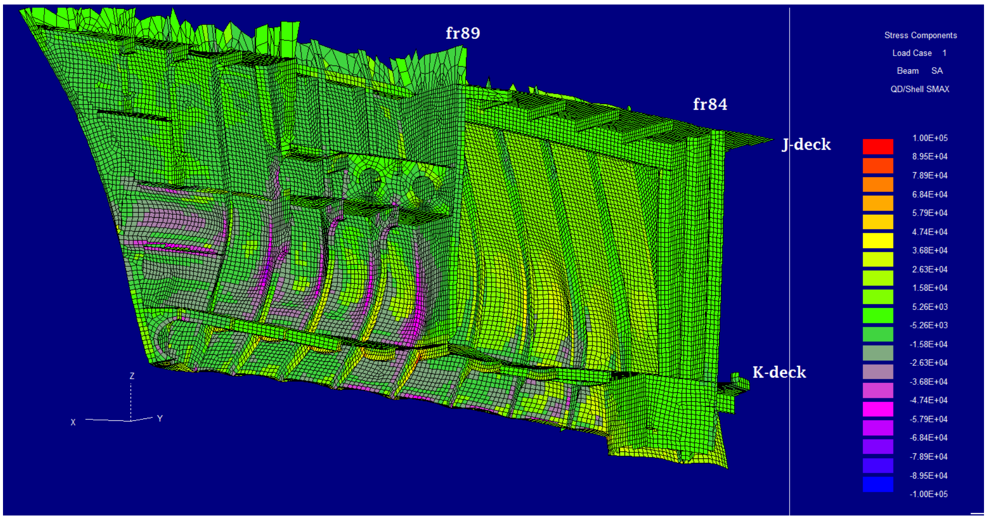

Figure 5.3: Response due to vertical flange load, Nz

Symmetric horizontal loading, Ny
Figure I.5 shows the response to the symmetric horizontal flange forces. The brackets and stiffeners on the K-deck will experience in general compressive loads. Which is a result of the global bending of the K-deck. The response to an unit load of the load component Ny is in general higher when compared with an unit load of load component Nz. However, for head sea conditions this load component is at least an order of magnitude lower compared to the vertical force components.

Asymmetric horizontal flange force due to sideward dome load, Ny_sideforce
Horizontal forces are introduced in the flange when the loading conditions of the sonar dome is asymmetric, as found in oblique waves. This loading results in mostly tension stresses on SB and PS is loaded in compression which can be observed in Figures I.7 and I.8. Compared to the symmetric horizontal load case, the maximum stress level increases for the same total force applied at the nodes from $0.28 MPa/kN$ to $0.34 MPa/kN$.

Asymmetric vertical flange force due to global bending of the dome, GMx
From Figure I.11 can be observed that this global bending moment results in relative high stress levels in the stiffeners on the bottom side of the K-deck. This can be explained by the fact that there are not so many structural members in transverse direction, which results in relative high shear forces in the transverse bulkheads and

stiffeners. Figure I.12 shows that the brackets at the K-deck are loaded in tension on one side and compression on the other side.

Pressure load, Press

The pressure load results in compressive stresses in the structural members above the K-deck, which is shown in Figure I.14. Relative large deflection of the K-deck is observed close to the bulkhead at frame 89. A closer investigation showed that at this location the longitudinal stiffener located at the centreline is discontinued. The effect of this non-continuous longitudinal stiffener will be studied in more detail in the next chapter. Figure I.15 shows the topside of the K-deck with the brackets. From this figure it can be seen that the discontinuity at the longitudinal stiffener on the centreline increases the structural response of the K-deck and the attached brackets.

Seakeeping loads at wetted steel hull

Figure 5.4 shows the middle layer von Mises stresses on all elements. The highest stress levels are found around the deck hull connections at the K- and J-deck, which is shown in more detail in Figure 5.5.
Since the wave load passes the bow, the maximum load varies in space and time. At other time steps during the loading, the location of the maximum stress level may change, however the observed stress levels are lower compared to the ones shown in the selected case at $t = 3.4s$ in Figure 5.4.

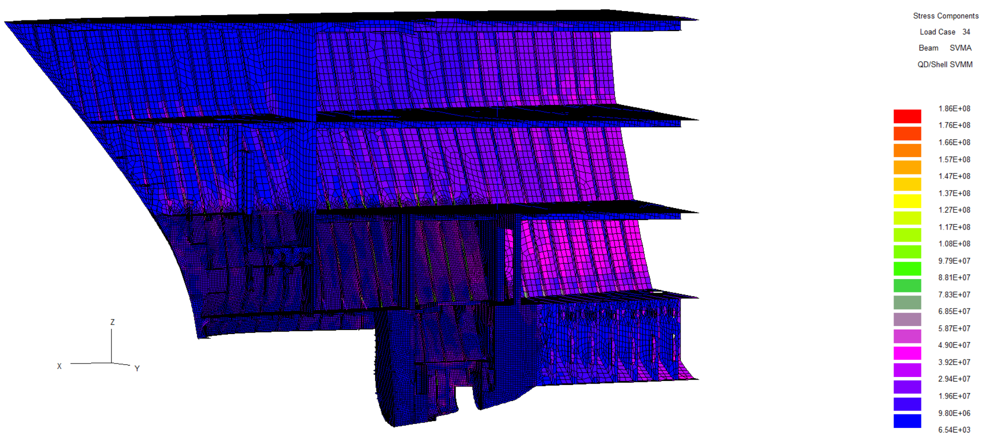

Figure 5.4: Response to seakeeping loads at the wetted steel hull load at $t = 3.4s$, SB half of model

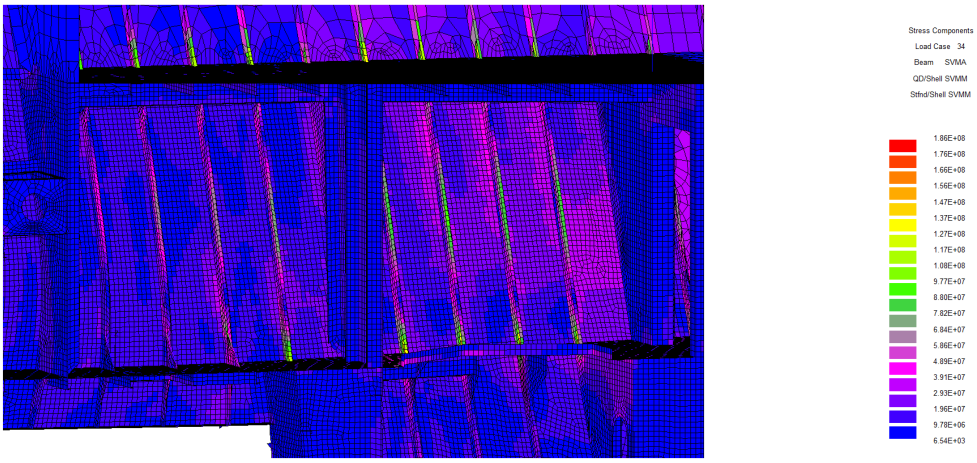

Figure 5.5: Response to seakeeping loads at the wetted steel hull load at $t = 3.4s$, deck-hull connections

5.4 Total structural response

Of interest is the total response of the bow structure subjected to all loading components. Using the total force components from the dynamic dome analysis, loads are imposed on the dome flange and the K-deck. The seakeeping loads are applied at the wetted steel hull. Using the superposition of these loads result in the total stress level in the structure.

Loads
The loads to be used at the dome connection are taken from Section 4.4. The loads shownin Figure 4.39 are used as input for the load history at the dome flange. One should note that the total force is multiplied by two since a full model of the bow structure is used, where a half model of the dynamic dome analysis was used. Within the calculations the response of four load cases are superimposed, the seakeeping loads on the steel bow structure, and the three unit load components at the dome connection. The loads at time $t = 3.4s$ are investigated in more detail since at this time the highest stress levels are observed. The total load consist of the following components:

- Vertical load of $1158kN$ at the flange
- Symmetric side force of $-6.83kN$ at the flange
- Pressure load of $1.0bar$ at the K-deck [1]
- Seakeeping loads at wetted hull

Response
Since the applied loads are fully symmetric, the SB side of the vessel is used to give an overview of the stress levels. Figure 5.6 shows the von Mises stress in the middle layer of the shell elements, thus only reflecting the membrane stresses in the elements. The yellow circles in Figure 5.6 indicate the areas where relatively high stress levels are found which are described below.
Figure 5.7 shows the stresses directly above the sonar dome. It can be observed that the top of the most aftward two brackets shows the highest stress level. The last stiffener on the right hand side of the figure, just before the bulkhead is not supported

[1] The exact geometry and area of the K-deck for the bow model and dynamic dome model differ. Chosen is to keep the total vertical load at the bow model equal to the load calculated using the dynamic dome model. Resulting in lower pressures in the bow model compared to the dynamic dome model.

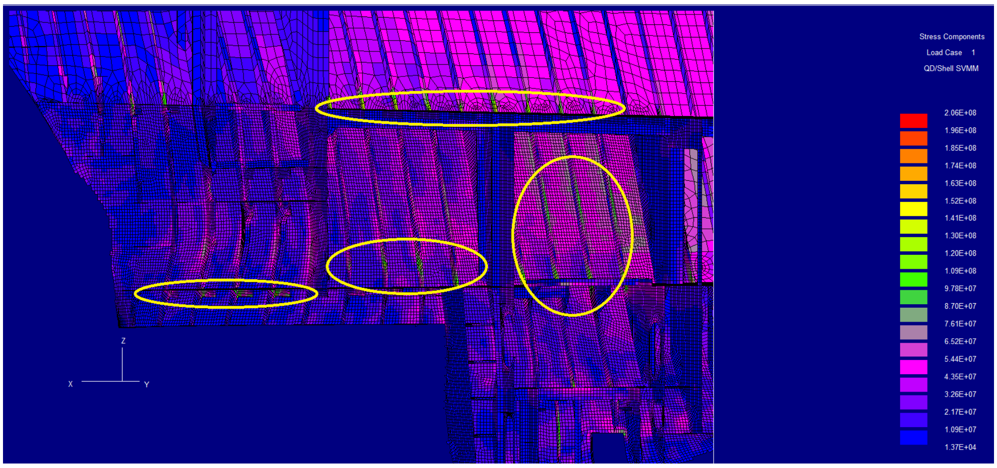

Figure 5.6: Areas with highest response in stress level due to the combined loading

by a bracket in this model, which result in a high stress level directly at the deck connection.

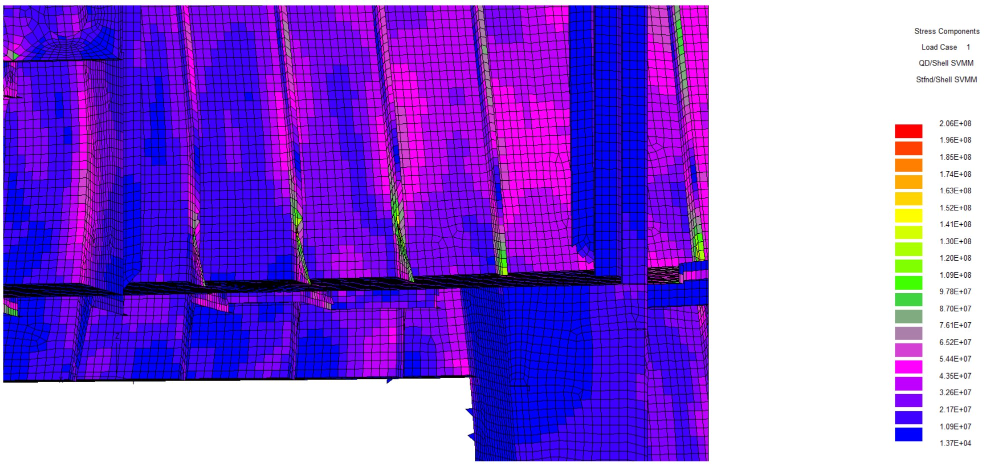

Figure 5.7: Middle layer von Mises stress level close to the K-deck

Figure 5.8 shows the stresses at the stiffeners at the bottom of the K-deck. Here it can be observed that the two stiffeners forward of the bulkhead at frame 89 show high stress levels due to the fact that the longitudinal stiffener at the centreline is not continued up to the bulkhead or even further.
Figure 5.9 show the stress concentration at the topside of the J-deck. At the top side of the J-deck, no brackets are fitted resulting in high compressive stresses in the stiffener flanges.
Figure 5.10 shows the structure directly above the location of the retractable bow thruster, located between frame 79 and 84 in Figure B. The lower part of this structure is relatively stiff due to the support structure of the bow thruster. However the vertical loading has to be introduced in the vertical hull stiffeners. Resulting in high stress levels in the stiffeners at the deck connection. Another aspect observed here is the relative high stresses at mid span of the vertical hull stiffeners. This is a result of the inward curved geometry of the shell, combined with wave pressure load at the hull.
From the analysis of the total response is concluded that the highest stresses are found around the deck hull connections and in the stiffeners on the bottom of the K-deck. In Section 5.6 the contribution of the different load components to the stress

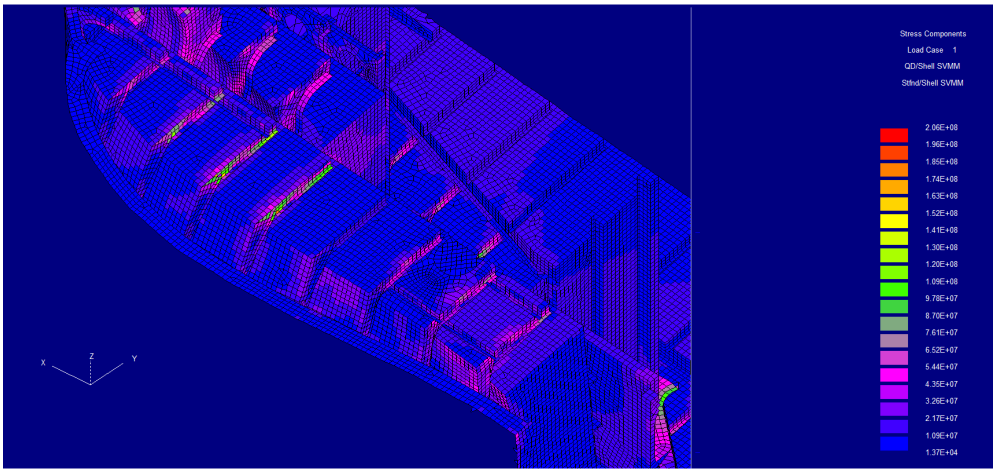

Figure 5.8: Middle layer von Mises stress level seen from bottom side of the K-deck

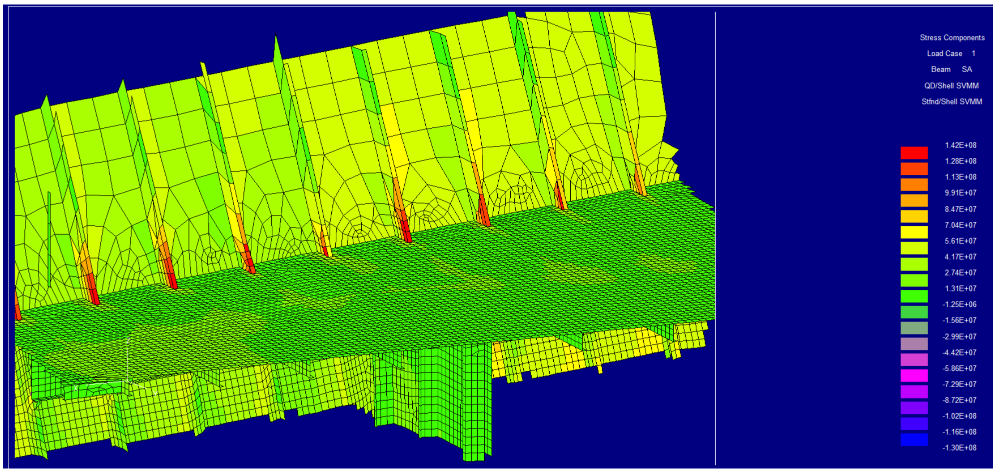

Figure 5.9: Middle layer von Mises stress level stiffener deck connection top side the J-deck

level of this structural detail will be investigated in more detail.

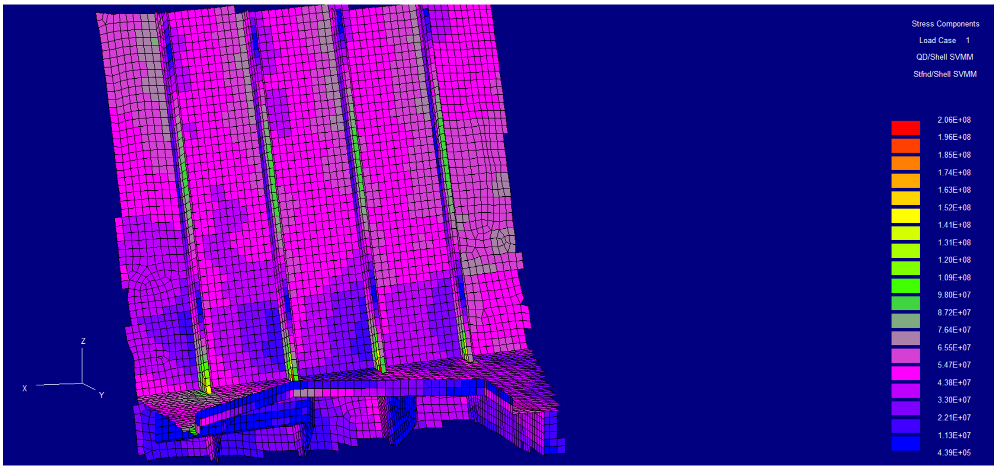

Figure 5.10: Middle layer von Mises stress level hull stiffener connection above bow thruster

5.5 Structural response in oblique sea conditions

In the current study, only cases in head wave conditions are simulated. In [21] it is shown that the total force for bow quartering waves does not lower significantly compared to the vertical force in head wave conditions. This results in a total vertical force that is similar for both conditions. In bow quartering waves it can be the case the total force will be applied to one side of the vessel. Resulting in a asymmetric loading where the load is reduced the at leeward of the vessel, and approximately doubled on the windward side.
Based on the response due to unit loads for the side force *Ny_sideforce* and global bending *GMx* an estimation can be made of the response due to loads in transverse direction at the sonar dome. When assuming that a sideforce may be in the same order of magnitude as the total vertical load observed in head wave conditions, stress levels of $340MPa$ are calculated in the brackets at the K-deck when only applying the sideforce load.
The sign of the stresses in the brackets for the side force load, and global bending loads are the same. Since these loads occur at the same time and in the same direction, the stress levels are increased by this combined load.

5.6 Maximum stress brackets at K-deck

Since the brackets at the K-deck have in general the highest stress levels, the response of these locations are investigated in more detail to determine which loading components contributes to this stress level. The response is calculated for 3 brackets on the SB side of the vessel, since the response is symmetric only minimal differences are observed between PS and SB. The brackets are located on the top of the K-deck and provide the support between the deck and vertical hull stiffeners at frames 86, 87 and 88.
The topside refers to the uppermost part of the bracket at the stiffener connection. The bottom refers to the corner at the connection at the K-deck. The stresses are extracted from the model using small beam element located along the flange of the bracket, functioning as numerical strain gauges. These locations are indicated in Figure 5.11.
The response due to the seakeeping load at the bow is directly calculated using loads at the wetted hull. The response due the dome load is calculated by determining the response for $1kN$ unit loads and scale this response linearly with the actual load level.

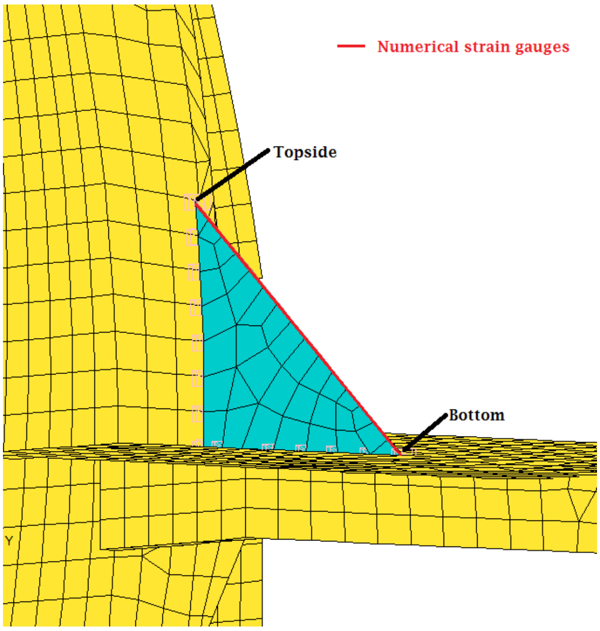

Figure 5.11: Locations at the brackets

In Appendix I an overview is given of the responses to the different unit load cases as defined in Section 5.2.
From the different load cases the maximum stress level in time is calculated for the three brackets at frame 86, 87 and 88 for the top and bottom side. The maximum stress level is listed in Table 5.1. It is observed that the top of the bracket at frame 86 shows the highest stress level.

Table 5.1: Maximum stress levels brackets

Locations	Stress level $[MPa]$
Bracket frame 88 top	-120
Bracket frame 88 bottom	-85
Bracket frame 87 top	-186
Bracket frame 87 bottom	-184
Bracket frame 86 top	-212
Bracket frame 86 bottom	-119

The stress levels of the bracket at frame 86 is studied in more detail. Contributions to the stress level from the seakeeping loading at the bow, internal pressure of the dome, vertical flange loading, horizontal flange loading and total response are shown individually in Figure 5.12. This shows that the largest contributions to the total stress level comes from the seakeeping loads at the wetted hull and pressure at the K-deck. The figures for the other bracket locations are shown in Appendix J. From the figures it is observed that the brackets show a large variation in stress levels. In general can be concluded that the highest contribution to the total stress level comes from the fluid pressure on the K-deck. The maximum loading occurs at the connection between the bracket and hull stiffener. The bracket at frame 86 has the highest total response of $212MPa$. Thee contribution of the different loads components is as follows: 58% by the seakeeping loads at the wetted hull, 32% by pressure on the K-deck, 11% by vertical flange load and -1% by horizontal flange load. A detailed plot of the von

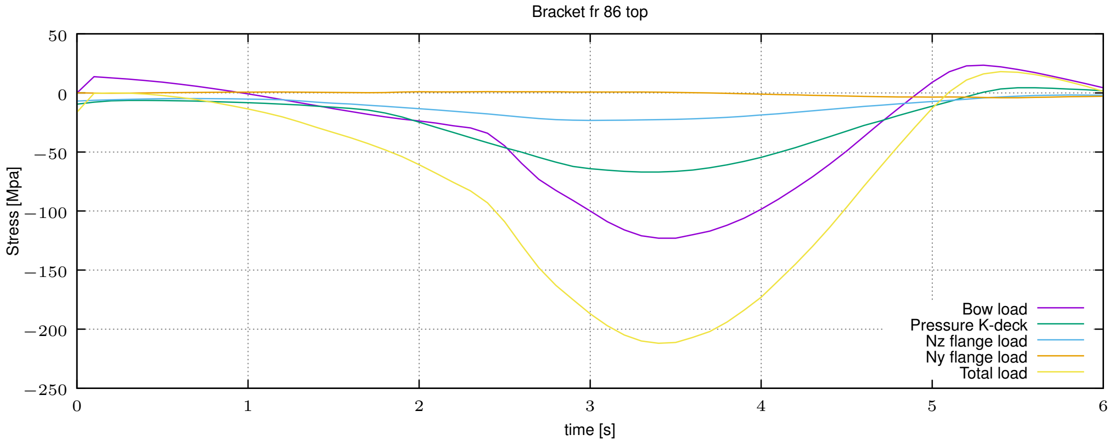

Figure 5.12: Stress components Bracket frame 86 topside

Mises stresses in and around the bracket at frame 86 is shown in Figure 5.13

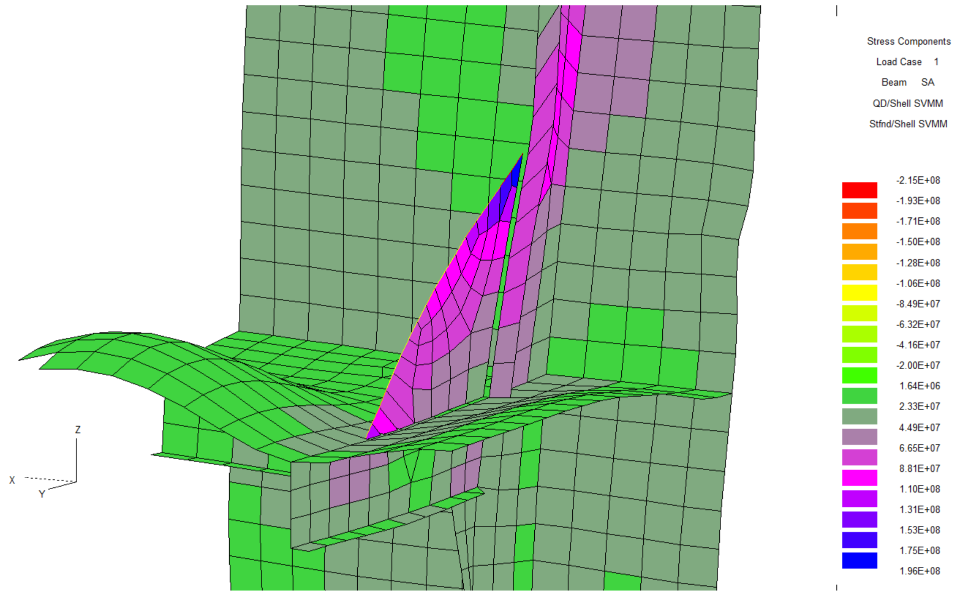

Figure 5.13: von Mises shell stresses and axial beam stresses at bracket frame 86 at $t = 3.4s$

5.7 Conclusion

It can be concluded that the wave loading at the wetted hull structure alone introduces relative high stress levels at the connections between the hull stiffeners and decks. The presence of the sonar dome result in additional load components in the bow structure, a pressure load on the K-deck and forces at the dome flange. These additional loads from the dome results in an increase of the maximum stress level of 42%.
The response of the sonar dome results in a fluid pressure at the bottom of the K-deck. Which results in a vertical load at this deck in positive z-direction. Above the dome, only one bulkhead is fitted. This has as result that the main portion of the vertical load at the K-deck has to be introduced into the outer hull and its vertical stiffeners, resulting in high stress levels in the connections between the K-deck and

the outer hull structure.
The loads at the dome flange results in additional stresses in mainly the outer hull and vertical hull stiffeners. The contribution to the stress level at the brackets on the K-deck seem to be significantly smaller compared to the stresses resulting from the other considered load components. However due to the inward curvature of the hull the vertical loads at the dome flange results in a bending moment in the outer hull and stiffeners, contributing to the stress levels at the connections between the decks and hull stiffeners.
Asymmetric loads, resulting from oblique sea conditions, at the dome flange seem to result in high stress levels when assuming that the total side force may be in the same order of magnitude as the total vertical load observed in head wave conditions. This side force will also introduce a global bending moment around the x-axis resulting in additional load components in vertical direction at the dome flange which results in a further increase of the stress level. The high stress levels are explained by the fact that the asymmetric loading results in high loads in the transverse members, which results in a high shear load in the bulkhead at frame 89 and the transverse stiffeners on the bottom of the K-deck.
The highest stress levels for the considered head sea slamming event are observed in the top of the bracket fitted at frame 86 on the K-deck, with a maximum stress of $212MPa$. The contribution of the different loads components to this stress level is: 58% by seakeeping loads at the wetted hull, 32% by pressure on the K-deck, 11% by vertical flange load and -1% by horizontal flange load. From which is concluded that the seakeeping loads at the wetted hull and pressure load at the K-deck are the largest contributors to the total stress level.

6 Structural response reduction

In Chapter 5 is concluded that the brackets at the K-deck experience high stress levels.
In Section 5.6, the contribution of each loading component to the total stress level at the brackets was shown. In the locations with the highest stress a large contribution due to the pressure load at the K-deck was shown. It will be investigated what the effects of changing the internal fluid pressure on these stress levels are.
To reduce the stress levels at the brackets, modifications of the structure are proposed. Modifications on two different locations will be investigated. The first location is the stiffening on the bottom of the K-deck. The second location consist of the vertical hull stiffeners located between the K- and J-Deck between frame 85 and 89.

6.1 Change internal fluid pressure

Based on the results from Chapter 5 it is assumed that the total response can be reduced by controlling the fluid pressure inside the dome. The effects of changing the internal pressure on the stress level in the brackets is studied.
Appendix J, Figure J.4 shows tat the contribution of the fluid pressure to the stress level at the bracket is about $122MPa$ to the total maximum stress level of $182MPa$, which is 67% of the total stress level. The contribution of the vertical flange load is $24MPa$, which is 13% of the total stress level.
From the analysis of the forces at the boundary of the sonar dome in Section 4.4 a total vertical force of $2105kN$ is derived. Using this total load, 2 load cases are set up. For the first load case a total vertical load of $2105kN$ is applied by a pressure on the K-deck, with a vertical flange load of $0kN$. The second load case consist of a vertical load of $2105kN$ applied at the flange, and a total force by the fluid pressure of $0kN$.

Case 1: The total vertical load applied by fluid pressure

Case 2: The total vertical load applied by vertical flange load

Case 1 results in a contribution of the vertical load to the stress level of $273MPa$ in the brackets. Case 2 results in a contribution of the vertical load to the stress level of $46MPa$ in the brackets. From the two load cases can be concluded that applying the vertical load at the flange results in lower stress levels in the brackets. The reason for this is that the flange load is directly transferred to the outer shell. The vertical load at the deck has to be transferred to the outer shell through the brackets.
A possible solution could be reducing the internal pressure increase in the dome, resulting in a higher loading of the composite shell in order to have a balance in total vertical force. This reduces the stress levels resulting from the vertical dome loads significantly. Reducing or even removing the internal pressure result in higher deformations of the dome, which introduces higher loads at the dome flange. One could design system that is capable of controlling the internal pressure. However one should take in mind when redesigning a sonar dome, with a mechanism that controls the internal pressure, that the reliability of this system should be at least at the level of the structure.

6.2 Modifications to the structure

Another method to reduce the structural response is by modifying the structure itself to reduce the stress levels. The proposed modifications focus on reducing the stress

levels in the brackets at the K-deck. The stress levels of the brackets of the original and modified structures will be compared.
A first review of the structural design of the bow shows that there is one longitudinal stiffener at the bottom of the K-deck which is discontinued between frame 87 and 91. Next to that, between frame 87 and 88 a manhole is fitted resulting in a less stiff deck. These detail result in a deck structure that is relatively flexible around the location of the vertical bulkhead at frame 89. When less loads are transferred to the vertical bulkhead, the loads have to be transferred to the outer shell by the brackets on this deck. Resulting in high stress levels in the brackets.
To reduce the stress level in the brackets, the stiffness of the K-deck is modified by making the longitudinal stiffener continuous. Next to that the thickness of the stiffeners on the bottom of the K-deck is varied.
The second modification is the increase of the stiffeners in the outer hull.
As loading the total combined load case is considered. This load case has been studied in Section 5.4.

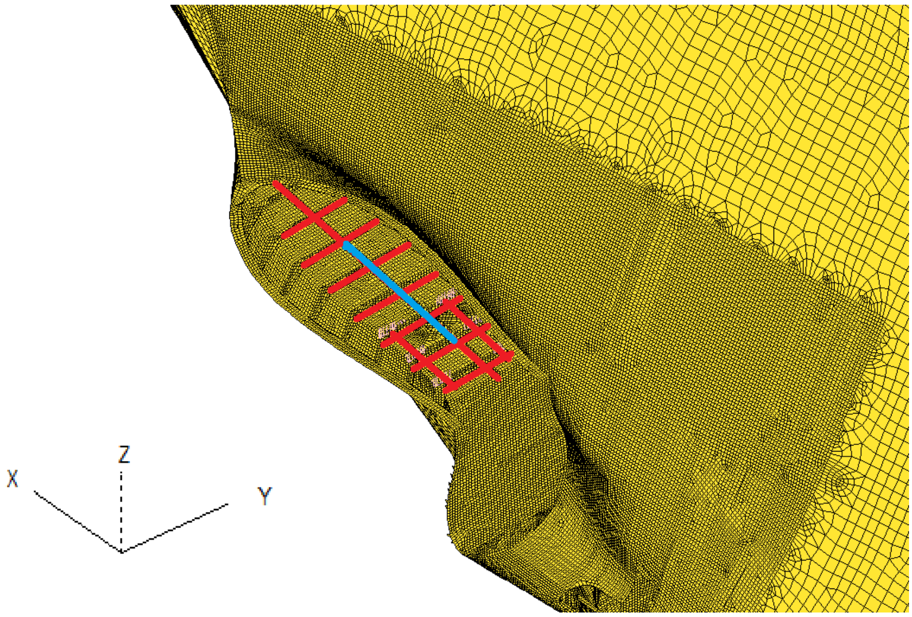

Figure 6.1: Modified stiffeners on bottom side K-deck

Modification stiffeners K-deck

To reduce these stress levels in the brackets, additional stiffening will be applied on the bottom of the K-deck. In Figure 6.1 the part of the longitudinal stiffener that is added is indicated in blue. The stiffeners indicated by the red lines in Figure 6.1 will be modified by changing the thickness for three different cases. The stiffening in the original configuration has a thickness of $7mm$. To investigate the effects of the additional stiffener and thickness variations, the following four cases are compared:

Case 1: Original configuration

Case 2: Configuration with a continuous longitudinal stiffener and original stiffener thickness of $7mm$.

Case 3: Configuration with a continuous longitudinal stiffener and decreased transverse stiffeners, to a thickness of $5mm$.

Case 4: Configuration with a continuous longitudinal stiffener and increased transverse stiffeners, to a thickness of $14mm$.

Table 6.1 shows the results for the four cases. The percentages for case 2 to 4 gives the stress level with respect to the original configuration of case 1. The first observation is that making the longitudinal stiffener continuous reduces the load at the brackets significantly. However, with increasing the thickness of the stiffeners, the stresses at the top of the brackets increase. The modifications of the stiffening at the K-deck has no significant contributions in the stress levels aft of the bulkhead at frame 85 and the outer shell-deck connections at the J-deck.

Table 6.1: Stress levels brackets, modifications of stiffening at the K-deck

Locations	Case 1 $[MPa]$	Case 2 $[MPa]$		Case 3 $[MPa]$		Case 4 $[MPa]$	
Bracket frame 88 top	-120	-66	55%	-113	94%	-71	59%
Bracket frame 88 bottom	-85	-49	58%	-75	88%	-45	53%
Bracket frame 87 top	-186	-105	56%	-186	100%	-114	61%
Bracket frame 87 bottom	-184	-95	52%	-179	97%	-77	42%
Bracket frame 86 top	-212	-150	71%	-211	100%	-158	75%
Bracket frame 86 bottom	-119	-114	95%	-111	93%	-102	86%

A viable solution is to make the longitudinal stiffener at the bottom of the K-deck continuous. This reduces the stress levels in the shell-hull connections. However, not all details about the equipment inside the sonar dome are known and a man-hole is fitted in the deck, a modification of the longitudinal stiffener may not be possible. It is expected that measures that increase the longitudinal stiffness of the K-deck around the location of the bulkhead result in a reduction of the stress levels in the deck-hull connections since a smaller portion of the total vertical load is introduced in the outer shell.

Modifications stiffeners outer shell

The loads at the bow structure causes inward deflection of the hull panels. A possible solutions to reduce these stress levels is by increasing the thickness of the hull stiffeners.

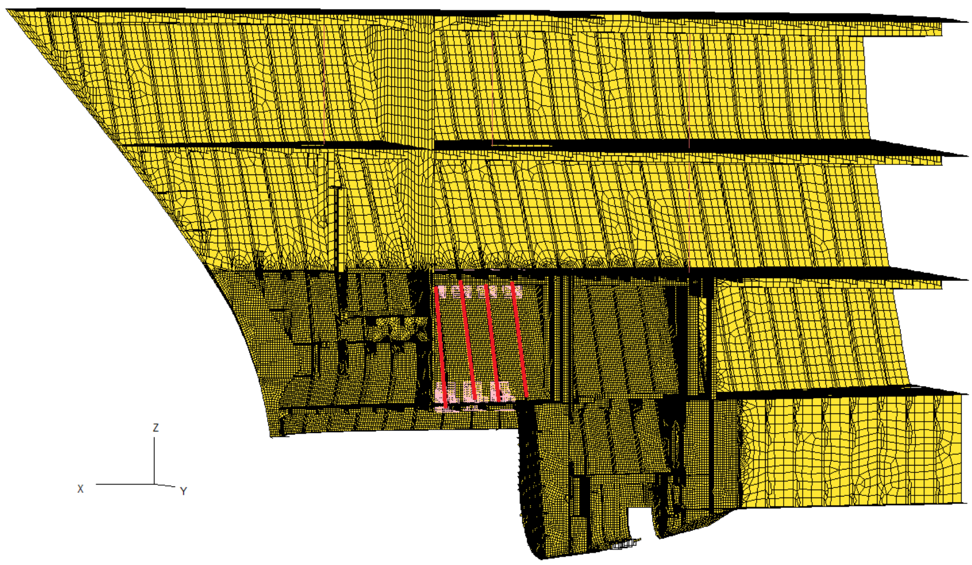

Figure 6.2: Modified stiffeners on outer shell between K- and J-deck

The thickness of the stiffeners between the bulkheads at frame 89 and 85 between the K-deck and J are modified. The stiffeners are a 'HP160x7' profile represented by shell elements with a web thickness of $7mm$ and a flat flange with a thickness of $15.4mm$. The thickness of the webs of the stiffeners are increased from $7mm$ to $14mm$ to investigate the difference in stress level in the brackets. The modified stiffeners are indicated in red in Figure 6.2. The results for the original structure and structure with increased thickness of the stiffener webs are shown in Table 6.2. It is observed that increasing the vertical stiffeners above the K-deck results in a reduction of the stress level at the top of the brackets of at least 29%, and in an increase in the stress level at the bottom of the brackets 8% with respect to the original configuration. The increased web thickness of the stiffeners result in an overall reduction of the stress level. However one should take in mind that the stress level at other locations is increased.

Table 6.2: Stress level brackets, modifications of the hull stiffening

Locations	Original stress level $[MPa]$	Stress level modified structure $[MPa]$	
Bracket frame 88 top	-120	-85	71%
Bracket frame 88 bottom	-85	-92	108%
Bracket frame 87 top	-186	-120	65%
Bracket frame 87 bottom	-184	-189	103%
Bracket frame 86 top	-212	-180	85%
Bracket frame 86 bottom	-119	-121	102%

6.3 Conclusion

It has been shown that the structural response of the brackets above the dome can be significantly reduced by preventing the increase of internal pressure. The response due to vertical flange loading is at least 6 times lower compared to the response due to the internal pressure loading. However, reducing the internal fluid pressure increase the loads at the dome shell and therefore the deformations of the dome, resulting in additional loads at the flange due to the deformations.

To reduce the response resulting from the internal pressure at the K-deck, the stiffening on this deck is modified. The longitudinal stiffener is made continuous. This modification results in a more stiff connection between the deck and bulkhead above, reducing the maximum stress level by 29%. Making the longitudinal stiffener continuous and increasing the thickness of the stiffeners on the K-deck to $14mm$ result in a total reduction of the maximum stress level of 25%.

The seakeeping loads at the wetted hull result in inward deflections of the outer shell. This response is reduced by increasing the web thickness of the vertical stiffening on the hull. This reduces the stress level on the top side of the brackets. However, on the bottom of the brackets the stress levels increase. The overall maximum stress level reduces with 11% for this modification.

7 Discussion

A study was performed to investigate the response of the fluid filled sonar dome and the response of the bow structure of the Zr.Ms. Mercuur in heavy seakeeping conditions.
During this study, seakeeping simulations were performed to determine the loads at the sonar dome and bow structure. A model of the sonar dome was created to study the effect of the fluid inside the dome on the response. From the response of the sonar dome, loads at the connection between the dome and the bow structure were derived. These loads in combination with the seakeeping loads at the wetted hull were applied to the bow structure. The response of the bow was studied with special interest in the stress in the brackets at the K-deck.

The seakeeping analysis of the vessel consists of 5 seakeeping simulations of $300s$ each. These runs were performed for head wave conditions with a significant wave height of $10m$, a peak period of $10.3s$ and a forward speed of the vessel of $5kn$. Out of these results a single slamming event was selected based on the highest slamming load calculated on a part of the bow structure. For this selected slamming event, the loads at the structural models were calculated. As a result of the peculiar distribution of slamming events, which shows a high probability of exceedance for rather extreme events, there is always the possibility of a more severe slamming event. One could expect to find more extreme slamming events when performing more seakeeping simulations in the same or other extreme sea states.
The loads were derived for two different structural models. These are the structural model of the bow excluding the dome and the model of the sonar dome only. The seakeeping pressure loads were mapped on these structural meshes, using forces at the nodes of the elements. Using the selected seakeeping results, 60 quasi-static load cases for the bow model were calculated. The 60 load cases describes a slamming event of $6.0s$.

The load of the considered slamming event results in a mainly static response. However, the rise-time of this slamming load could result in an initial overshoot compared to the static responses. The dynamic response of the dome to different rise-times of the load was studied. The seakeeping simulations showed that the rise-time of the load is generally longer than $0.2s$. The overshoot of the vertical displacement response at the bottom of the dome was less then 5% with respect to the static result for rise-times longer than $0.2s$. The dynamic response of the dome was mainly observed in the force transferred to the bow structure through the composite dome shell. The loads at the dome were calculated with a time step of $0.1s$, this time step is relatively large compared with the rise times of the load. A fast increase of the load with a short duration increases the dynamic response which may be missed due to the time step used. An effect that is note taken into account is the effect of the fluid surrounding the dome when submerged. This fluid acts as an added mass and will lower the response periods further, which may result in a natural period closer to the periods of the loads.
An expansion container is connected to the fluid inside the dome, resulting in the in- and outflow of water from the dome during loading. The equations for the flow rate are derived from pipe-flow theory and implemented in the calculation of the dynamic response of the dome. The outflow of water during loading reduces the increase of

the internal pressure. The maximum outflow of water from the dome is calculated to be 10 litres during the slamming event considered, reducing the maximum pressure increase with only 5%. To prevent any increase in pressure during the slamming event, over 50 litres should flow in and out of the dome, which is the total volume of the expansion container installed.
The expansion container on board of the Zr.Ms. Mercuur has a volume of 50 litres and is filled in static conditions up to a certain level. Outflow volumes from the dome within the order of the container volume results in an overflow of the expansion container, which is not ascertained by the crew in heavy seakeeping conditions. This indicates that the outflow volume is at least significantly smaller compared to the total volume of the expansion container. The 10 litres of outflow calculated for the rather extreme head sea slamming event is possible based on the observations on board. However the actual outflow volume is not known, neither if the considered extreme slamming loading has occurred.
In the initial phase of the slamming event, the pressure rises quickly and the outflow volume is limited due to the short duration. For this stage of the slamming event considered, no noticeable differences were observed for both, the model with the assumption that no fluid will flow out of the dome and the model where the outflow of the fluid is incorporated.
Observing load components with longer periods than the slamming loads, the in- and outflow from the dome reduces the total pressure increase during loading. However this in- and outflow from the dome is not preventing any pressure increase resulting from wave loading. The wave loading will result in a oscillating pressure on the K-deck, possibly resulting in fatigue loading as result of the structural response to this load which is reflected upon later.
The method used to calculate the outflow is based on pipe flow theory, with a friction factor derived from the Moody chart [26]. The Reynolds number is assumed to be constant in the calculations, which allows to include a constant friction factor. Assuming that the flow is fully turbulent shows that the friction factor only varies significantly for a small range of Reynolds numbers. The range where the friction factor changes is for the lowest flow speeds occurring with a small pressure difference over the pipe, which are hardly observed in the considered slamming event. These flows under low pressure differences do not contribute significantly to the outflow volume and the assumption of the constant friction factor should not have a large influence on the total outflow volume.
The presence of the internal fluid lowers the stress levels in the composite shell for the considered slamming event. A reduction of 69% of the maximum stress level is calculated between the dome with and without internal fluid. This is the result of the part of the load that will be transferred by the internal fluid pressure. Altering the fluid pressure, which is reflected upon later, has a serious effect on the stress level in the composite shell.
To investigate the contribution of dynamic effects, the dome response was also calculated using a quasi static method based on the linear responses and changes in volume of the dome. For the slamming event considered, the maximum pressure calculated using the quasi static method is 5% lower compared to the pressures obtained using dynamic simulations. Since the dynamic effects are rather limited, the difference is assumed to be due to the linear response assumption made.
The vertical location of the expansion container relative to the dome has an influence on the internal pressure. The response was calculated for two levels of the expansion container relative to the top of the dome, $0m$ and $5m$. The resulting maximum pressure increase for the slamming event is $0.59bar$ for the $0m$ case and $0.64bar$ for the $5m$ case. The $5m$ elevation of the container results in an overall pressure increase

of 8.5%. The difference in internal pressure is limited since a higher hydrostatic pressure component in the dome fluid is partly compensated by a smaller increase of the uniform internal pressure due to the slamming loading.

The forces at the flange location were calculated to derive the loads to be applied at the steel bow structure. The total vertical force at the upper boundary of the dome is separated into two components: the force due to the internal fluid pressure and the force exerted by the shell elements representing the composite dome structure. Both force components, shell and fluid, are equal in order of magnitude for the design and slamming event considered. In the latest designs of the sonar domes for the Zr. Ms. Mercuur some of the internal stiffeners are removed since these members were assumed to not contribute significantly to the strength of the dome. Expected is that this modification affects the global response of the dome and is expected to result in a slightly higher pressure increase in the dome during seakeeping loading. This pressure increase results in lower stresses in the dome composite and the load at the K-deck will be increased when compared with the model including the stiffeners.
The forces in transverse direction in the dome shell are at least a factor 20 smaller compared to the vertical shell forces. However, one should note that this true for a head wave slamming event only. Asymmetric loads in oblique sea conditions increase the transverse forces significantly. The forces in longitudinal direction are about a factor 10 smaller compared to the vertical load at the dome for head sea conditions. The force in this direction was not studied in detail since it is assumed that the load in this direction is transferred through the bulkhead and not through the dome flange. By calculating the total force at the boundary of the sonar dome model, local effects and distribution of the loads were neglected. Also, the model is clamped at the whole boundary, resulting in a more stiff connection compared to the real bow structure which may increase the total load at the flange location.

The total load at the flange found in dynamic calculations on the dome was applied to the bow model. The total flange load is equally distributed over all flange nodes. The total vertical force due to the internal pressure is applied by a pressure load on the bottom of the K-deck. The exact geometry and area of the K-deck for the bow model and dynamic dome model differ slightly.
The total vertical load at the bow model was kept equal to the load calculated using the dynamic dome model, resulting in slightly lower pressures in the bow model compared to the dynamic dome model.
The application of the loads from the sonar dome and the seakeeping loads to the bow model results in high stress levels in the brackets on the K-deck. The location with the highest stress level is the bracket at frame 86 at the top. The total stress level is $212MPa$ and the contribution of the different loads components is as follows: 58% by seakeeping loads at the wetted hull, 32% by pressure on the K-deck, 11% by vertical flange load and -1% by horizontal flange load.

Oblique sea conditions will result in sideward loads at the sonar dome, leading to asymmetric loads at the dome flange. To estimate the effects of a load in sideward direction at the dome, the assumption was made that the total side force in oblique seakeeping conditions at the dome is of the same magnitude as the total vertical load observed in head wave conditions. A load equal to the vertical load in head sea conditions is used. The sidward loads results into two force components at the flange: a sideways flange load and a global bending moment around the x-axis at the dome. Both load components result in an increase of the stress level at the brackets on the

K-deck. Applying a sideforce equal to the amplitude calculated for the vertical loads at the flange results in a stress level of $340MPa$ due to this side load component only. The high stress levels are explained by the fact that the asymmetric loading results in high shear loads in the transverse members, which results in a high load in the bulkhead at frame 89 and the traverse stiffeners on the bottom of the K-deck. Further research is needed to determine the actual occurring stresses in extreme oblique conditions.

The structural response of the brackets above the dome can be significantly reduced by preventing the increase of internal pressure in the dome. The maximum stress level due to vertical flange loading is at least 6 times lower compared to the response to the internal pressure loading for the brackets considered. However, reducing the internal fluid pressure increases the stress in the dome shell and the deformations of the dome, resulting in additional loads at the flange due to the deformations. The resulting response shifts more towards the results found for an empty dome, the significance of this influence is determined by the extend of the pressure reduction. Based on the results the stress level in the composite dome shell could be three times as high when fully preventing the increase of pressure in the dome fluid.
A few suggestions from modifications of the bow structure are given and investigated. The first suggestion is to modify the stiffening on the K-deck to reduce the response due to internal pressure. On the bottom of the K-deck the longitudinal stiffener is made continuous. This modification results in a more stiff connection between the K-deck and bulkhead above. Reducing the stress levels in the brackets on top of the K-deck significantly, reductions of the stress levels at the considered brackets are between 30% and 50% of the total stress level of the original structure of $212MPa$ for the considered slamming event.
The pressure load at the outer hull results in an inward deflection of the hull panels. This is reduced by increasing the thickness of the vertical stiffening on the hull. The web of the stiffener is increased from $7mm$ to $14mm$ while the flange thickness of $15mm$ is kept constant. This increased web thickness results in a reduction of the maximum stress of 12%. However, on the bottom side of the brackets the stress level will increase with approximately 8%. The overall reduction of the stress level is 8% with respect to the stress level of $212MPa$ of the original structure.

Comparison with previous studies

In [21] a quasi static method is introduced to incorporate the effect of the internal fluid in the dome in the FEM calculations. Comparison of this method with the fully dynamic computation has shown that this method gives a good estimation of the internal pressures as the response is hardly dynamic. However using this linearised approach results in a slight under prediction of the response. Thereby is the outflow of fluid to the expansion container neglected in this method, however this could be easily implemented. Only for the initial phase of the loading this can be neglected. The pressures inside the dome calculated in [21] are expected to be close to the values that would be observed when modelling the full dome including the fluid as performed in the current study.
In [12] a slamming load with a maximum of $5bar$ pressure at the bottom of the dome and a cosine distribution over the height is applied as a design load case. Compared with the seakeeping loads calculated in the current study, this load seem to be an overprediction of the occurring slamming loads. The response for a dome without internal fluid are reported in [12]. From the results observed in the current study it is concluded that the internal fluid lowers the response of the dome. Neglecting the

internal pressure in this report results in a rather conservative approach.
In [10] the buckling load of the dome shell is investigated without internal fluid. The calculations in the current report has shown that the response of the dome shell is less localized when the internal fluid is included. The approach without the internal fluid as used in [10] results in a conservative approximation.

Practical application of this research

A sonar dome introduces loads that should not be neglected when designing the steel bow structure. When designing a sonar dome placed at the forefoot of a new vessel at least the following aspects should be taken into consideration.
The slamming loads show a impact type of character which may results in a dynamic amplification of the response of the sonar dome. For the design considered, the response of the dome was mainly static since the response period was much faster compared to the rise-time of the slamming loads considered. In new designs the response periods should be calculated in order to determine whether the response of the dome may be dynamic in nature. The effect of the internal and external fluid should be taken into account when computing the natural frequencies of the sonar dome. The dynamic response is mainly observed in the loads in the composite shell, and contribute therefore directly to the flange loads.
Seakeeping loads at the dome result in an increase of the internal fluid pressure inside the dome. When connected to the vessels bow structure, the internal fluid pressure is directly applied to the deck above the dome. This pressure load is applied to a deck that would not be loaded in such a way in a normal bow structure without dome. The pressure load at this deck has to be taken in consideration when designing the bow structure around the dome.
The current research has shown that the change of volume method for accounting for the fluid inside the dome gives a good estimation of the internal pressure, however is not conservative. The linear quasi static method is far less computational expensive compared to the dynamic simulations including the internal fluid in LS-DYNA and can also be used with an FE-model of the structure without modelling the fluid, which makes this method most suitable for design purposes. The method for accounting for the outflow towards the expansion container used could be implemented in the linear quasi static calculations. This allows to calculate the pressure increase in the dome for loads with a longer durations, such as non-impulsive wave and acceleration loads. These loads could have significant contributions regarding the fatigue lifetime since the number of occurrence of wave loads is much higher compared with the number of occurrence of slamming events.

Limitations

The seakeeping load cases considered for this study consist of one, rather extreme, condition for head waves. However, maximum responses resulting from this load case are reported but may be not the most severe conditions in general. Using a estimated side force at the dome has shown that the response resulting from oblique seas could be quite large.
The dynamic dome calculations show instabilities when the deformations increase. The problem is avoided since the considered loads and resulting deformations remain small enough to avoid this problem. Looking at other load cases, resulting in larger deformations this problem may arise.

8 Conclusion

The structural response of the sonar dome and bow structure of the Zr.Ms. Mercuur has been investigated. The seakeeping response of the vessel, the (dynamic) response of the sonar dome itself and the response of the steel bow structure have been studied to answer the main research question:
'How does a sonar dome respond to different types of loads and what is the influence of the loads at the dome on the structural response of the steel bow structure in heavy seakeeping conditions?'. A model of the sonar dome including the internal fluid is set up to investigate the response of the dome and calculate the loads at the bow structure. The calculated dome loads and seakeeping loads are applied to the bow model to investigate the stress levels in the steel bow structure.

The seakeeping load at the dome results in deformations of the composite dome shell. Including the internal fluid in the model results in a reduction of these deformations. The reduced deformations results in a large decrease of the stresses in the composite shell. For the slamming event considered the maximum stress level showed a reduction of 69%. The seakeeping loads result in an increase in the pressure of the fluid inside the dome. The relatively long duration of the seakeeping loads and its rise-times compared to the natural response periods, result in a nearly static response for the load cases considered.

The internal fluid is allowed to flow in and out of the dome to an expansion container. During the initial phase of the loading the outflow is not large enough to result in a notable difference of internal pressure increase in the dome. Therefore the assumption that no fluid flows out of the dome is valid. However for loads with longer durations the internal pressure reduces due to the outflow of water in time. The from the seakeeping simulations selected slamming event results in a maximum outflow volume of 10 litres. This outflow volume reduces the maximum internal pressure increase with 5%.

The loads at the dome result in forces on the steel hull structure. The combination of the composite dome shell loads and internal fluid pressure loads results in a decomposition of the total vertical load over these two components. The total force in the dome shell and the total force exerted by the fluid on the steel bow structure are roughly equal in magnitude. The forces in the dome shell are transferred via the flange to the bow structure. The internal pressure results in a pressure load on the K-deck of the steel bow structure.

The loads transferred from the dome to the bow structure results in additional stresses in the structural members. The pressure loads on the K-deck results high stress levels in the brackets located directly above the dome. The contribution of the pressure load at the K-deck to the maximum stress level is 32%. The contributions of the flange loads to this stress level is 10% and the remaining 58% is due to the seakeeping loads at the whole bow.

Especially the seakeeping loads and internal pressure results in high stress levels at the brackets at the K-deck. Modifications of the bow structure are proposed in order to reduce these stress levels. On the lower side of the K-deck at the centreline the longitudinal stiffener which is discontinuous in the original design is made continuous.

Resulting in a more stiff connection between the deck and the bulkhead fitted above. This modification results in a reduction of 25% of the maximum stress level.

Seakeeping loads result in inward deflection of the hull panels. This response is reduced by increasing the web thickness of the vertical hull stiffeners from $7mm$ to $14mm$ while the flange thickness is kept constant at $15mm$, the webs and flanges represent a HP bulb profile. This modification results in a reduction of 11% of the maximum stress level of $212MPa$.

To conclude, the presence of a sonar dome in a bow structure results in additional load components at the bow structure. These components introduce forces at the dome flange and a pressure load on the K-deck. This results in an increased stress level of the structural elements directly above the dome, where the contribution of the internal pressure to the stress levels is most relevant. The maximum stress level in the bow structure shows an increase from $128MPa$ to $212MPa$ when the loads are included. Vessels without a sonar dome do not have a deck in the forefoot of the vessel that is highly loaded by a fluid pressure. There will be less load transfer between the decks and outer shell, when the deck is not loaded vertically. The seakeeping pressure will still load the outer hull. However, normally, many transverse frames are fitted at the forefoot of a vessel to transfer the load at the forefoot into the bow structure.

8.1 Recommendations

Full scale validation

To validate the calculated pressure, full scale measurements of the pressures inside the dome have to be performed under seakeeping conditions. The outflow of fluid into the expansion container has to be measured as well to tune the parameters used in the outflow model, this could be done by measuring the flow to the expansion container for different pressure differences between the dome and container. The pressure inside the dome is simulated using a FE model including the internal fluid and a method to compensate for the outflow of water to the expansion container is applied. The pressure increase shows to be the main contributor to the stress levels in the structure when looking at the loads originating from the response of the sonar dome. In order to validate the relation between the pressure loads at the K-deck and the stress levels in the structure, stain measurements should be performed.

Less extreme sea conditions

The response to a rather severe hydrodynamic load which includes slamming is studied. Less severe wave loading results in an increase of internal pressure in the dome as well, which is not fully prevented by the outflow of water to the expansion container. It is recommended to calculate the increase of internal pressure for different wave conditions to calculate the contribution to the fatigue lifetime due to this internal pressure loading.

Seakeeping simulations to derive extreme loads

More seakeeping simulations have to be performed to be able to derive a load case that will describe a maximum response which require on to account for slamming. Slamming shows a statistical distributions that is highly non-linear resulting in a relative high probability for relatively high responses.

Sideward loads at the dome

Focus was on head sea conditions resulting in symmetric loads at the bow and sonar dome. Assuming that sideward loads at the dome in oblique sea conditions are in the same order of magnitude as the total vertical load at the dome in head sea conditions showed rather high stress levels. It is recommended to study the response of the dome and bow structure for oblique sea conditions.

9 References

[1] John M. Brett. Numerical modelling of shock wave and pressure pulse generation by underwater explosions. *Defence science and technology organisation, Australia*, 09-09-1998.

[2] Holland Composites. Interio sonar dome. http://www.naval-technology.com/contractor_images/23825/images/212791/large/inside-dome-lrg.jpg. Accessed: 12-01-2016.

[3] Livermore Software Technology Corporation. *LS-DYNA® Theory Manual*, 27-12-2015. revision 7046.

[4] Livermore Software Technology Corporation. *LS-DYNA® Keyword User's Manual*, May 2007. revision 7163.

[5] W.E. Cummins. The impulse response function and ship motions. *David Taylor model basin*, 1962.

[6] A. de Boer, M.S. van der Schoot, and H. Bijl. Mesh deformation based on radial basis function interpolation. *Computers and Structures*, 85(11 - 14):784 – 795, 2007. Fourth {MIT} Conference on Computational Fluid and Solid Mechanics.

[7] Odd M. Faltinsen. Impulsive pressure loading and response management. In *International Ship and Offshore Structures Congress 2012*, 2012.

[8] Odd M. Faltinsen, J. Kvalsvold, and J. van Aarsnes. Wave impact on a horizontal elastic plate. *Marine Science and Technology*, 1997.

[9] Odd M. Faltinsen, Maurizio Landrini, and Marilena Greco. Slamming in marine applications. *Journal of Engineering Mathematics*, 48(3-4):187–217, 2004.

[10] Peter Globevnik. Sonar dome lcf/m-fregat knikberekening. Report, Solico, DMO/Martech, 10-06-2001.

[11] Peter Globevnik. Analyse van scheepsflens voor sonardome, effect van extra geplaatste knieën. Report, Solico, DMO/Martech, 26-07-2007.

[12] Peter Globevnik. Modificatie sonardome. Report, Solico, DMO/Martech, 26-07-2007.

[13] Owen F. Hughes and Jeom Kee Paik. *Ship Structural Analysis and Design*. Society of Naval Architects and Marine Engineers (SNAME), 2010.

[14] J.M.J. Journee and W.W. Massie. *Offshore Hydromechanics*. Delft University of Technology, 2001.

[15] Livermore Software Technology Corporation (LSTC). Ls-dyna website. http://www.lstc.com/products/ls-dyna. Accessed: 24-02-2016.

[16] Martec Limited. *Trident FEA 2004 Users's Manual*, sm-04-06 edition, August 2004.

[17] L. Olovsson, M. Souli, and I. Do. Ls-dyna ale capabilities (arbitrary-lagrangian-eulerian) fluid-structure interaction modeling. Livermore Software Technology Corporation, 07-01-2003.

[18] Gijs Portengen. De boeg inclusief de sonardome van hr.ms. van nes komt los van de golven tijdens een storm op zee. (foto: still uit film van de koninklijke marine). http://marineschepen.nl/dossiers/images/storm-op-zee-m-fregat-van-nes.jpg. Accessed: 12-01-2016.

[19] Gijs Portengen. Figure: Op het droge in den helder. http://marineschepen.nl/schepen/images/PICT0112kl.jpg. Accessed: 12-01-2016.

[20] J. Tuitman. *Hydro-elastic response of ship structures to slamming induced whipping*. Phd thesis, TU Delft, TNO, 2010.

[21] J.T. Tuitman. Effect of sonar dome on response of bow structure under hydrodynamic loading. 2012.

[22] J.T. Tuitman. *User manual Hydro Elastic Tool Set*. TNO, May 13, 2001.

[23] J.T. Tuitman, T.N. Bosman, and E. Harmsen. Local structural response to seakeeping and slamming loads. *Marine Structures*, 2013.

[24] K. Tuomo, R Sakari, and R. Antti. Mv estonia accident investigation. 1995.

[25] Bureau Veritas. Hydrostar, 14-12-2014. hydrodynamic software developed by Bureau Veritas.

[26] Frank M. White. *Fluid Mechanics*. Mc Graw Hill, 2010.

A Research overview

B General Arrangement Zr. Ms. Mercuur

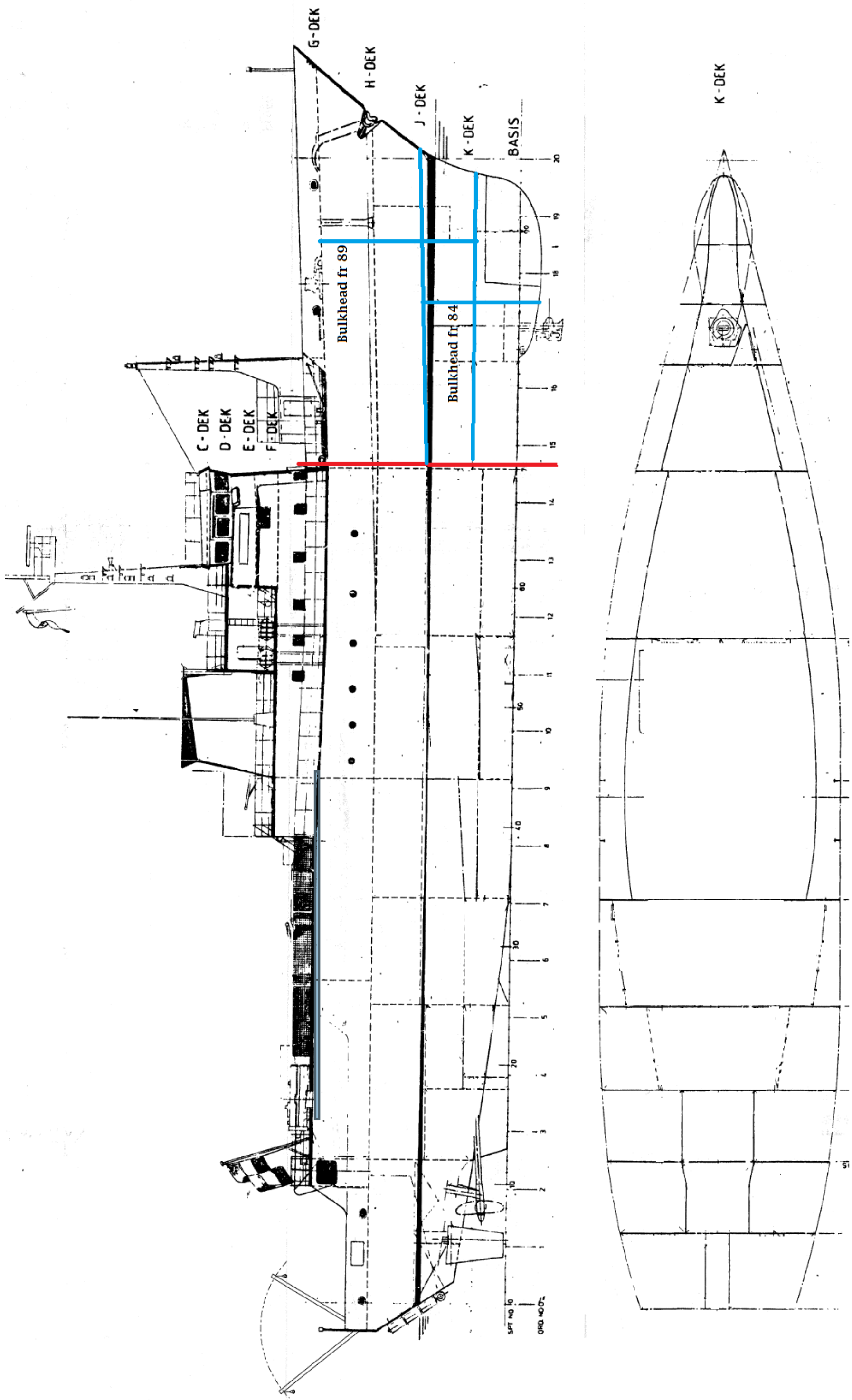

Figure B.1: General Arrangement

C Seakeeping Results

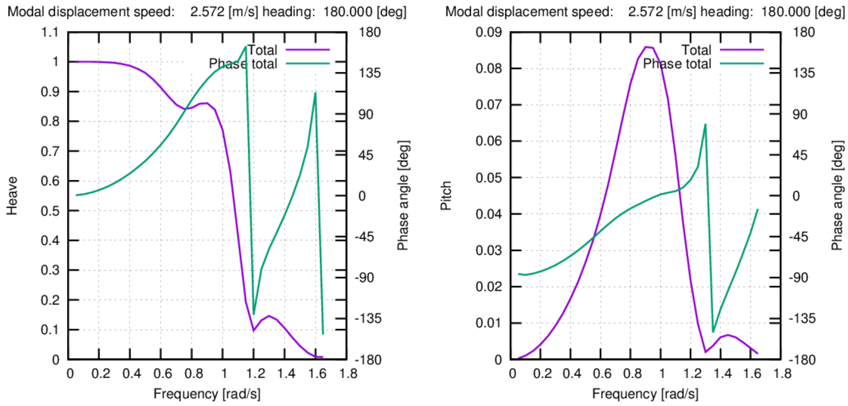

Figure C.1: Linear seakeeping frequency response, heave and pitch

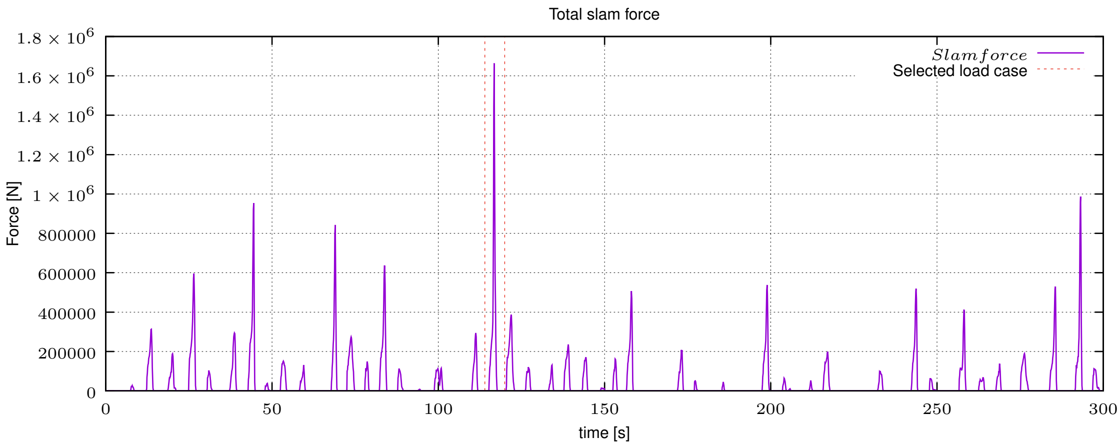

Figure C.2: Slam force from seakeeping simulation

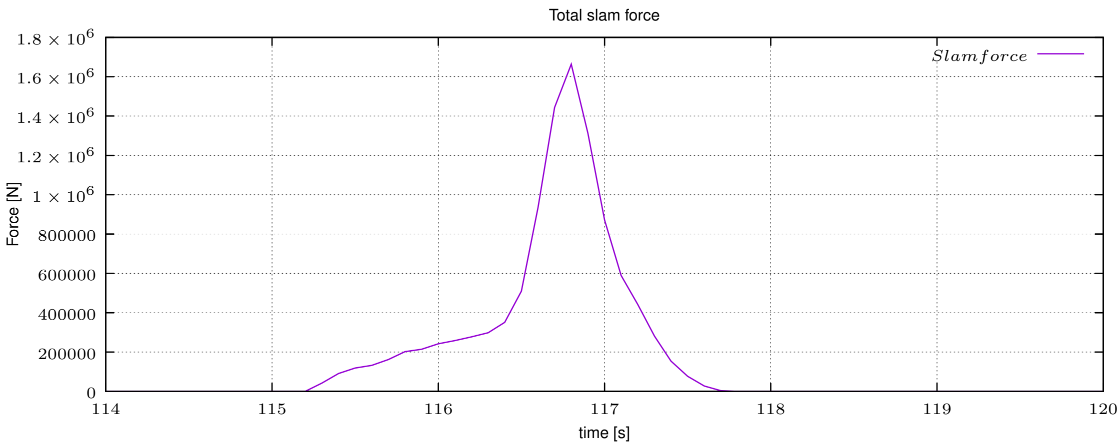

Figure C.3: Slam force from seakeeping simulation, selected load case

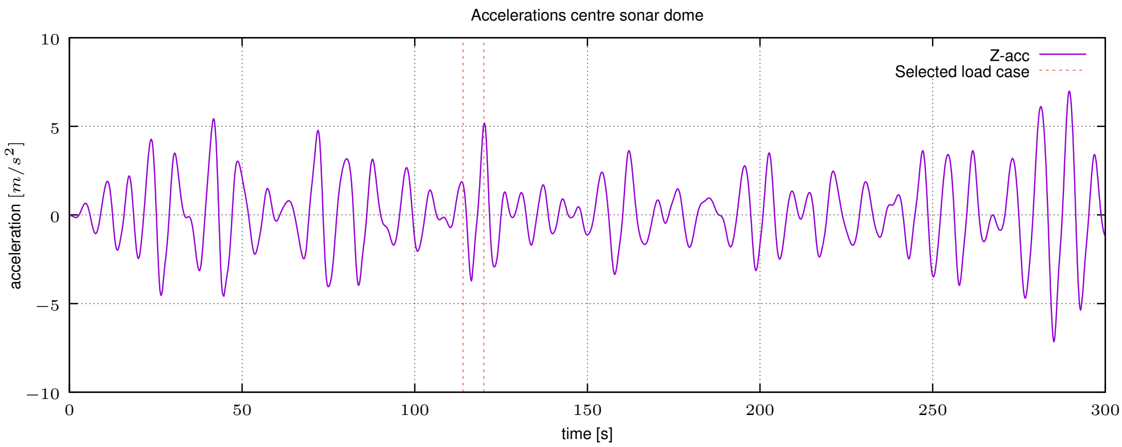

Figure C.4: Acceleration levels at centre sonar dome

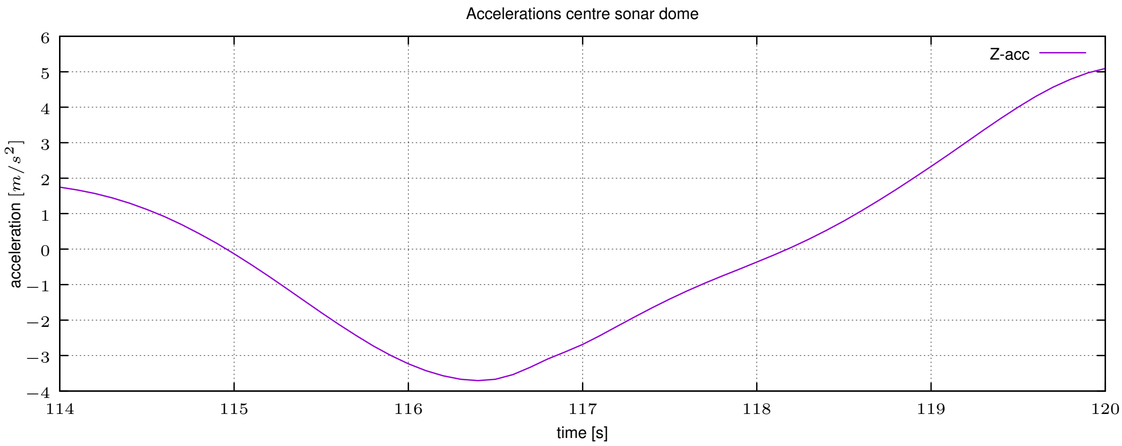

Figure C.5: Acceleration levels at centre sonar dome within selected load case

D Comparison ALE vs Langrangian

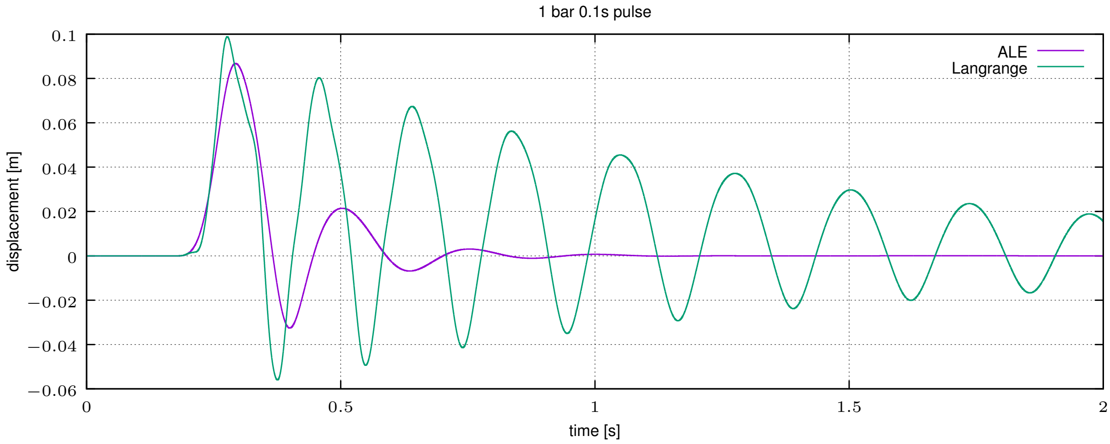

Figure D.1: Vertical displacement node 218, comparison ALE vs Langrangian formulation

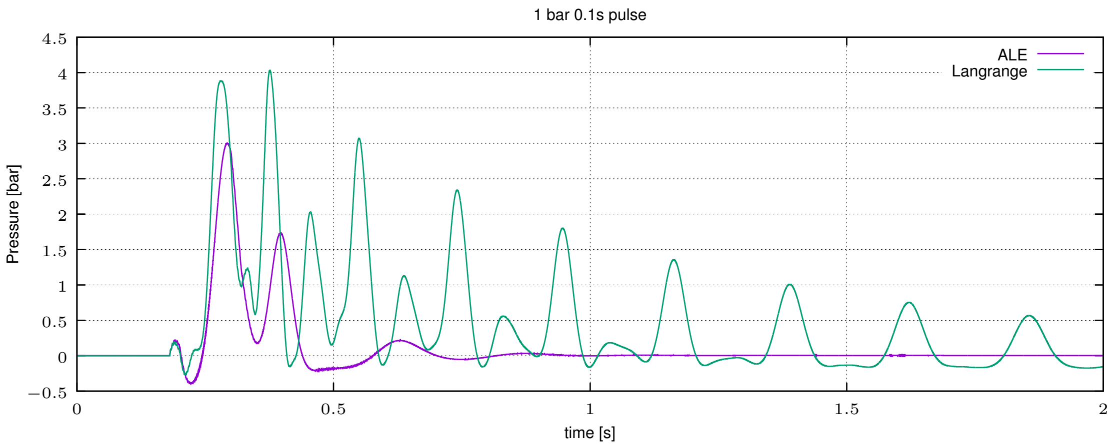

Figure D.2: Internal pressure, comparison ALE vs Langrangian formulation

E Mesh generation using RBF interpolation

This appendix describes the method where the Radial Basis Function is used to interpolate the internal nodes of the deformed mesh. This method is derived from [6]. First the geometry of the dome is derived from a existing geometrical model of the vessel. This geometry is reduced to a set of nodes describing the contour of the geometry. The points used for de sonar dome of the Mercuur are shown in E.1.

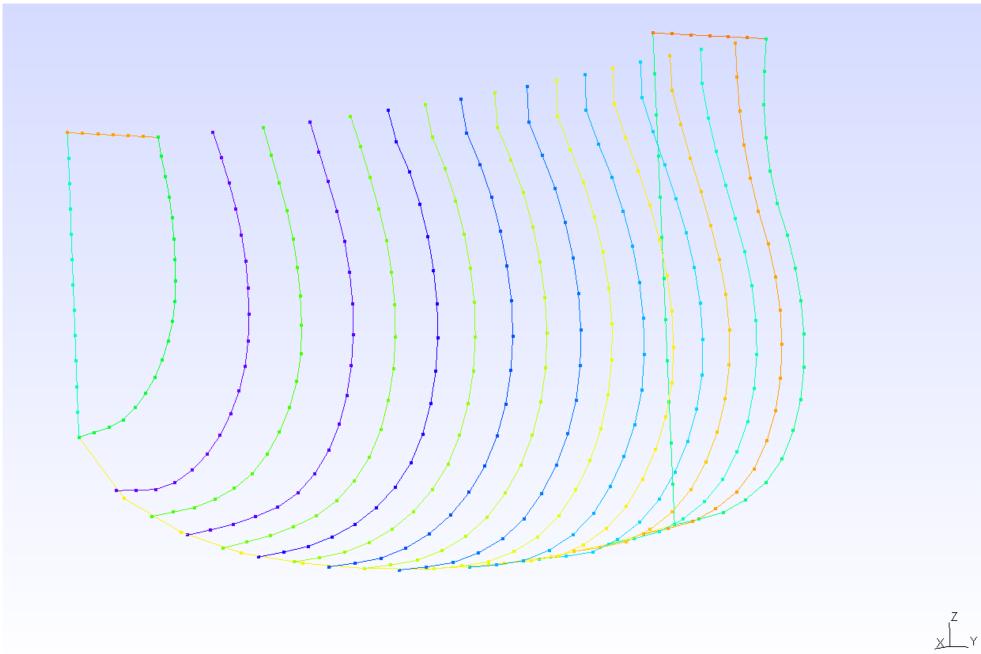

Figure E.1: Dome geometry boundary points

Secondly a simple shape is generated to create a 3D structured mesh. In this case a box shape is chosen which largely overlaps the sonar dome. This box is illustrated by Figure E.2

The nodes at the boundary of the 3D box mesh are relocated using a connectivity matrix relating these nodes to the nodes in the dome geometry file. These boundary nodes will form the constrains of the RBF interpolation method to relocate the nodes without a prescribed location.

The function used within the RBF is the Thin Plate Spline (TPS) given by Equation E.1 where x represent the nodal coordinates. The TPS is implemented in the radial basis function $s(x)$ given by Equation E.2.

$$\phi||x|| = ||x||^2 \ln ||x|| \tag{E.1}$$

$$s(x) = \sum_{j=1}^{Nb} \gamma_j \phi||x - x_{bj}|| + q(x) \tag{E.2}$$

Where:

Nb	Number of boundary points
γ	is a set of mapping coefficients
$q(x)$	linear pronominal given by: $c0 + c_x x + c_y y + c_z z$

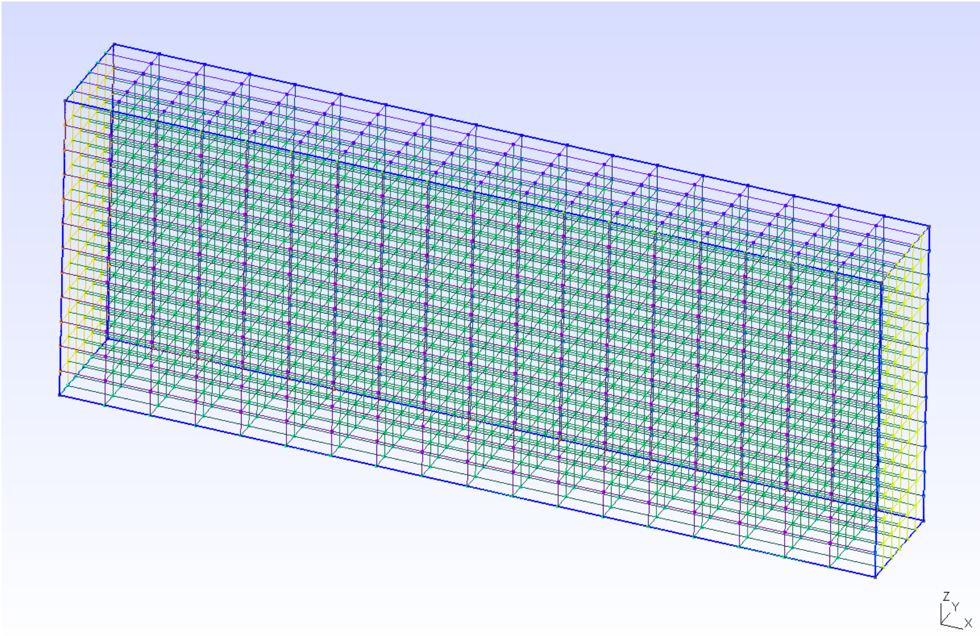

Figure E.2: Dome box mesh

To recalculate the internal nodes the mapping coefficients γ and the polynomial coefficients from $q(x)$ are calculated. This is done by solving the system of equations for the boundary nodes. The internal nodes can be easily repositions using the obtained coefficients by evaluating Equation E.2 for each node.
The result is a reshape 3D mesh representing the sonar dome as shown in Figure E.3.

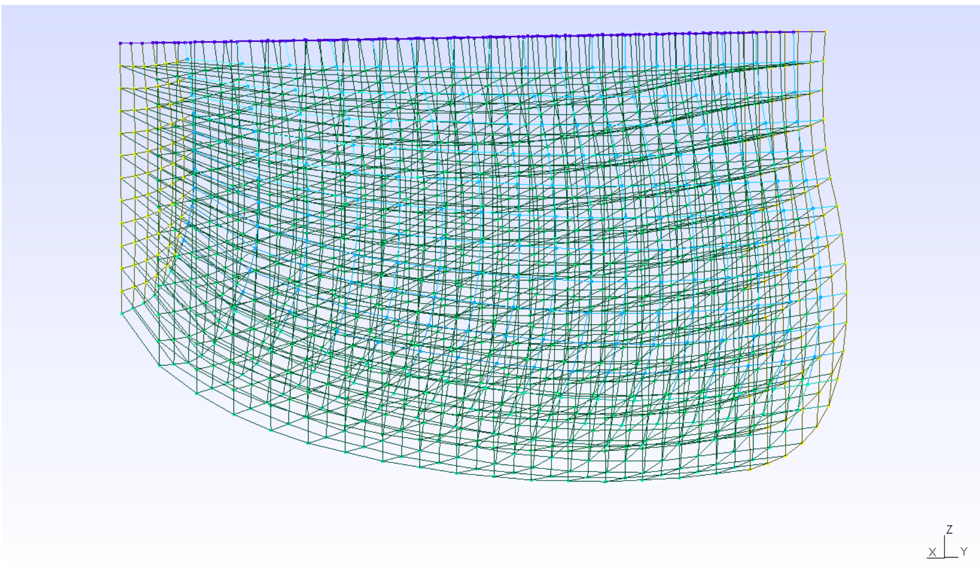

Figure E.3: 3D sonar dome mesh

F Deformations 3D dome models

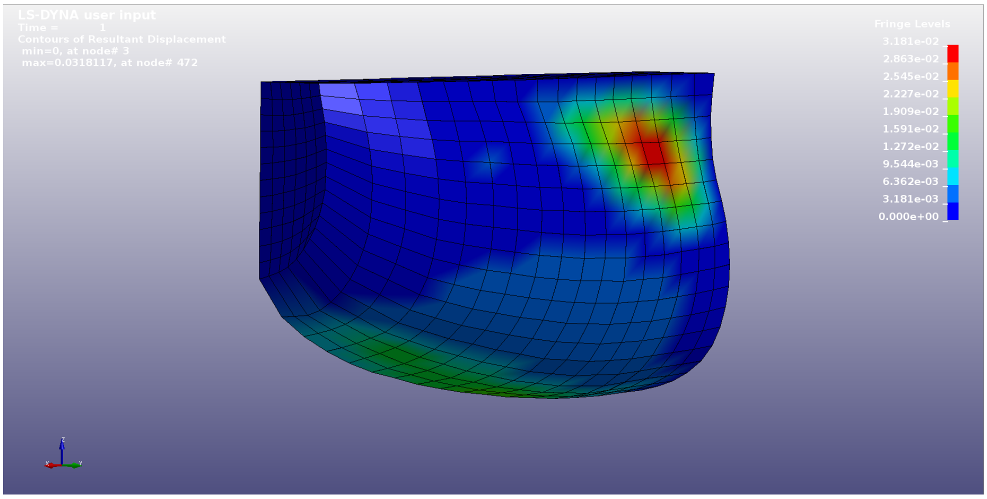

Figure F.1: Maximum displacement in static condition, without internal fluid

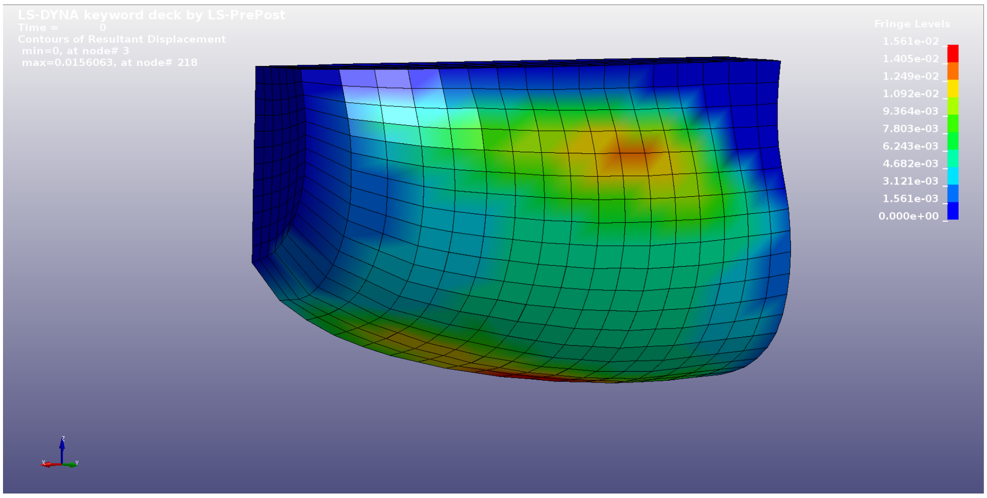

Figure F.2: Maximum displacement in static condition, with internal fluid

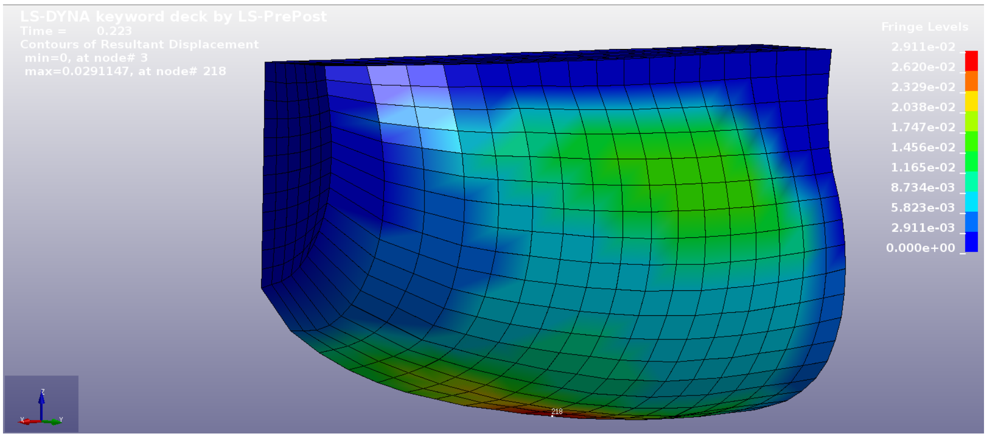

Figure F.3: Maximum displacement dynamic, with internal fluid

G Outflow calculations

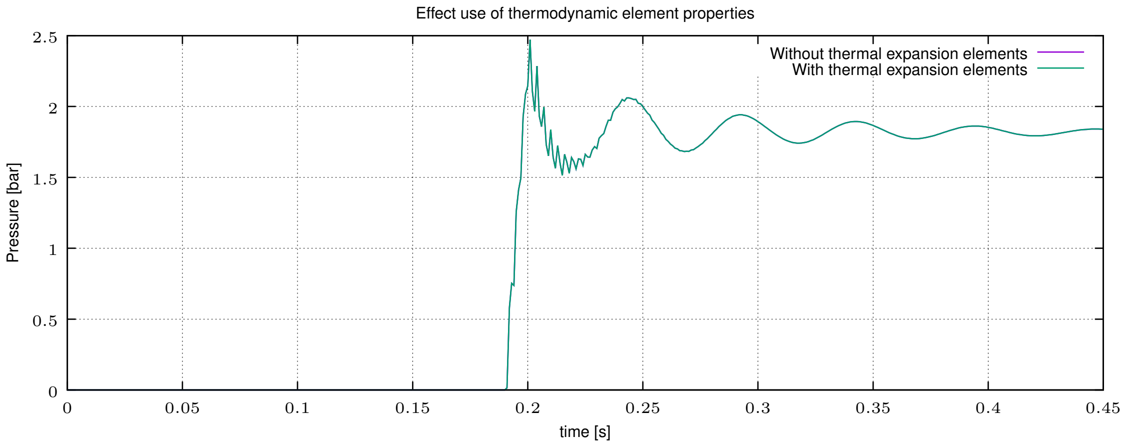

Figure G.1: Comparison model with and without thermodynamic elements

Results including overflow for different rise times

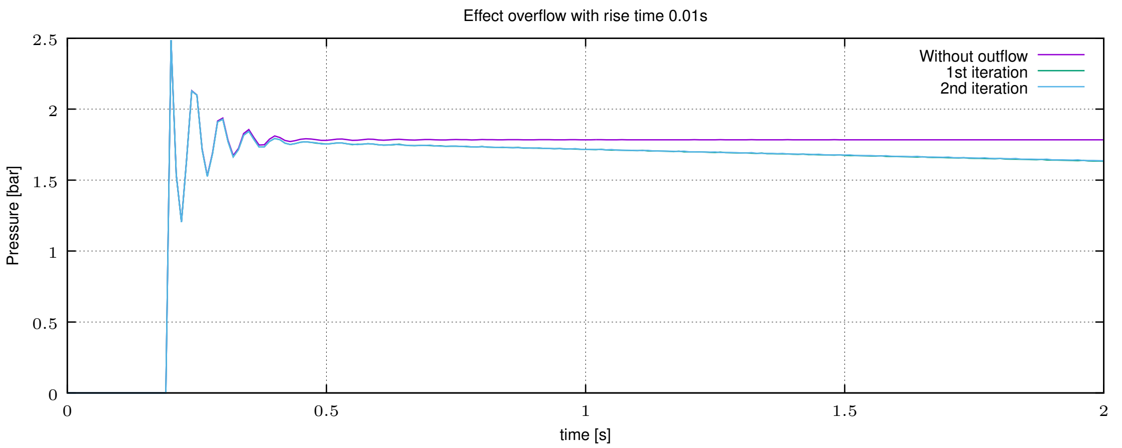

Figure G.2: Influence overflow on internal pressure, with a load rise-time of 0.01s

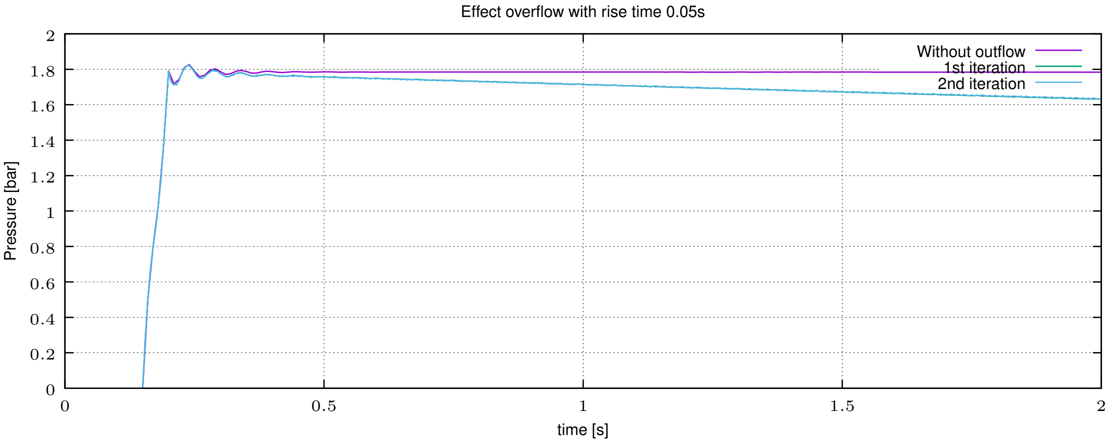

Figure G.3: Influence overflow on internal pressure, with a load rise-time of 0.05s

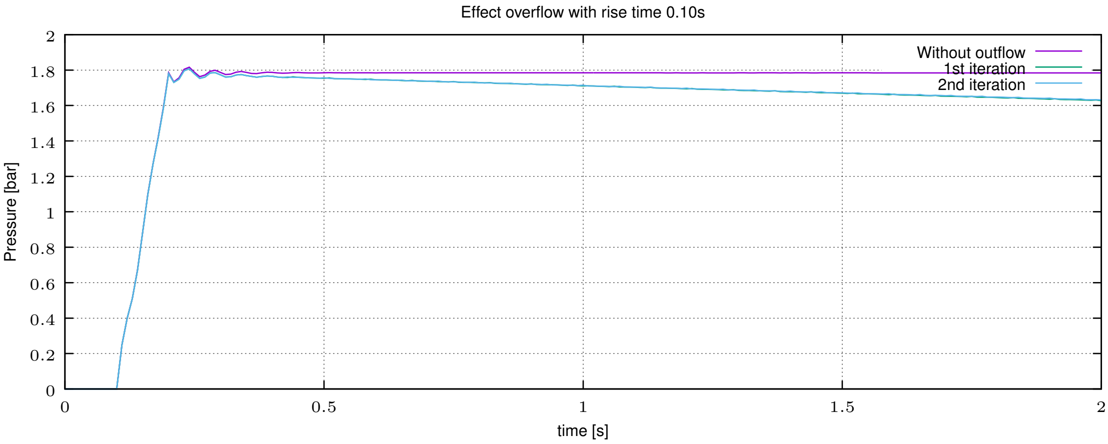

Figure G.4: Influence overflow on internal pressure, with a load rise-time of 0.10s

Wave loading including overflow

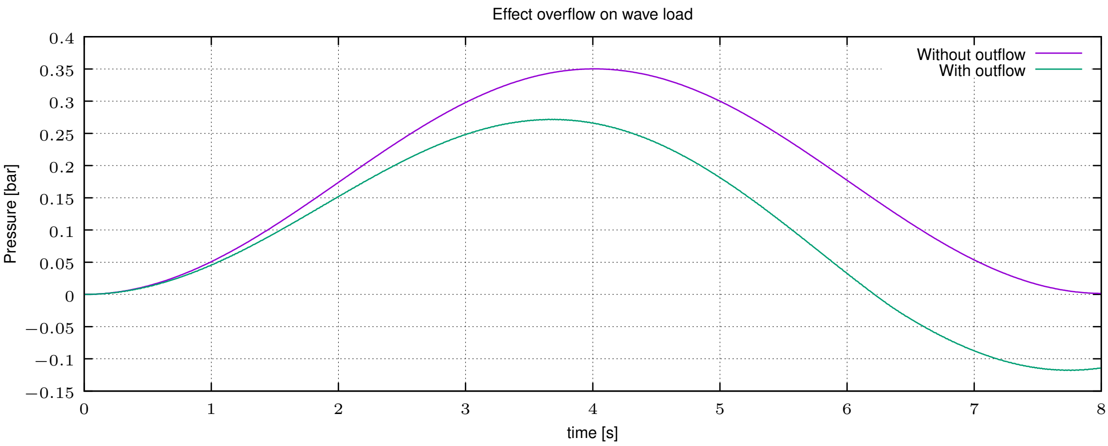

Figure G.5: Influence overflow on internal pressure for wave loading

H Dome stress

The figures show the maximum von mises stress of each element. On the right hand side of each figure the actual position of the vessel relative to the wave surface is shown.

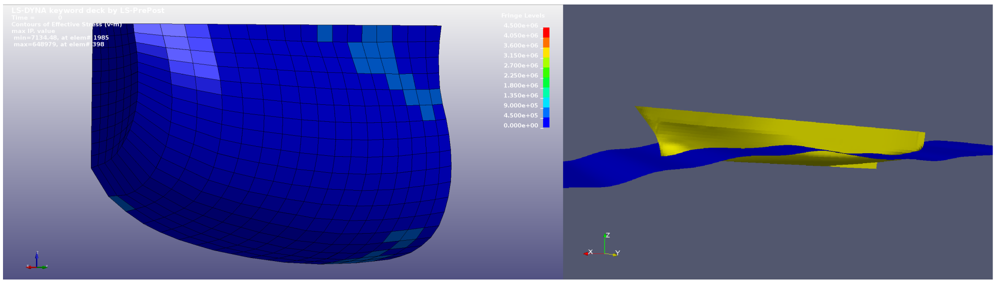

Figure H.1: Domestress, t=0s

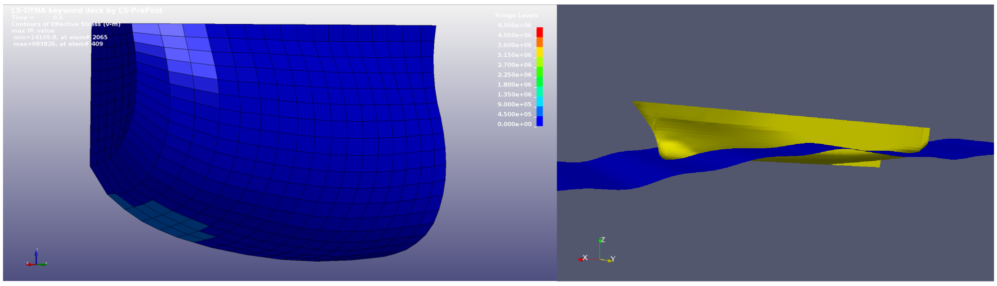

Figure H.2: Domestress, t=0.5s

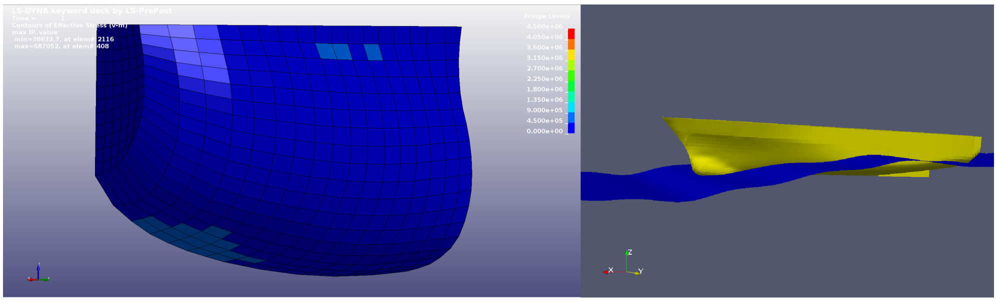

Figure H.3: Domestress, t=1.0s

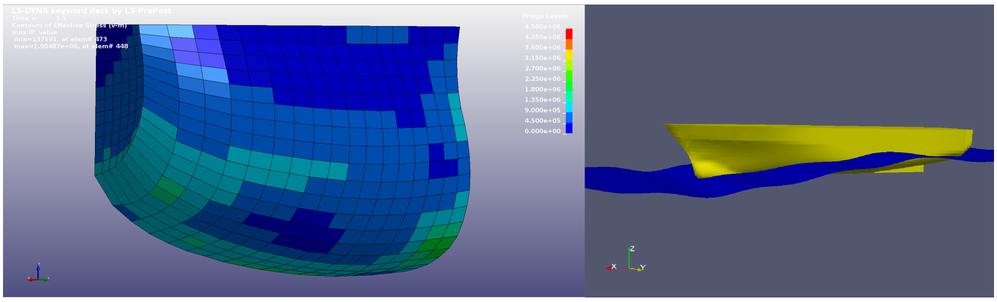

Figure H.4: Domestress, t=1.5s

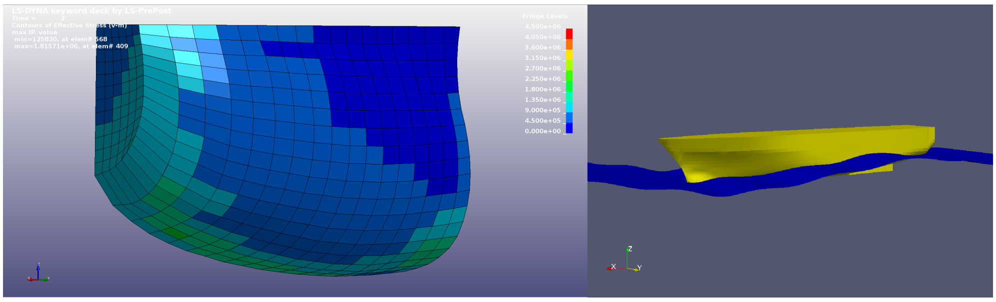

Figure H.5: Domestress, t=2.0s

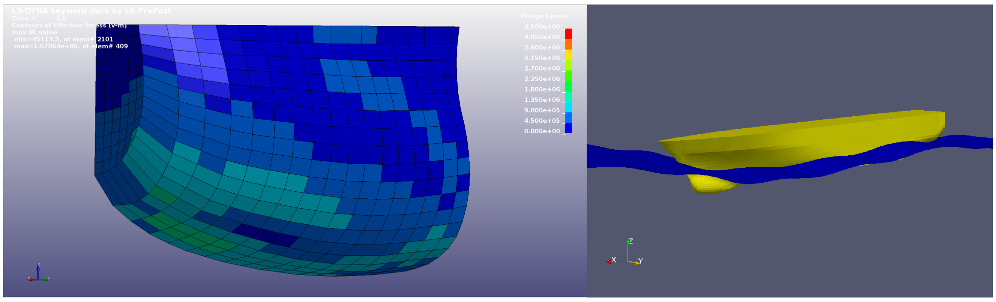

Figure H.6: Domestress, t=2.5s

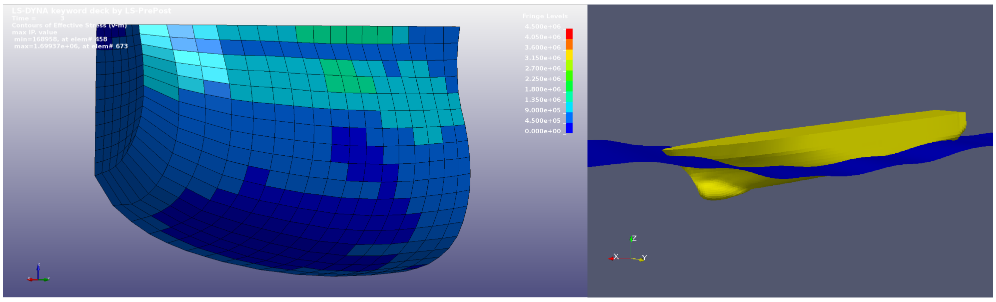

Figure H.7: Domestress, t=3.0s

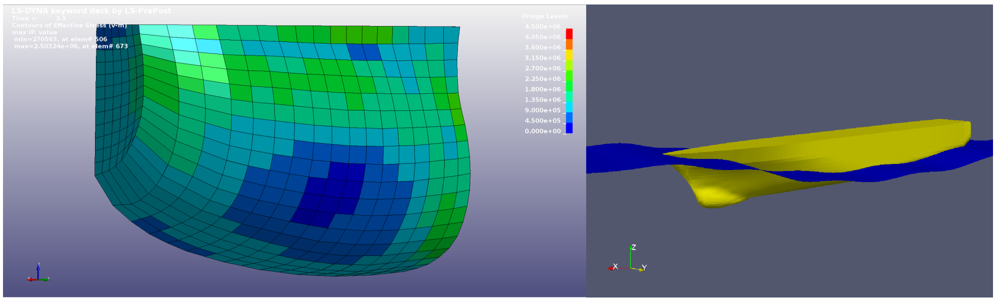

Figure H.8: Domestress, t=3.5s

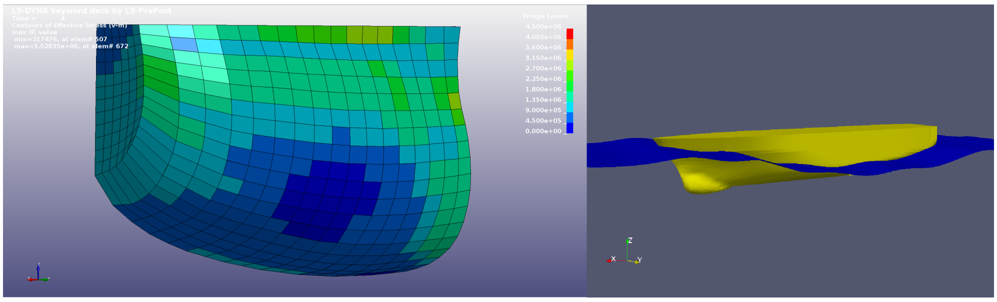

Figure H.9: Domestress, t=4.0s

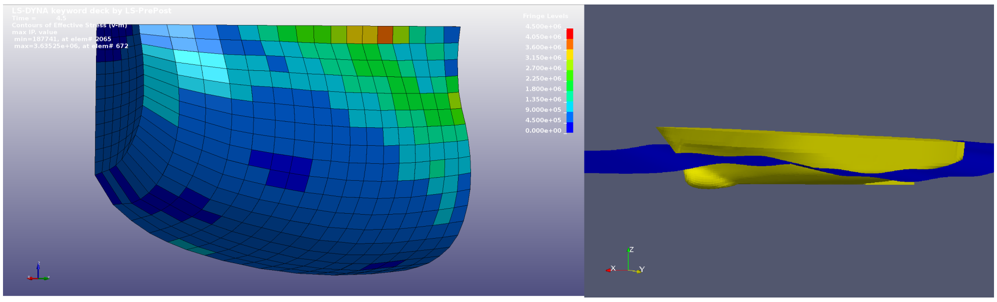

Figure H.10: Domestress, t=4.5s

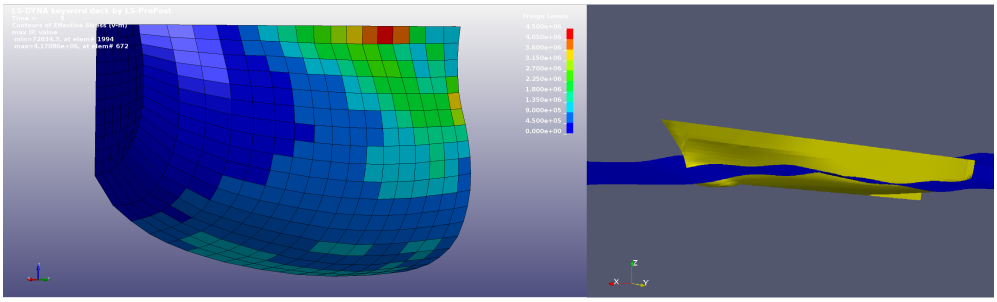

Figure H.11: Domestress, t=5.0s

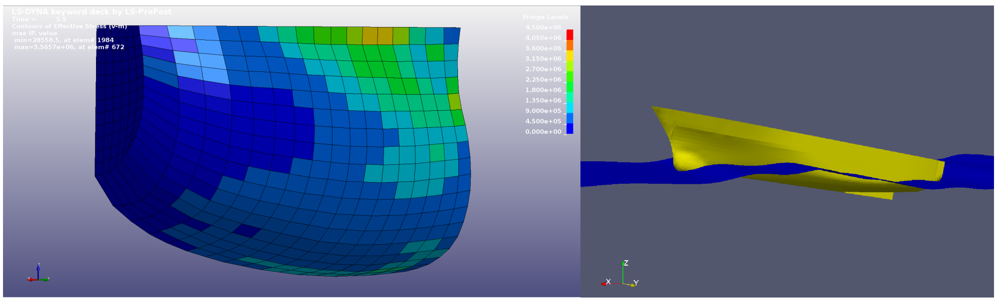

Figure H.12: Domestress, t=5.5s

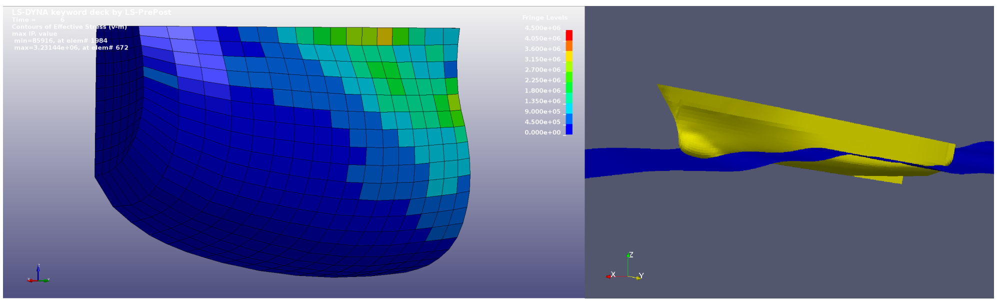

Figure H.13: Domestress, t=6.0s

I Structural response, unit loads

I.1 Vertical flange load, Nz=1kN

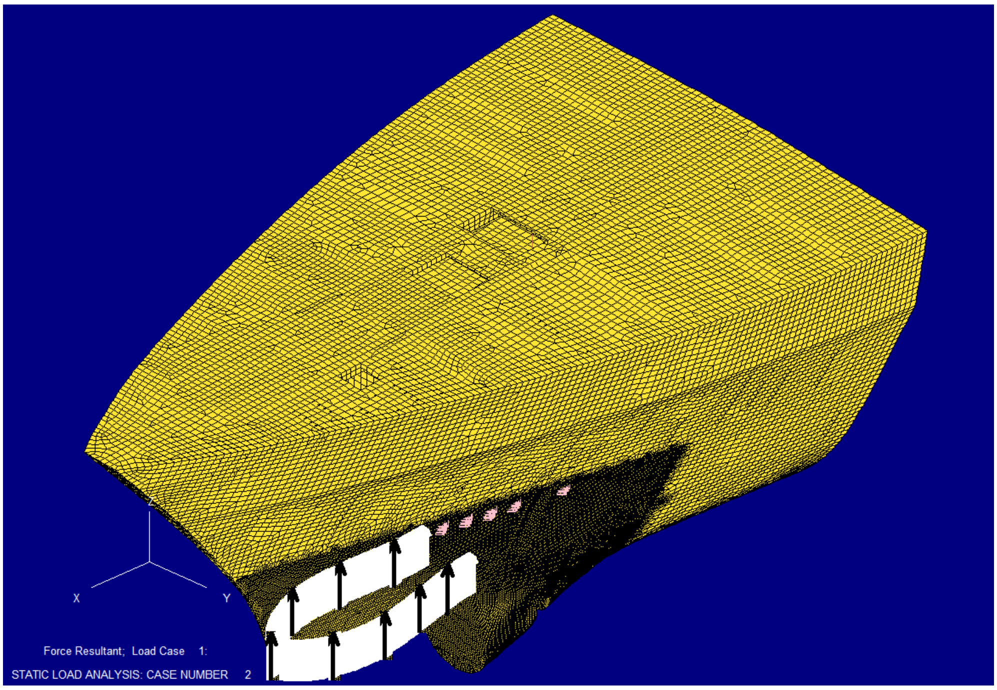

Figure I.1: Vertical flange load, Nz

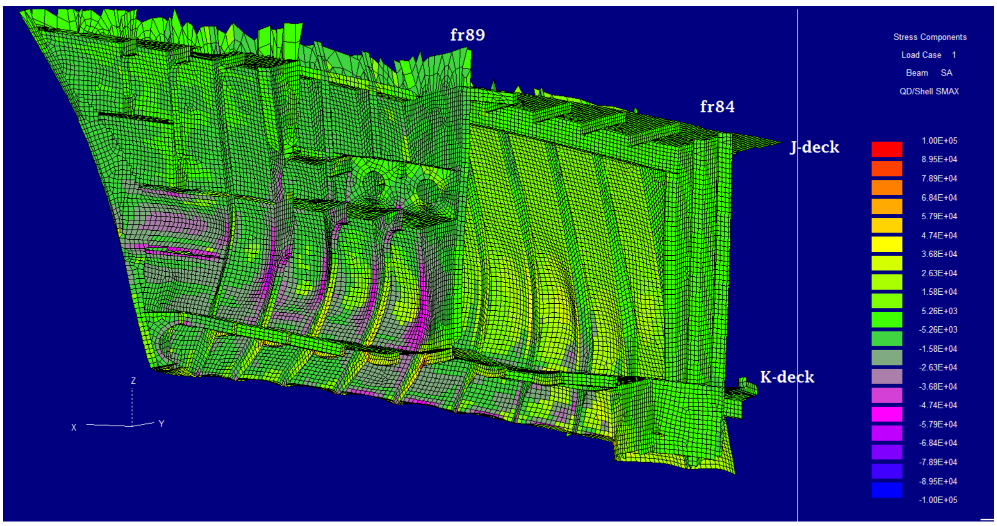

Figure I.2: Response to vertical flange load, Nz

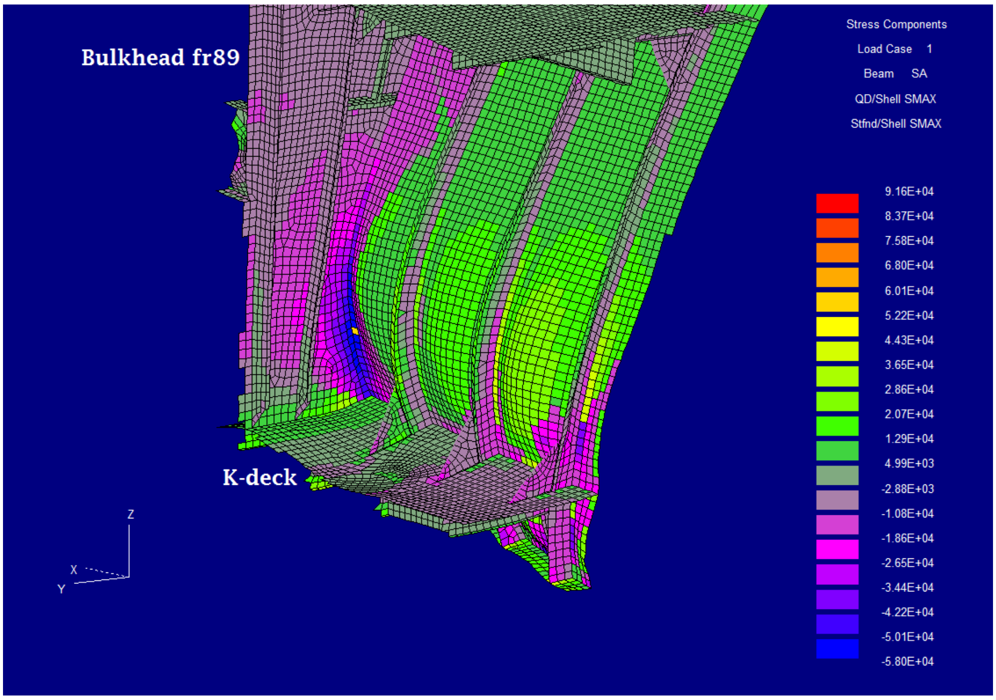

Figure I.3: Resposne to vertical flange load, Nz

I.2 Symmetric horizontal loading, Ny=1kN

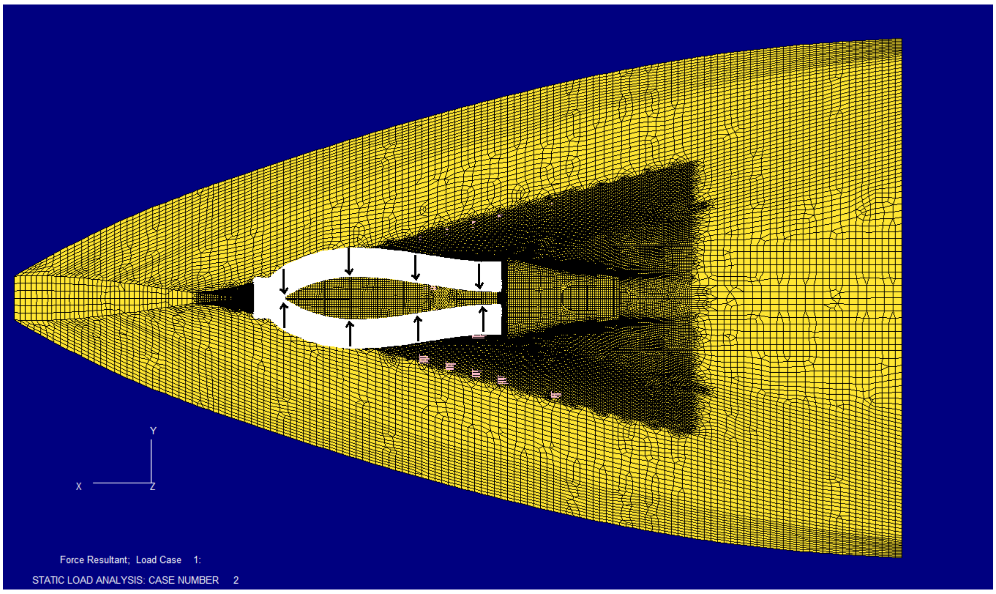

Figure I.4: Horizontal flange load, Ny

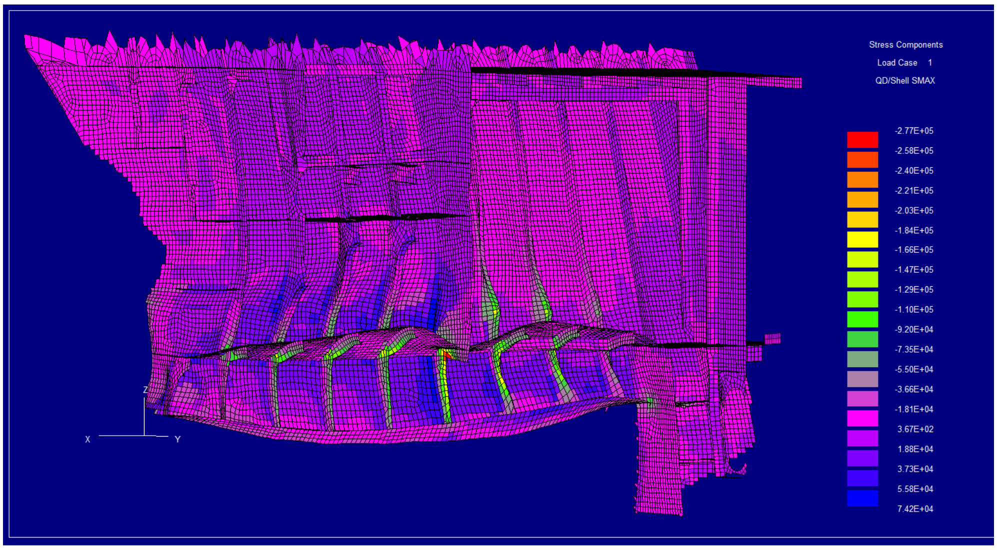

Figure I.5: Response to horizontal flange load, Ny

I.3 Asymmetric horizontal flange force due to sideward dome load, Ny_sideforce=1kN

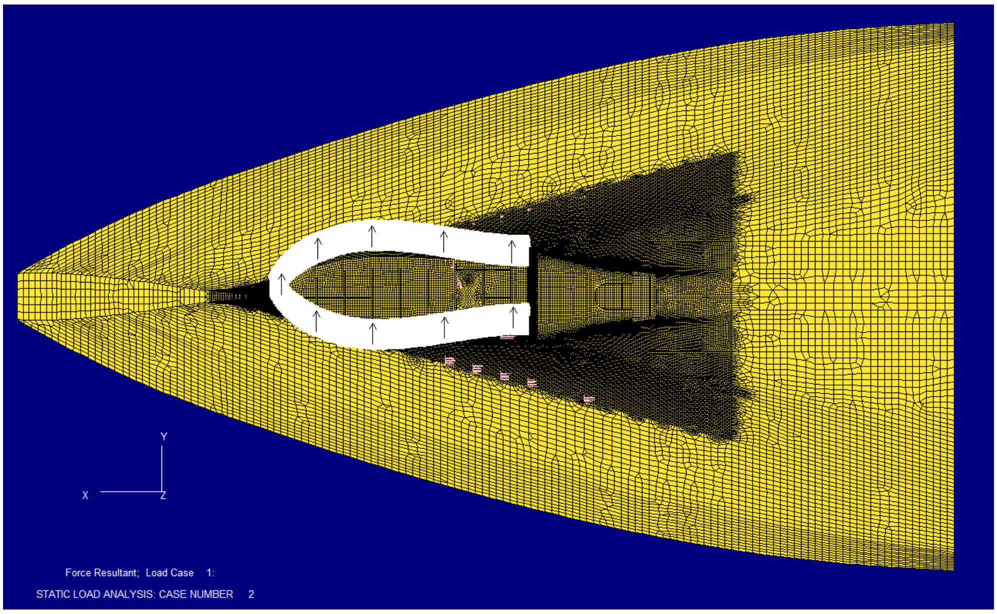

Figure I.6: Side force, Ny

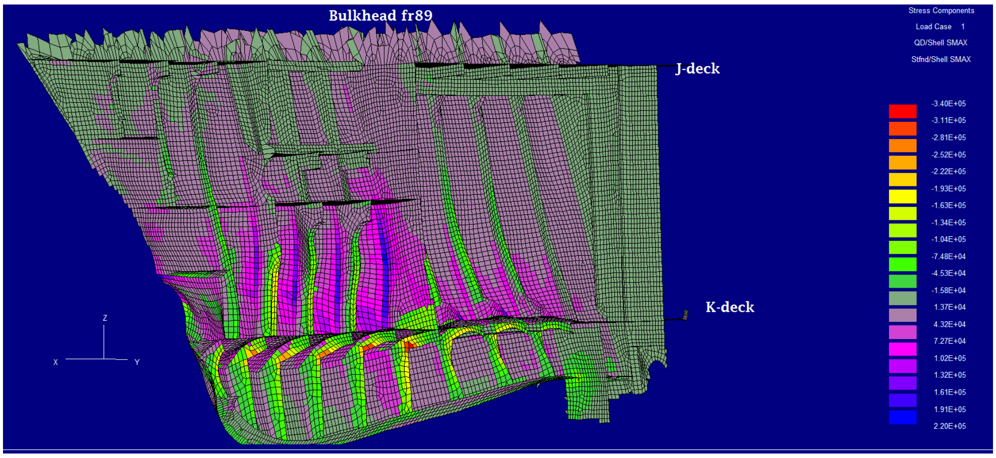

Figure I.7: Response to side force, Ny

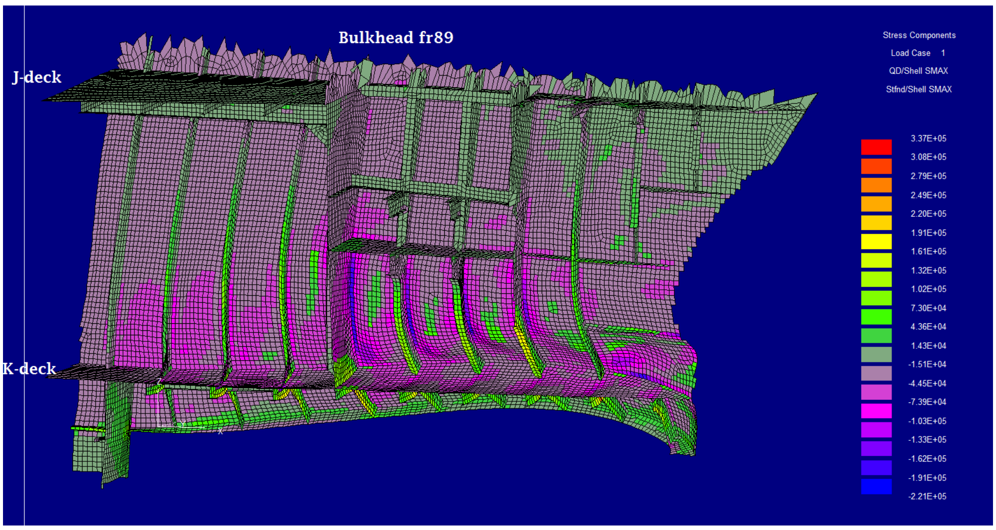

Figure I.8: Response to side force, Ny

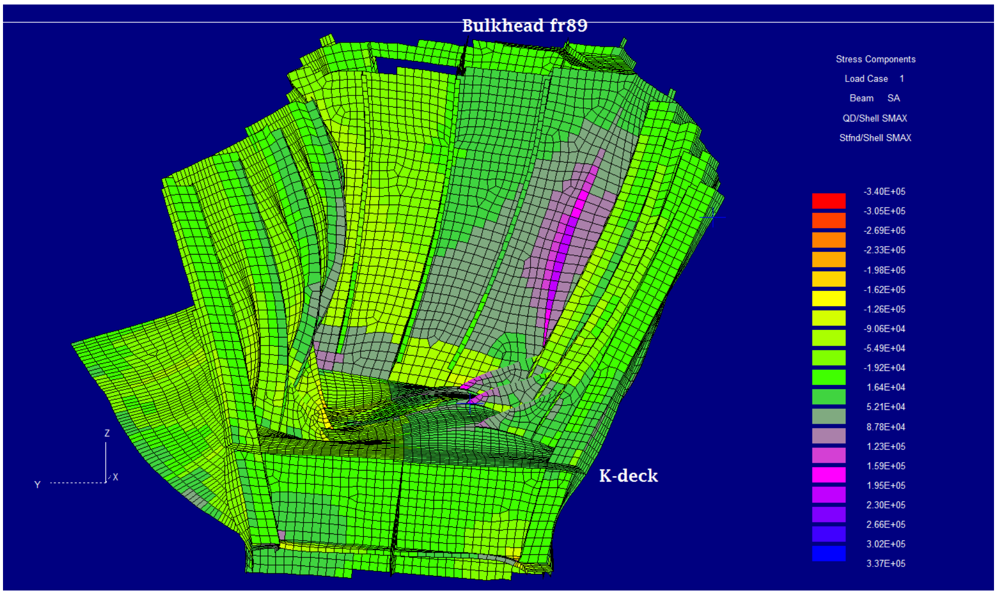

Figure I.9: Response to side force, Ny

I.4 Asymmetric vertical flange force due to global bending of the dome, GMx

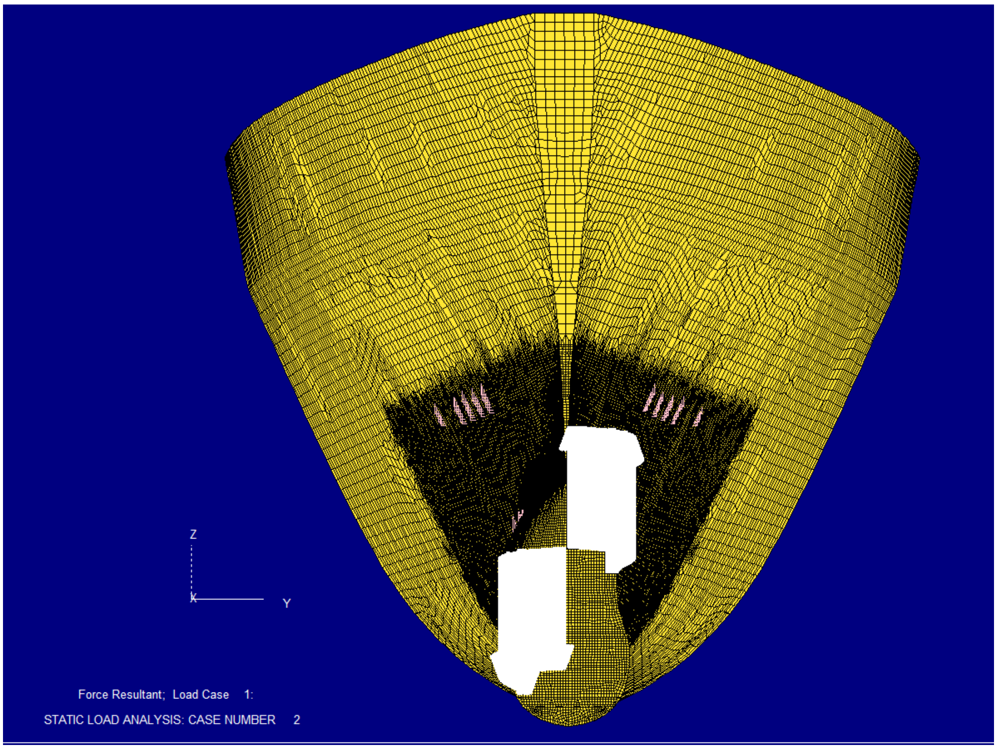

Figure I.10: Global bending flange load, GMx

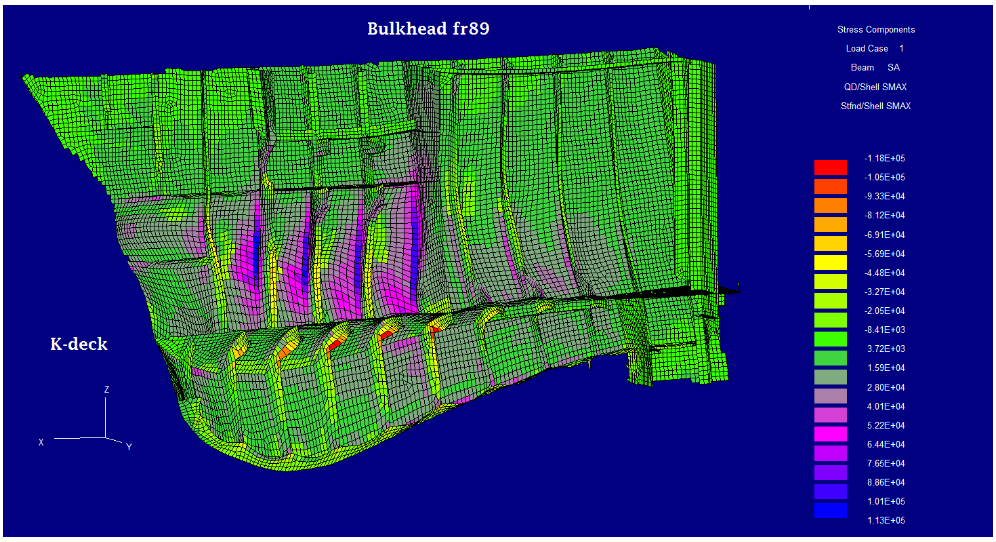

Figure I.11: Response to global bending flange load, GMx

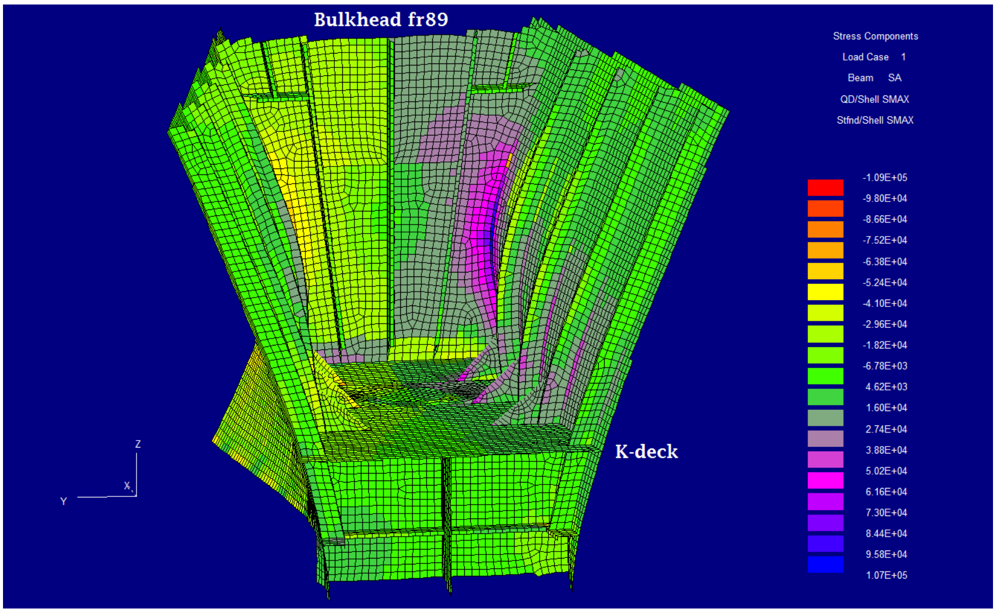

Figure I.12: Response to global bending flange load, GMx

I.5 Pressure load, Press=1bar

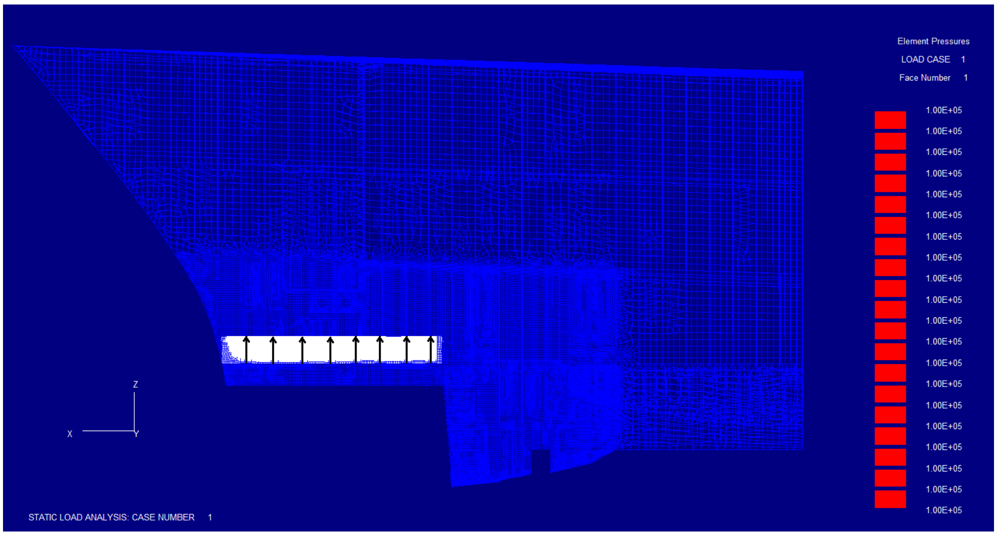

Figure I.13: Pressure load, Press

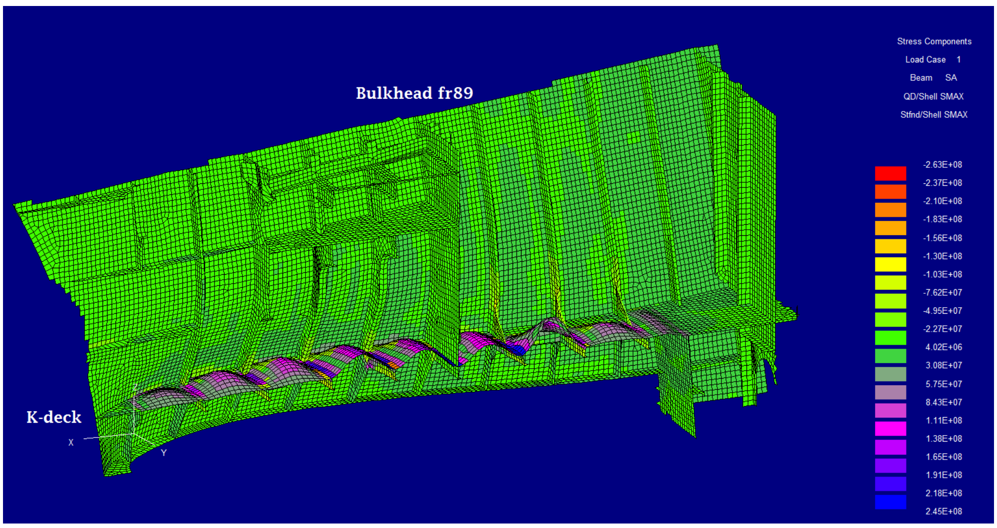

Figure I.14: Response to pressure load, Press

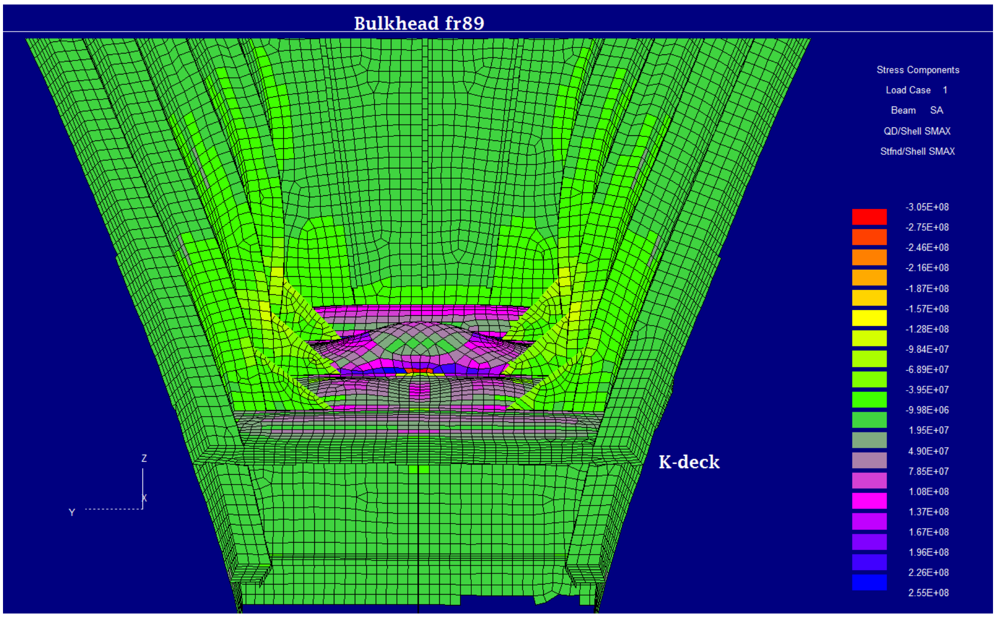

Figure I.15: Response to pressure load, Press

J Stress Brackets K-deck

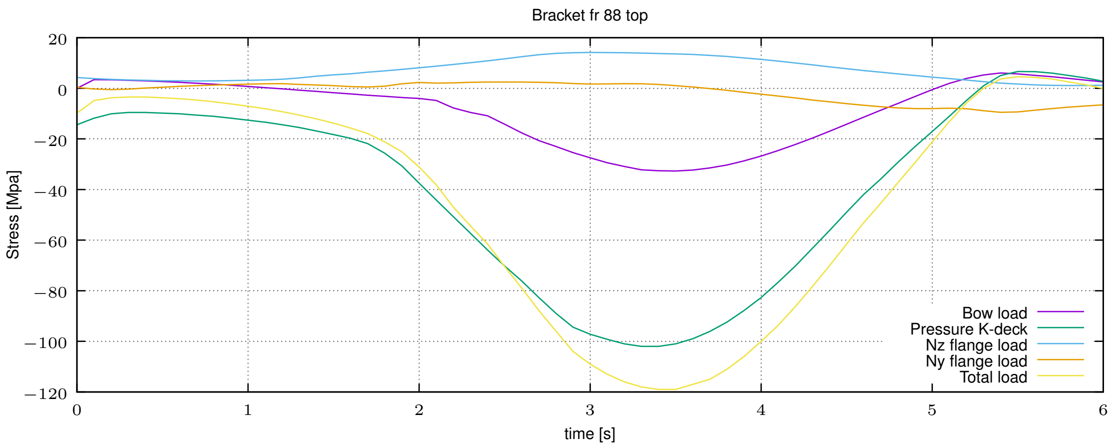

Figure J.1: Stress components Bracket frame 88 topside

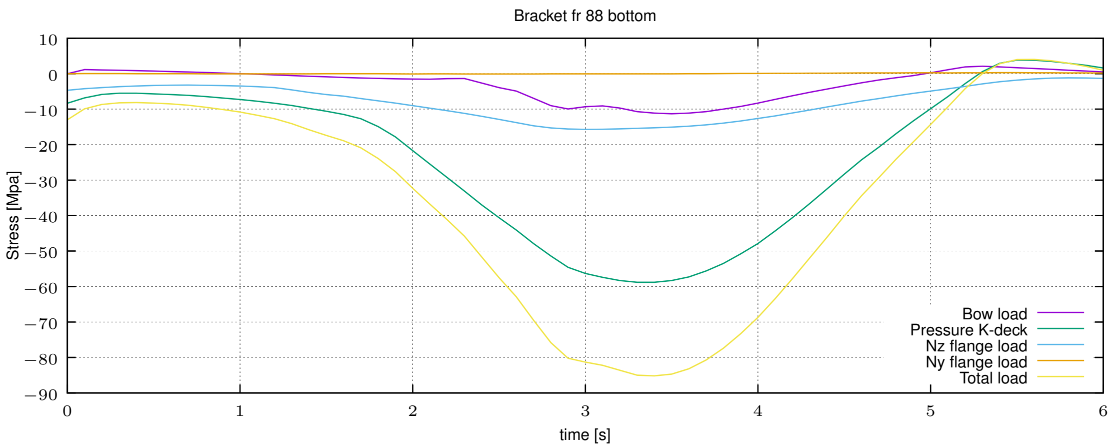

Figure J.2: Stress components Bracket frame 88 bottom

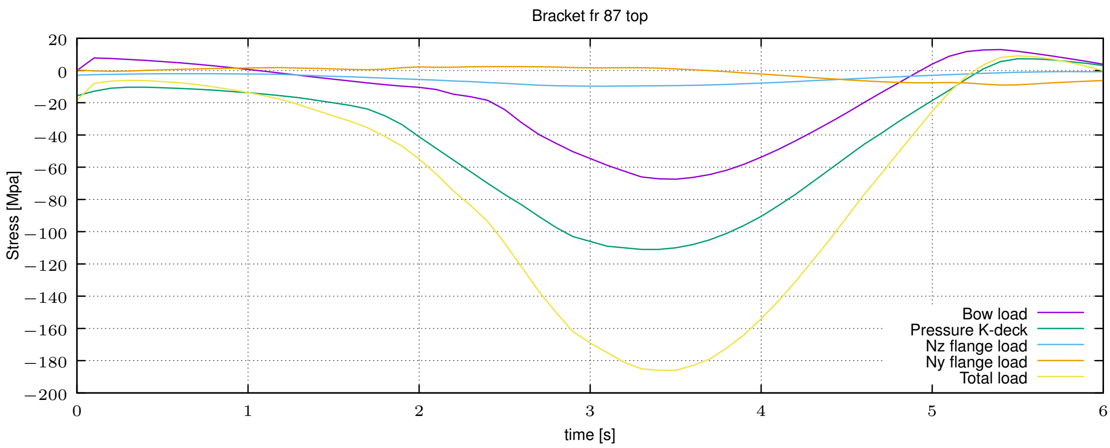

Figure J.3: Stress components Bracket frame 87 topside

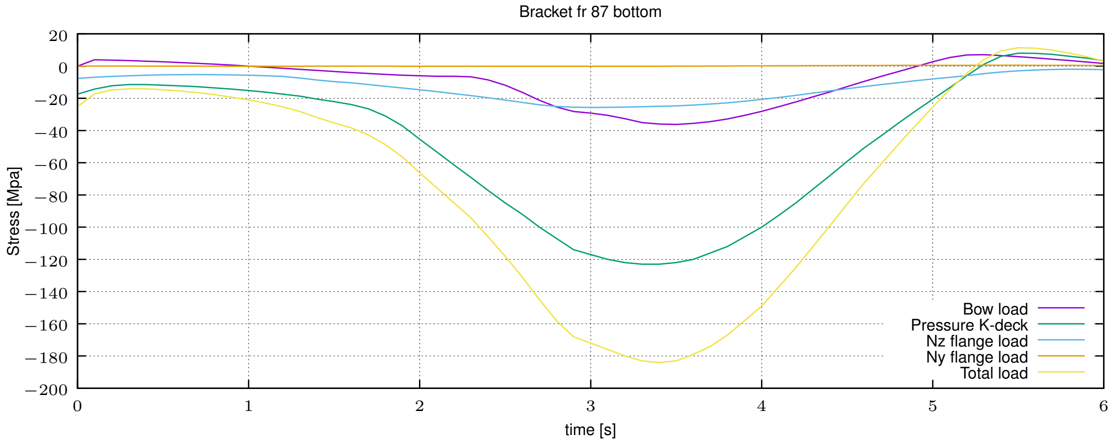

Figure J.4: Stress components Bracket frame 87 bottom

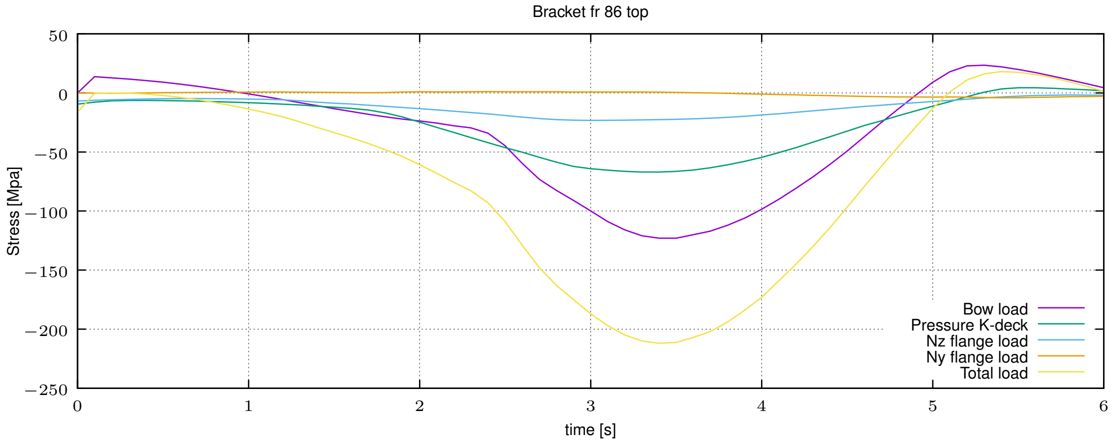

Figure J.5: Stress components Bracket frame 86 topside

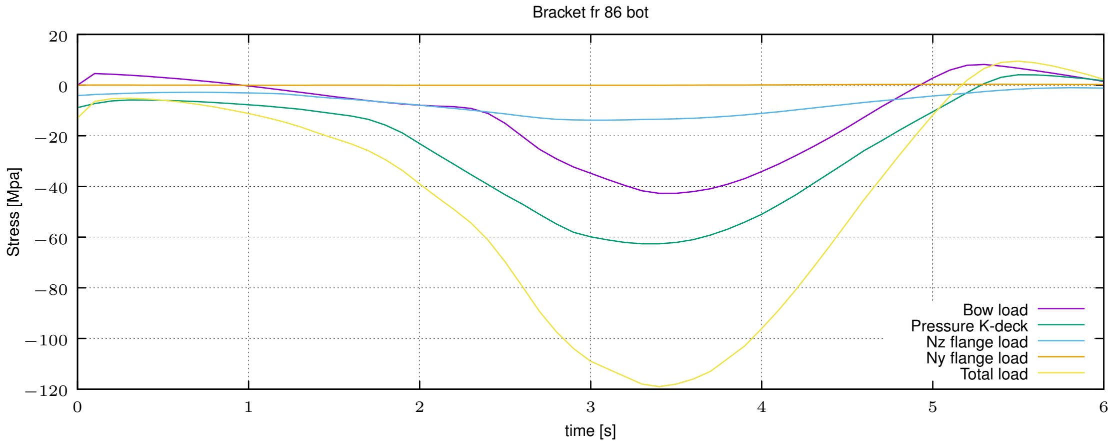

Figure J.6: Stress components Bracket frame 86 bottom